

# Irradiation-induced degradation of amorphous silicon solar cells in space

Proefschrift

ter verkrijging van de graad van doctor  
aan de Technische Universiteit Delft,  
op gezag van de Rector Magnificus prof. J. T. Fokkema,  
voorzitter van het College voor Promoties,  
in het openbaar te verdedigen  
op maandag 3 december 2007 om 12:30 uur

door

Arjen KLAVER

Ingenieur  
van de Technische Universiteit Eindhoven  
geboren te Helmond

Dit proefschrift is goedgekeurd door de promotor:

Prof. dr. C. I. M. Beenakker

toegevoegd promotor:

Dr. R. A. C. M. M. van Swaaij

Samenstelling promotiecommissie:

Rector Magnificus, voorzitter

Prof. dr. C. I. M. Beenakker, Technische Universiteit Delft, promotor

Dr. R. A. C. M. M. van Swaaij, Technische Universiteit Delft, toegevoegd promotor

Prof. H.-C. Neitzert, Università degli Studi di Salerno

Prof. dr. ir. M. C. M. van de Sanden, Technische Universiteit Eindhoven

Prof. dr. W. C. Sinke, Universiteit Utrecht

Prof. dr. P. M. Sarro, Technische Universiteit Delft

Dr. G. L. Oomen, Dutch Space b.v.

The work described in this thesis was supported by the Technology Foundation STW and SenterNovem.

The work was carried out at the laboratory of Electronic Components, Technology and Materials (ECTM), Delft Institute of Microsystems and Nanoelectronics (DIMES), Delft University of Technology.

Klaver, A.

Irradiation-induced degradation of amorphous silicon solar cells in space,  
Ph. D. thesis Delft University of Technology, with summary in Dutch, 2007.

ISBN 978-90-9022469-5

NUR 959

# Contents

<b>1</b>	<b>Introduction</b>	<b>1</b>
1.1	Crystalline Si and hydrogenated amorphous Si solar cells . . . . .	2
1.2	Space radiation and radiation-induced degradation of c-Si solar cells	4
1.2.1	Space radiation . . . . .	4
1.2.2	Crystalline silicon solar cell degradation . . . . .	5
1.3	Solar-cell and material analysis . . . . .	7
1.3.1	Characterization of electrical properties of a-Si:H . . . . .	8
1.3.2	Optical absorption . . . . .	9
1.3.3	Solar-cell characterization . . . . .	11
1.4	Motivation and outline . . . . .	12
<b>2</b>	<b>Degradation of solar cell material by high-energy electrons</b>	<b>15</b>
2.1	Introduction . . . . .	15
2.2	Degradation in optical and electrical properties of solar cell material.	17
2.2.1	Optical properties of glass substrates . . . . .	17
2.2.2	Electrical properties of intrinsic a-Si:H . . . . .	19
2.2.3	Optical properties of intrinsic a-Si:H . . . . .	21
2.2.4	Activation energy of doped a-Si:H . . . . .	23
2.3	Time-resolved microwave-conductivity spectroscopy . . . . .	25
2.3.1	Introducing TRMC . . . . .	25
2.3.2	Experimental details . . . . .	26
2.3.3	Model description . . . . .	27
2.3.4	Results and discussion . . . . .	29
2.4	Conclusions . . . . .	33

---

<b>3</b>	<b>Computer modeling of degraded amorphous silicon solar cells</b>	<b>35</b>
3.1	Introduction . . . . .	35
3.2	The ASA device simulator . . . . .	37
3.2.1	Recombination statistics . . . . .	38
3.2.2	Optical simulations . . . . .	39
3.3	Procedure to simulate degraded solar-cell performance . . . . .	39
3.4	Sensitivity study of simulation procedure . . . . .	42
3.4.1	Increase of light absorption in glass substrates . . . . .	42
3.4.2	Changes in activation energy doped a-Si:H and defect density intrinsic a-Si:H . . . . .	42
3.4.3	Defect creation depth profile . . . . .	48
3.5	Procedure to predict the EOL performance . . . . .	52
3.6	Conclusions . . . . .	53
<b>4</b>	<b>Degradation of solar cells by light soaking</b>	<b>55</b>
4.1	Introduction . . . . .	55
4.2	Experimental details . . . . .	57
4.3	Experimental results . . . . .	58
4.3.1	Experimental results for the as-deposited solar cells . . . . .	58
4.3.2	Degradation under open- versus short-circuit condition . . . . .	60
4.4	Simulation details . . . . .	63
4.5	Simulation results . . . . .	66
4.5.1	Simulations of the as-deposited solar cells . . . . .	66
4.5.2	Simulation of light soaking of a-Si:H solar cells . . . . .	68
4.6	Conclusions . . . . .	72
<b>5</b>	<b>Degradation of solar cells by high-energy electrons</b>	<b>75</b>
5.1	Introduction . . . . .	75
5.2	Experimental details . . . . .	78
5.3	Experimental results . . . . .	78
5.3.1	Experimental results for the as-deposited solar cells . . . . .	78
5.3.2	Fluence dependency . . . . .	80
5.3.3	Flux dependent degradation . . . . .	85
5.3.4	Degradation under open- versus short-circuit condition . . . . .	88
5.4	Simulation results . . . . .	91
5.4.1	Simulations of the as-deposited cells . . . . .	91
5.4.2	Simulations of electron-beam irradiated cells . . . . .	93

---

5.5	Conclusions . . . . .	98
<b>6</b>	<b>Degradation of solar cells by high-energy protons</b>	<b>101</b>
6.1	Introduction . . . . .	101
6.2	Experimental details . . . . .	103
6.3	Experimental results . . . . .	104
6.3.1	Experimental results for the as-deposited solar cells . . . .	104
6.3.2	Degradation with 1-MeV and 65-MeV protons . . . . .	105
6.4	Comparison with light soaking and electron-beam irradiation . . .	109
6.5	Conclusions . . . . .	114
<b>7</b>	<b>Conclusions and discussion</b>	<b>117</b>
<b>A</b>	<b>Generation, drift and recombination along the incident-particle trajectory</b>	<b>121</b>
	<b>Bibliography</b>	<b>127</b>
	<b>List of abbreviations and symbols</b>	<b>141</b>
	<b>Summary</b>	<b>143</b>
	<b>Samenvating</b>	<b>149</b>
	<b>Curriculum Vitae</b>	<b>155</b>
	<b>List of publications</b>	<b>157</b>
	<b>Dankwoord</b>	<b>159</b>

---

# Chapter 1

## Introduction

To a large extent solar-cell technology has been pioneered by space industry, as solar energy is one of the main power sources for satellites. Space, however, is a harsh environment for electronic devices, such as solar cells. In this environment the devices mounted in or on satellites and are subjected to large temperature cycles, atomic oxygen, space dust, and high-energy charged-particle irradiation. Mostly, conventional solar cells based on crystalline silicon (c-Si) are used to provide electric power to satellites, although nowadays gallium-arsenide (GaAs) solar cells are also frequently used because of their higher efficiency and radiation tolerance [1]. However, they also cost more and are heavier due to their higher thickness and mass density.

Hydrogenated amorphous silicon (a-Si:H) solar cells have great potential for space applications, because they can be produced inexpensively, are lightweight, and are relatively radiation hard. Furthermore, they show favorable annealing properties at working temperatures in space, which may reverse some performance degradation of the solar cells [2]. If these cells are applied in a space environment, it is important to be able to predict their End-of-Life (EOL) efficiency for a given mission. Typically, an indication for the EOL efficiency in a space environment is obtained by irradiating cells with a 1-MeV electron beam. However, the degradation mechanism of a-Si:H solar cells by high-energy charged-particle irradiation is still unclear and more research is needed to predict the EOL performance more accurately for a given space mission.

In this chapter we will give a brief introduction on the operation of solar cells, more particular a-Si:H solar cells that we have used in this work. We will

then shortly explain the circumstances under which solar cells operate in a space environment and focus on the effects of high-energy charged-particle irradiation. Then we will explain experimental techniques that we have used. In the last section we present the motivation for this work.

### 1.1 Crystalline Si and hydrogenated amorphous Si solar cells

At present, for most solar cells semiconducting materials are used and the market for solar cells is dominated by cells made from c-Si. Solar-cell operation is based on the photovoltaic effect, which consist of two steps. First, electron-hole pairs are generated in the semiconductor by light absorption and subsequently the electron-hole pairs are separated and the carriers are collected.

Solar cells of c-Si are in fact single large-area p-n junction diodes. Throughout the diode light is absorbed and electron-hole pairs are generated. The generated minority carriers (i.e., electrons in p-type Si and holes in n-type Si) diffuse through the solar cell towards the depletion region. When the electrons and holes reach the depletion region charge separation occurs. Electrons generated in the p-layer will be swept across the depletion region to the other side under the influence of the internal electric field, and visa versa for holes generated in the n-layer. The holes generated in the p-layer and the electrons in the n-layer will not be able to cross the depletion region and drift towards the contacts. Because the generated minority charge carriers first diffuse to the depletion region before the charge separation, c-Si solar cells are often characterized as diffusion-type devices. Due to the low light absorption of c-Si as a result of its indirect bandgap, these solar cells must be relatively thick to absorb enough light, around  $10\ \mu\text{m}$ . However, in solar cell production wafer thicknesses of about 250 to  $300\ \mu\text{m}$  are required for reasons of mechanical stability. Alternatively, thin films of c-Si have been deposited on glass and using high-quality light-trapping techniques reasonable module efficiencies above 8% have been obtained for a film thickness of  $1.4\ \mu\text{m}$  [3].

Solar cells of a-Si:H differ from their crystalline counterparts due to differences in electrical and optical material properties. In contrast to c-Si, a-Si:H lacks long-range order, which gives rise to weak or strained silicon-silicon bonds. As a result the conduction and valence bands have tail states that extend into the bandgap.

In addition, a-Si:H has a relatively high density of defects, usually threefold coordinated Si atoms, so-called dangling bonds, leading to a quasi-continuous density of defect states in the band-gap. These defect states may act as recombination and trapping centers for free charge carriers and result in a low charge-carrier diffusion length for a-Si:H. Fortunately, most of these dangling bonds are passivated by hydrogen that is incorporated in the material during the deposition.

Thin films of a-Si:H can be deposited using plasma-enhanced chemical vapor deposition, using silane gas ( $\text{SiH}_4$ ) as the precursor [4]. By adding different gasses to the plasma the material properties of the a-Si:H may be altered. For instance, by adding germane ( $\text{GeH}_4$ ) [5] or methane ( $\text{CH}_4$ ) [6] to the gas mixture, an a-Si:H alloy is obtained with lower or higher band gap, respectively. To create p-type material diborane ( $\text{B}_2\text{H}_6$ ) is added in the gas mixture and boron is incorporated in the material [7]. Similarly, for n-type material phosphine ( $\text{PH}_3$ ) is used.

In contrast to c-Si, a-Si:H has a direct bandgap and a higher light absorption for energies above the a-Si:H bandgap. Because of this higher absorption, a-Si:H solar cells can be made much thinner and therefore lighter than their crystalline counterparts, typically less than 500 nm for a single-junction solar cell. However, the charge-carrier diffusion length in doped a-Si:H is too low to allow a high-efficient diffusion-type solar cell. To overcome this problem solar cells a p-i-n or n-i-p structures are used in which an intrinsic layer is sandwiched between a n- and p-doped layer. Here, the intrinsic layer is sometimes called the active or absorber layer. The p- and n-doped layer create an electric field over the intrinsic layer in the solar cell, which facilitates in the charge separation, improving the solar cell performance considerably. Light is now primarily absorbed in the intrinsic layer in which the charge carriers are generated. Under operating conditions the generated electrons will drift towards the n-layer, while the holes drift towards the p-doped layer, because of the internal electrical field over the intrinsic layer. Therefore, a-Si:H solar cells are classified as drift devices.

The main drawback of a-Si:H solar cells is the lower beginning-of-life efficiency as compared to c-Si cells. Green et al. [8] reported that the efficiency record for a-Si:H single-junction cells is 9.5 % [9], while for multijunction a-Si:H/ $\mu\text{c-Si:H}$  cells it is 11.7 % [10], and for a-Si:H/a-SiGe:H/a-SiGe:H triple-junction production modules it is 10.4% [11]. Note that these are stabilized efficiencies, i.e., after 1000 hours of light soaking before their efficiency was determined. The performance of a-Si:H solar cells decreases upon prolonged illumination, the so-called Staebler-Wronski effect [12], as additional defect states are created in the band gap

leading to increased recombination rate. This performance degradation stabilizes eventually and may be reversed by moderate annealing at elevated temperatures. For c-Si, the record lab cells have an efficiency 24.7% [13], and modules have 22.7% [14].

## 1.2 Space radiation and radiation-induced degradation of c-Si solar cells

### 1.2.1 Space radiation

Solar cells in space are continuously bombarded by high-energy charged-particle irradiation, most often electron and proton radiation. In most cases the radiation flux is low and the solar-cell performance is hardly affected by the radiation over longer periods of time. However, in some particular orbits or during a space-wind storm the radiation levels may be much higher.

In many cases solar-wind storms are related to solar flares and coronal mass ejections (CME), which result from magnetic-field instabilities in the sun. During a CME or flare a cascade of high-energy particles may be ejected from the sun towards the earth, although the exact relationship between CMEs and solar flares is still under discussion [15]. Most flares are found around sunspots and occur on an 11-year cycle of these spots. The mass of a CME may be up to 10 billion tons of solar material. The ejected material is a plasma consisting primarily of electrons and protons (in addition to small quantities of heavier elements such as helium, oxygen, and iron), accompanied by the entrained coronal magnetic field. Near earth, intensities of  $> 10$  MeV-protons ranging from  $10^0$  to  $10^5$  protons  $\text{cm}^{-2} \text{s}^{-1} \text{sr}^{-1}$  have been recorded during such a storm [16]. These space-wind storms can last up to a few days and may lead to a significant efficiency decrease of solar cells on satellites. For instance, on July 14, 2000, the efficiency of solar cells on the solar heliospheric observatory satellite dropped from 14% to 12% [17] due to such a solar-wind storm. Two big solar wind storms in the next year led to another decrease to only 8% efficiency. A CME on January 7, 1997, hit the Earth's magnetosphere on January 10 and caused the loss of the AT&T Telstar 401 communication satellite (estimated costs: \$200 million). The effects of CMEs may even be observed on earth as auroras when the ejected plasma cloud connects with the Earth upper atmosphere. In addition, in 1989 a CME knocked out the power to all of Quebec, Canada. Here, the space-wind storm induced large current

in power and communication lines, leading to overload conditions.

The particles from the space winds may be trapped in the earth magnetic fields and further accelerated, leading to the so-called Van Allen radiation belt. The belts starts 200-1000 km above the earth's surface extends up to 7 earth radii. Typical Low Earth Orbit (LEO) missions (300-500 km) are characterized by low radiation levels but a high amount of thermal cycles each year. High inclination LEO missions may lead to higher radiation levels, because the shielding of the earth's magnetic field against space wind is not as effective on the poles as on the equator. In addition, solar cells on satellites in an orbit crossing the southern Atlantic Ocean anomaly are more susceptible to damage because the trapped electrons belts dip there to lower altitudes, increasing the radiation levels.

If the altitude of the satellites is increased, they may be able to cover a larger part of the earth surface, which implies that fewer satellites are required to provide global coverage. However, for missions in geostationary earth orbits (GEO) and medium earth orbits (MEO) the radiation levels are greatly increased due to the higher density of trapped electrons and especially protons at these high altitudes. Furthermore, the earth magnetic field does not protect the satellites anymore against solar winds. The annual damage induced in a c-Si solar cell by trapped protons at  $100^\circ$  inclination at an altitude of 4000 km is equivalent to an 1-MeV electron fluence of approximately  $5 \times 10^{16}$  electrons/cm<sup>2</sup>/year [18]. c-Si solar cells hardly survive such high irradiation levels.

As solar cells on satellites are exposed to radiation for prolonged periods, the cells are often protected with cover glass to reduce the performance degradation by the radiation, because the cover glass blocks a large part of the incident particles in the glass. This must be radiation hard glass of which the transmission is not or hardly affected upon irradiation. The disadvantage of this solution is the higher launch weight and thus mission cost.

### 1.2.2 Crystalline silicon solar cell degradation

In planning a space mission, the degradation of solar cells in the space environment needs to be predicted, which is usually realized by correlating the results from ground testing to the degradation in space. However, the degradation rate of solar cells is dependent on the kinetic energy of the incident particle, which complicates the analysis.

There are two important methods to analyze the degradation of c-Si and other

crystalline solar cells for their radiation tolerance in a space environment. The first method was introduced by the Jet Propulsion Lab (JPL) more than 25 years ago [19]. In this method using ground tests with various particle energies an equivalent 1-MeV electron-beam fluence is determined, which produces the same amount of the degradation as the specified space environment. Therefore 12 single-energy degradation curves are measured, 4 using electron and 8 using proton irradiation. The kinetic energy of the incident particles is varied from 0.6 to 12 MeV for electron irradiation, while for protons this is in between 50 keV and 9.5 MeV. For each particle a Relative Damage Coefficient (RDC) is calculated, which correlates the observed degradation by electron-beam irradiation to the degradation by 1-MeV electrons and for protons to the 10-MeV proton degradation. With the RDCs and the expected electron and proton spectra incident on the solar cells for a specified mission, the equivalent 1-MeV electron fluence is calculated and the EOL-performance is determined from the 1-MeV electron degradation curve.

In the second method the energy dependence of the degradation is determined by calculations of the energy deposition of the incident particles in the solar cell [20, 21]. This method was developed by the US Naval Research laboratory (NRL). In the calculations the energy loss of the incident particle having an energy,  $K$ , in the irradiated material is determined, where a distinction is made between non-ionizing (NIEL) and ionizing energy loss (IEL); a high NIEL value implies low tolerance of the material for that beam energy. It has been determined that c-Si solar cell degradation is related to NIEL [20]. Using the NRL method, RDC values can be calculated and these are in agreement to the values obtained by the JPL method and therefore both methods lead to similar EOL values.

Figure 1.1 presents the NIEL and IEL functions collected from various sources [20, 22]. In the NIEL calculations a minimum atom displacement energy in the Si lattice of 12 eV was used. Electrons with an energy lower than the 300 keV threshold energy are unable to transfer 12 eV or more to the material in a head-on collision. Increasing the kinetic energy leads to an increase in NIEL, because in a larger fraction of the collisions at least 12 eV will be transferred to the Si atom. Protons are much heavier and therefore are able to knock-out Si atoms at a much lower kinetic energy.

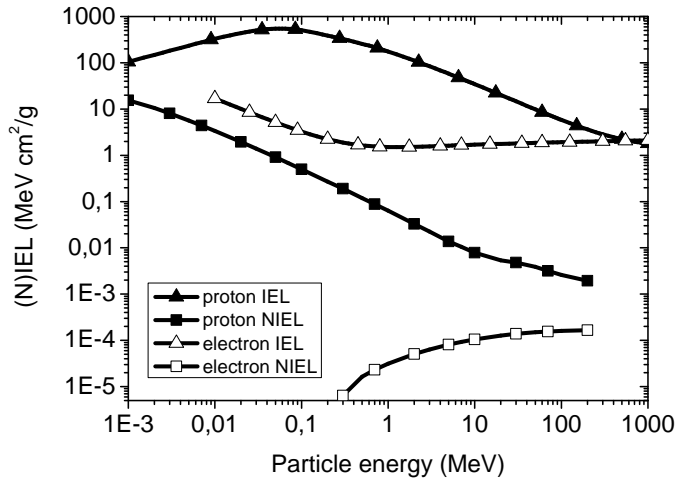


**Figure 1.1:** IEL and NIEL values for c-Si found in literature [20, 22] for proton- and electron-beam irradiation.

### 1.3 Solar-cell and material analysis

Various techniques were utilized in this work to study the material properties of a-Si:H and characteristics of a-Si:H solar cells following high-energy charged-particle irradiation and light soaking. The change in material properties is needed in order to understand the variations in solar-cell characteristics. Therefore, the absorption of the material was measured, from which the band gap and the sub-bandgap absorption is determined. In addition, photo- and dark conductivity measurements were carried out, as well as a determination of the Fermi level position of single layers of a-Si:H. Solar cells were characterized by extracting the external parameters from current density versus voltage measurements and by quantum-efficiency measurements. In the following we will give a brief description of measurement techniques that we have used in this work.

### 1.3.1 Characterization of electrical properties of a-Si:H

The conductivity,  $\sigma$ , is a measure for the free electron and hole density,  $n$  and hole,  $p$ , respectively, with their corresponding mobility,  $\mu_n$  and  $\mu_p$  in the material:

$$\sigma = n \cdot \mu_n + p \cdot \mu_p. \quad (1.1)$$

$n$  and  $p$  are dependent on material properties, like the activation energy, and on charge-carrier generation and recombination statistics.

At thermal equilibrium charge carriers are generated by thermal emission to the extended states. The dark conductivity is determined by the density of free charge carriers in the material at thermal equilibrium. The density of these free charge carriers is in turn related to the Fermi level position,  $E_f$ , with respect to the conduction and valence band, according the relations

$$n_0 = N_c \exp\left(\frac{-(E_c - E_f)}{kT}\right) \quad (1.2)$$

$$p_0 = N_v \exp\left(\frac{-(E_f - E_v)}{kT}\right), \quad (1.3)$$

where  $N_c$ ,  $N_v$ ,  $E_c$ ,  $E_v$ ,  $k$  and  $T$  are the conduction- and valence-band state density, their energy position of the bottom of the conduction band and top of the valence band, the Boltzmann constant, and the temperature, respectively. For undoped a-Si:H the Fermi level is nearly in the middle of the bandgap, resulting in low  $n$  and  $p$  values. Using n-type doping the Fermi level is shifted towards the conduction band and towards the valence band for p-type doping. In addition, a non-uniform defect state distribution in otherwise intrinsic a-Si:H may lead to a shift in the Fermi-level away from middle of the bandgap. Note that the Fermi-level of a-Si:H in thermal equilibrium is closely related to the activation energy of the dark conductivity.

Under illumination, the free charge-carrier generation rate,  $G$ , and thus  $n$  and  $p$ , are highly increased and the photoconductivity may be determined. Under steady-state conditions measurement of the photoconductivity may provide information on the defect density. Using the continuity equations the following relationship between the inverse of the photoconductivity,  $\sigma_{ph}$ , and the defect density may be deduced:

$$\frac{1}{\sigma_{ph}} \propto \frac{N_d}{G} \quad (1.4)$$

To measure the conductivity of the material, two parallel 300-nm thick Al bars are deposited on the 600-nm thick a-Si:H. The bars are spaced 0.5 mm apart

and are either 20 mm or 5 mm long, for respectively the photoconductivity and dark conductivity measurements. Between those contacts a voltage,  $V$ , is applied and the current,  $I$ , is measured using a two-point probe measuring system. The conductivity is then derived from the slope of the  $I - V$  curve from 0 to 100 V. In this work, the photoconductivity is determined under AM 1.5 illumination [23] with an intensity of 1000 W/m<sup>2</sup>.

The activation energy is determined from the slope of the Arrhenius plot of the dark conductivity, while assuming that the carrier mobility is temperature independent. The temperature was varied from 60 °C to 90 °C, with a step of 5 °C using a temperature-controlled stage. These relatively low temperatures were chosen to reduce the effect of annealing of irradiation-induced defects during the measurement. A measurement usually lasted less than 30 minutes, but still some annealing of defects was observed. Instead of using a  $I - V$  curve to determine the conductivity at each temperature, in the activation energy measurements, only a single  $I - V$  point was used to determine the conductivity.

### 1.3.2 Optical absorption

Optical properties of the material determine the electron-hole pair generation profile in solar cells, but can also give information about the electrical material properties, with the use of sub-band gap absorption measurements. An example measurement of the absorption spectrum including the sub-bandgap absorption is shown in figure 1.2. A self convolution of the density of states of a-Si:H  $N$ , determines the absorption spectra:

$$\alpha(h\nu) = \frac{C}{h\nu} \int_{E_f - h\nu}^{E_f} N(E)N(E + h\nu)dE, \quad (1.5)$$

with  $h\nu$  the photon energy and  $C$  a constant. In the a-Si:H absorption spectrum three energy ranges can be identified: in the high-energy range the absorption is due to transition between the extended states, below this energy range the absorption associated to tail states and defect states.

The first parameter we consider is the optical bandgap,  $E_g$ , which characterizes the extended state absorption. For a-Si:H typically the so-called Tauc-gap definition [24] is used to determine the bandgap:

$$\sqrt{\alpha h\nu} = A(h\nu - E_g), \quad (1.6)$$

where  $\alpha$ ,  $h\nu$ , and  $A$  are the absorption, the photon energy, and a constant (determined by a fitting procedure), respectively.

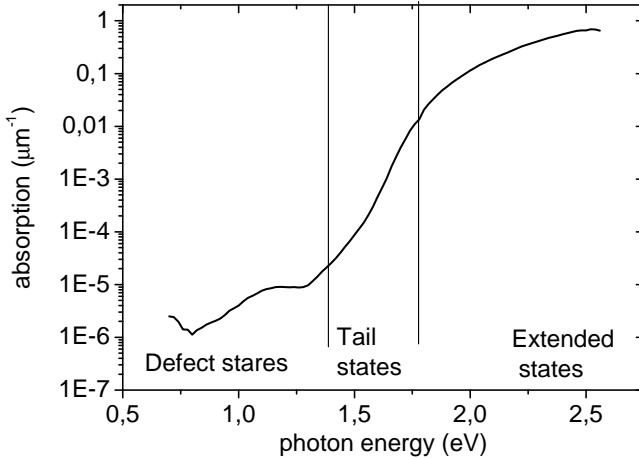


**Figure 1.2:** Example measurement of the absorption spectrum of intrinsic a-Si:H. Three energy ranges are identified, namely absorption associated with the extended states, tail states, or defect states

The sub-bandgap absorption is mainly governed by excitation processes of charge carriers from the valence or conduction band into the localized states, either tail or defect states. The second part of the a-Si:H absorption spectra, between approximately 1.8 eV and 1.4 eV is related to the tail states. In this energy range  $\alpha$  is exponentially dependent on the photon energy by a characteristic energy, the so-called Urbach energy,  $E_u$ :

$$\alpha = \alpha_0 e^{(E-E_u)/kT}. \quad (1.7)$$

As the characteristic energy of the valence-band tail is much higher than that of the conduction-band tail, it is generally accepted that the Urbach energy reflects the characteristic energy of the valence-band tail.

Finally, below 1.4 eV, the light absorption is associated with the defects states in a-Si:H. The defect density of states can be obtained by the integration of the absorption related to defect states using the procedure as proposed by Jackson et al. [25]. The defect density of the material is found to be:

$$N_{def} = 7.9 \times 10^{15} \int \alpha_d dE \quad (1.8)$$

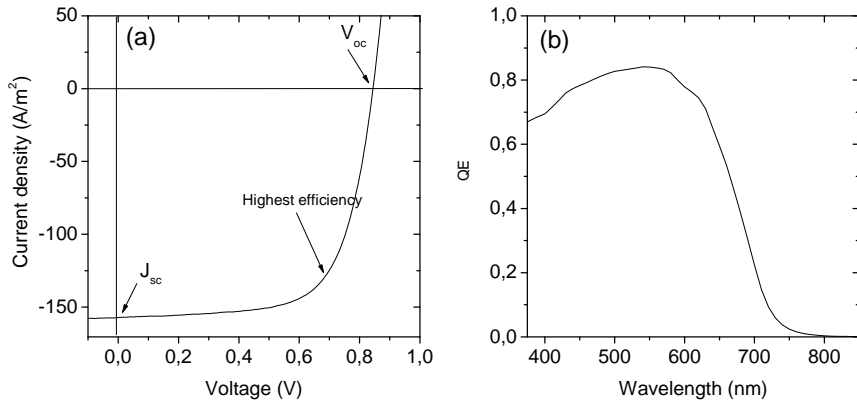


**Figure 1.3:** Example measurements of (a) the current density versus voltage ( $J-V$ ) for an a-Si:H solar cell, including the external parameters, and (b) the quantum efficiency.

### 1.3.3 Solar-cell characterization

In order to measure the energy conversion efficiency of solar cells, current density versus voltage ( $J-V$ ) curves under AM1.5 [23] illumination were measured. An example measurement is presented in figure 1.3a. The energy conversion efficiency is the maximum power output of the solar cell under illumination divided by the incident power. For the measurement the voltage is swept from  $-0.1$  to  $0.9$  V while measuring the current. From the  $J-V$  curves the external solar-cell parameters are extracted: the open-circuit voltage,  $V_{oc}$ , the short-circuit current density,  $J_{sc}$  and the fill factor,  $FF$ . The fill factor is defined as the ratio of the efficiency over the  $V_{oc}$ - $J_{sc}$  product and is an indication of the recombination rate in the solar cell.

The spectral response of the solar cell is characterized by the quantum efficiency (QE) and an example measurement is presented in figure 1.3b. This quantity indicates which fraction of generated electron-hole pairs is collected per photon of given energy (i.e., wavelength). The wavelength of the incident light is varied from 380 to 950 nm using a filter wheel with 35 band transmissions filters. The transmitted light is then focused onto the solar cell and the current at short-circuit condition is determined. No additional bias lighting was used. A light chopper coupled to a lock-in amplifier is used to increase the signal-to-noise ratio

of the measurements. The setup is calibrated using a calibrated photo diode.

### 1.4 Motivation and outline

For a-Si:H solar cells to be used in space they have to be cost-competitive with conventional c-Si and GaAs solar panels. The costs may be divided into three groups: fabrication costs, launching costs, and operational costs. These costs are in turn dependent on the required power of the mission, the radiation levels encountered, and the mass of the panels. An important parameter in choosing the type of solar cells for a particular mission is the power-versus-mass ratio of the solar panels, because the launch cost of the panels into a LEO orbit may be up to about \$20 000/kg [26, 27]. Solar cells of a-Si:H may have an advantage over c-Si and GaAs cells, because of the higher radiation tolerance, their better annealing properties, and lower weight if no cover glass is used. However, a-Si:H solar cells have a significant lower beginning of life efficiency. Therefore, a-Si:H solar cells will probably be most cost-effective for high radiation missions. If a-Si:H solar cells are going to be used for space applications it is essential that the EOL-performance for a particular mission can be predicted. With the EOL performance, the solar-panel area needed for the power consumption of the satellite can be determined and the deployment cost of the a-Si:H solar panels can be calculated and compared to panels based on c-Si and GaAs solar cells.

The aim of the work presented in this thesis is to develop a model with which the EOL performance of a-Si:H solar cells during high-radiation space missions can be predicted. In the model, changes in material properties of each individual layer in the solar cell following irradiation by various incident particles (either protons or electrons having varying kinetic energies) are linked to the overall performance degradation of the cell. In order to obtain this correlation the mechanism underlying the degradation of the a-Si:H is investigated.

In chapter 2 the changes in material properties following 1-MeV electron-beam irradiation are studied. We have investigated optical and electrical properties of intrinsic and doped silicon as well as the transmission of the glass substrates. The analysis focuses mostly on the changes in defect density of the intrinsic layer, because it is expected that these changes play a major role in the degradation of a-Si:H solar cells. The defect density following irradiation will be investigated using the photoconductivity, dual-beam photo-spectroscopy, and time-resolved microwave conductivity measurements.

Based on changes observed in the material, a procedure is proposed in chapter 2 to link these changes in material properties to the performance degradation. We utilize in this procedure the simulation program called *Advanced Semiconductor Analysis* (ASA), with which the performance as well as the internal parameters (e.g., the electric field distribution and the recombination rate) of the solar cell can be calculated using electrical and optical material properties of the various layers in the solar cells. In this chapter we also study the effect of changes in various parameters on the solar cell performance.

In order to verify our procedure to simulate the degradation in a-Si:H solar cells, we have performed light-soaking experiments under both open- and short-circuit condition. These results are presented in chapter 4. Here we will present the first performance and quantum efficiency simulations of a series of solar cells with varying thickness under both open and short-circuit conditions. We have opted for different circuit conditions in order to alter the recombination profile in the solar cells, as it is generally accepted that defect creation is linked to recombination events in the intrinsic layer.

In chapter 5 we present the results of degradation of a-Si:H solar cells by 1-MeV electrons. We will study the fluence and flux dependence, and compare the effect of short-circuiting the cells to open-circuit degradation. The latter two experiments are performed in order to find out if degradation by charged-particle irradiation is similar to the so-called Staebler-Wronski effect [12]. We then show the simulation procedure and results of the degradation by 1-MeV electrons; these are compared to experimental results. In addition, we extract the defect density versus the fluence, because it may provide further insight in the defect creation mechanism.

The kinetic energy and mass dependence of the incident particle on the a-Si:H solar cell degradation is investigated in chapter 6. Here, we will show results of a-Si:H solar cells irradiated using two high-energy proton beams: 1 MeV and 65 MeV. The results are compared to literature and to results of electron-beam irradiated cells. Using these comparisons we discuss various possible damage mechanisms for a-Si:H solar cell degradation by charged-particle irradiation.



## Chapter 2

# Degradation of solar cell material by high-energy electrons

### 2.1 Introduction

The performance of a-Si:H solar cells is determined by the electrical and optical properties of the material of each individual layer and the interface properties between the layers. In order to understand the performance degradation of a-Si:H solar cells following high-energy charged-particle irradiation the major degradation processes in each layer should be studied and quantified. It is generally accepted that the major degradation process in a-Si:H solar cells is due to increases in the defect density of the intrinsic layer [28–30], but changes in activation energy of the doped layers [31–33] may also play a significant role in the degradation. Not only a-Si:H degrades under irradiation, but other components in the cell as well. In particular we are interested in changes in the optical properties of the glass substrates, as these may seriously affect the solar-cell performance.

Already in 1979 it was reported by Voget-Grote et al. [34] that mainly dangling bonds and vacancy-type defects are created in a-Si:H following 1-MeV electron-beam irradiation. Schade et al. [35] concluded using photoluminescence measurements that the changes in a-Si:H following keV electron-beam irradiation not only occur on the surfaces but also in the bulk of the material. Kazanskii et al.

[36] reported on changes in photoconductivity and optical absorption spectra and related these to increases in dangling bond density. They observed a decrease in the photoconductivity by almost 3 orders of magnitude following a dose of 5000 J/cm<sup>2</sup>. In addition, it was found that the absorption of light with an energy below 1.5 eV was significantly increased, while the absorption was unchanged for light having a higher energy. The fluence dependency of increases in defect density has been studied by Gangopadhyay et al. [37], using space-charge-limited current measurements, and Schröder et al. [38], using electron spin resonance (ESR) spectroscopy. Both found a linear dependence of the defect density on the irradiation fluence. However, Diehl et al. [39] used a stretched exponential dependence of the induced defect density as a function of the fluence following irradiation with 40 keV electrons. This fluence dependency was chosen to include relaxation of defects at saturated defect density. Woodyard et al. [40] concluded that the degradation observed in the a-Si:H following irradiation could not be explained by only taking the displacement damage of the incident particles into account and suggested that ionizing events play a role in the degradation. Finally, Danesh et al. [41, 42] and Yelon et al. [43] indicated that the degradation of a-Si:H by electron-beam irradiation may be closely related to degradation by light soaking and may be described using the hydrogen-related models for light-induced degradation.

In this chapter we present quantitative data of changes in the electrical and optical properties following high-energy electron irradiation of a-Si:H based materials that are used in our solar cells. These data on the material properties are required in order to understand the degradation of irradiated solar cells. Later, we will correlate these observed changes in material properties to the degradation of solar cells by 1-MeV electron irradiation in chapter 5 with computer simulations using the method presented in chapter 3.

This chapter is organized as follows. In section 2.2 the changes in the electro-optical properties of intrinsic and n-doped a-Si:H layers, as well as p-doped a-SiC:H and glass substrates are presented. In the following section 2.3 time-resolved microwave conductivity (TRMC) measurements are shown, which were used to study changes in electron-hole pair recombination kinetics in intrinsic a-Si:H quantitatively and in-situ during the irradiation. This technique also allowed to monitor changes in the electron mobility. In order to interpret the results a model is proposed to extract the total defect density in the a-Si:H from the recombination kinetics. Finally, all results presented in this chapter are summarized and conclusions about the major degradation processes in the solar cell material

are drawn in section 2.4.

## 2.2 Degradation in optical and electrical properties of solar cell material.

Samples of intrinsic and n-doped a-Si:H , p-doped a-SiC:H, Corning 1737 glass and CMZ glass have been subjected to 1-MeV electron-beam irradiation. At this beam energy a uniform energy-deposition profile in the samples is expected, because the so-called continuous-slowing-down-approximation stopping range of 1-MeV electrons in silicon is  $5.4 \times 10^{-1} \text{ g/cm}^2$  [22]. Given a mass density of a-Si:H of  $2.1 \text{ g/cm}^3$  it is then estimated that the average path length of the incident electron is 0.26 cm. The electron flux was  $5 \times 10^{11} \text{ electrons/cm}^2\text{s}$  and a maximum fluence of  $2 \times 10^{16} \text{ electrons/cm}^2$  was used. Intrinsic a-Si:H layers have been characterized by measuring the photo- and dark conductivity, the activation energy of the dark conductivity, the optical bandgap and sub-bandgap absorption. The photoconductivity can be used as a measure for the defect density in the material, whereas the dark conductivity and the activation energy provide information on the Fermi-level position and thus indirectly on the energy distribution of the defects. Doped a-Si:H and a-SiC:H layers are only characterized by the activation energy. For glass only the changes in transmission are taken into account.

### 2.2.1 Optical properties of glass substrates

Two types of glass were used in the irradiation experiments in this thesis: Corning 1737 glass, which is used generally in the thin-film transistor (TFT) field, and radiation tolerant CMZ glass fabricated by Thales Space Technology. The latter is typically used as cover glass to protect crystalline Si and GaAs solar cells from low- to medium-energy charge-particle space radiation to enhance the lifetime of the solar cell. It is known that the light transmission of both glass types will be reduced after electron-beam irradiation [44]. This loss in transmission will lead to less light being coupled into the a-Si:H solar cells and thus lowering the electron-hole pair generation rate. Therefore, quantitative data are needed of the light transmission following electron-beam irradiation in order to simulate the electron-beam degradation of solar cells correctly. Both types of glass have only been used as substrate for the deposition of our a-Si:H cells and a-Si:H layers and not as a cover-glass to protect the solar cells from the irradiation.

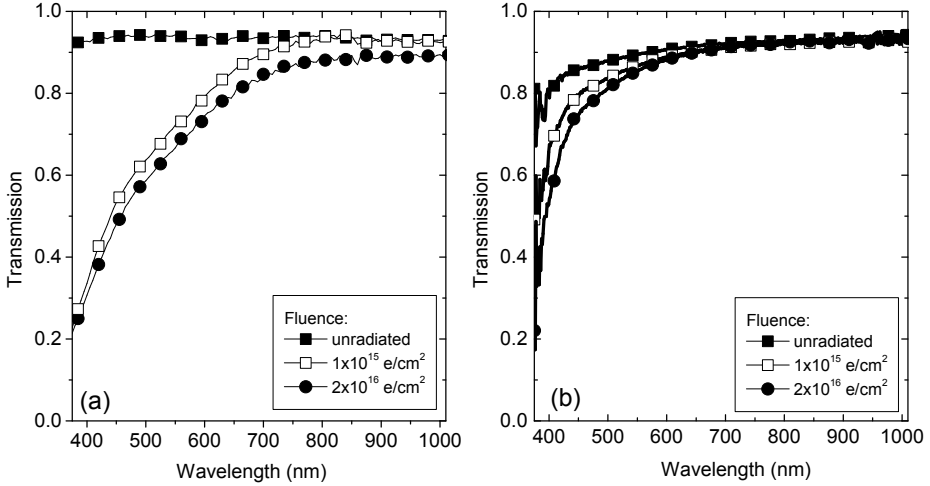


**Figure 2.1:** The transmission of (a) Corning 1737 glass and (B) CMZ glass before and after 1-MeV electron-beam irradiation with a fluence of  $1 \times 10^{15}$  and  $2 \times 10^{16}$  electrons/cm<sup>2</sup>.

Figure 2.1a shows the transmission of Corning 1737 glass after various irradiation fluences. The transmission of the glass is reduced considerably for wavelengths below 800 nm. Increasing the irradiation fluence does lead to additional loss of transmission, but large part of the reduction in transmission is already obtained at the lowest fluence of  $1 \times 10^{15}$  electrons/cm<sup>2</sup>. By convoluting the transmission spectra with the AM1.5 spectrum, we estimate that after electron-beam irradiation 23% of the incident photons with a wavelength between 300 nm and 750 nm is absorbed in the glass before entering the solar cells.

The transmission of CMZ glass after various irradiation fluences is plotted in figure 2.1b. The transmission before irradiation is lower than for Corning 1737 glass, especially at shorter wavelengths. This glass also shows reduction of transmission following irradiation, although this glass is more tolerant to radiation than Corning 1737. As can be seen in the figure, the transmission of this glass is reduced somewhat for wavelengths below 600 nm and also in this case most reduction is already obtained at the lowest fluence. We estimate that with CMZ glass following irradiation 12% of the incident light having a wavelength between 300 nm and 750 nm is absorbed in the glass. The results found here compare

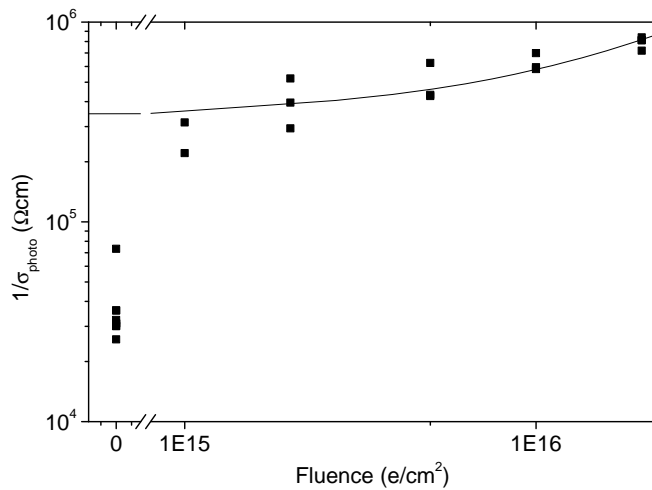


**Figure 2.2:** The inverse of the photoconductivity of intrinsic a-Si:H versus the irradiation fluence. The solid line represents a fit to the data using a linear dependence on the fluence.

well with the results obtained by Russel and Jones [44] who performed a large study on the degradation behavior of several coverglasses using various incident particles.

### 2.2.2 Electrical properties of intrinsic a-Si:H

In order to characterize the changes in electrical properties following irradiation, 500-nm thick a-Si:H layers have been deposited on CMZ glass and subjected to 1-MeV electron-beam irradiation. Before and after irradiation, the photo- and dark conductivity was measured along with the activation energy of the dark conductivity. Figure 2.2 presents the inverse of the photoconductivity (measured using AM1.5 illumination) versus irradiation fluence. A maximum fluence of  $2 \times 10^{16}$  electrons/cm<sup>2</sup> was used. At each fluence multiple samples were irradiated and the result of each separate sample is presented in figure 2.2. As discussed in the chapter 1, the inverse of the photoconductivity is proportional to the total defect density in the material. We clearly observe an increase of the inverse of the photoconductivity with the irradiation fluence, which implies an increase in the

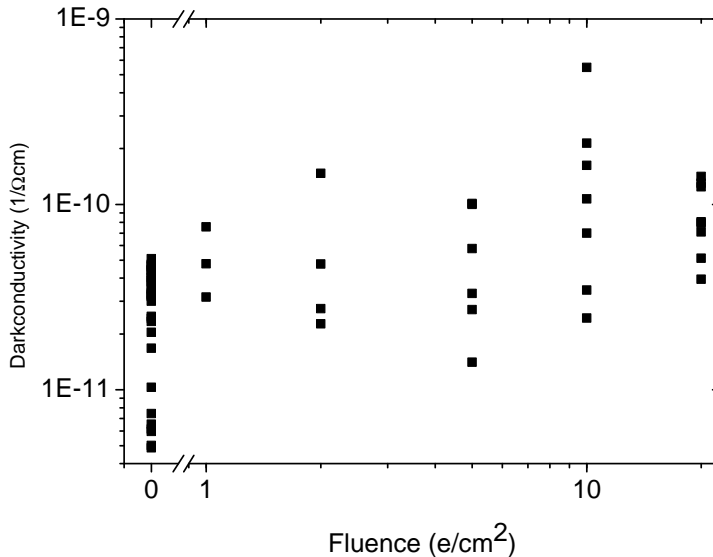


**Figure 2.3:** The dark conductivity of intrinsic a-Si:H versus the irradiation fluence.

defect density following electron-beam irradiation. The results shown in figure 2.2 suggest that the defect density in this material increases by approximately a factor of 30 during the irradiation and a factor of 3 to 4 between the highest and lowest fluence. However, it is difficult to extract the fluence dependence of the inverse of the photoconductivity, due to the large spread in the data for each fluence. A standard deviation up to 10% in photoconductivity has been found between samples irradiated with equal fluence. The results of the inverse of the photoconductivity can be reasonably well fitted to a  $\frac{1}{3}$  power dependence on the fluence, indicating similarities with the Staebler-Wronski effect where in steady-state light soaking degradation experiments the defect density follows a  $\frac{1}{3}$  power dependence on time. We should remark, however, that also an  $\frac{1}{2}$  power or even a linear dependence as presented by the line in figure 2.2 could be used to fit the results well. Note that the linear fit only has a mismatch for the as-deposited samples. In addition, it should be noted that the relation between the photoconductivity and the light-induced defect density is not unique [45, 46]. Von Roedern et al. [47] showed that the spin-density increase determined by ESR spectroscopy can be higher than expected from the observed decay in photoconductivity following light soaking.

The dark conductivity exhibits an overall increase of approximately one order of magnitude following irradiation as is seen in figure 2.3. Generally, an increase in dark conductivity suggests either an increase in electron or hole mobility, a change in the defect-density distribution in the band-gap, or more thermal generation of charge carriers [48]. The latter reason is because of an increase in defect state density, which may act as donor or acceptor states for thermally-activated transitions. The results from the photoconductivity and from TRMC presented in section 2.3 indicate that the irradiation increases the defect density but no effect on the electron mobility is found. However, in activation energy measurements on these layers a small shift of less than 0.1 eV was found, indicating a shift in Fermi-level and a change in the defect state energy distribution. Thus we assume that the increase in dark conductivity in this experiment is due to an increase in the defect density accompanied by a change in defect density energy distribution.

A typical method to determine the quality of the a-Si:H material for use as intrinsic layer in a solar cell is to calculate the so-called photo-response, defined as the ratio between the photo- and dark conductivity [49]. If the photo-response is above  $10^5$  the material is considered to be solar grade [50]. Both effects, the increase in dark conductivity and the decrease in photoconductivity, reduce this photo-response and following electron-beam irradiation using the highest fluence it is only 100. The low photo-response after irradiation already indicates that the solar cells with this intrinsic a-Si:H layer will show a large degradation as will be found in chapter 5.

### 2.2.3 Optical properties of intrinsic a-Si:H

To investigate changes in the light absorption profile, the optical absorption spectra of a-Si:H layers following electron-beam irradiation are studied by reflection-transmission measurements. In addition, sub-bandgap absorption, related to the defect density of a-Si:H was measured using dual-beam photoconductivity (DBP). The optical absorption spectra of a-Si:H following electron-beam irradiation are shown in figure 2.4. The absorption curve for light having an energy above 1.5 eV appears to be shifted slightly towards lower photon energies, although the curve shape is not altered by the irradiation. Similar to Kazanskii et al. [36], for energies below 1.5 eV the absorption is increased considerably and is dependent on the fluence. This experiment was also performed on a-Si:H layers deposited on CMZ cover glass and here no shift for the absorption curve was found in agree-

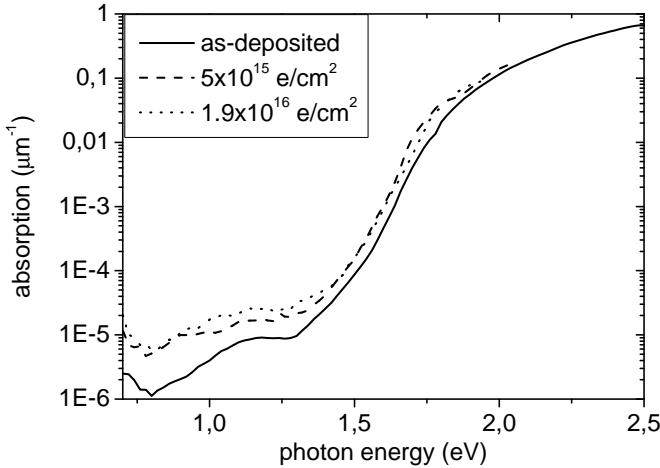


**Figure 2.4:** (Sub-bandgap) Optical absorption spectra of a-Si:H following electron irradiation

ment with the results obtained by Kazanskii et al. [36] and Danesh et al. [41], although a possible difference in material properties of a-Si:H grown on CMZ as compared to Corning 1737 may be noted in these measurements. The difference between the absorption curves of the as-deposited and the irradiated samples in figure 2.4 for energies above 1.5 eV may therefore be attributed to transmission loss of the Corning substrates. Thus, we conclude that no significant changes of the band gap were observed after electron-beam irradiation. In addition, we do not observe a significant change in the Urbach energy,  $E_u$ , as a result of electron irradiation, indicating that no changes in the valence-band tail were induced.

There is a substantial increase in sub-band gap absorption, which is correlated to defect-state absorption [25]. Using equation 1.8 we estimate that the defect density increases from  $4.4 \times 10^{14}$  to  $1.2 \times 10^{15} \text{ cm}^{-3}$ . The rest of the absorption curve is unaffected by the irradiation, suggesting that only that part of the curve correlated to the defect density is altered. The results also suggest that the concentration of weak bonds (WB) is not affected significantly as the concentration of WBs is linked to the valence-band tail and Urbach energy [51]. The conclusion that first the defect density is altered before the valence band tail or the band gap change has also been observed in Continuous Random Network

(CRN) theoretical models of the density-of-states distribution in degraded a-Si:H [52]. They reported that the introduction of different types of defects causes no strong changes in the principal structure of the conduction and the valence band, but only leads to states in the band gap.

A similar effect has been observed in 17-MeV proton irradiated a-Si:H where the band structure did not show a significant change up to  $1.7 \times 10^{14}$  protons/cm<sup>2</sup> [53]. Using the ionizing dose as reference, this proton fluence may be equivalent to an 1-MeV electron beam fluence of  $2.5 \times 10^{15}$  electrons/cm<sup>2</sup> [28]. This fluence is comparable to the fluence range used in our irradiation experiments, indicating that their results with proton irradiation may be extrapolated to our case.

### 2.2.4 Activation energy of doped a-Si:H

Individual n-doped and p-doped layers as used in a-Si:H solar cells were irradiated to study the effects of irradiation on the activation energy. For these films the same deposition parameters were used as for the doped layers in the solar cells, however, the thickness was increased to 500 nm.

The conductivity of the doped layers is much higher than that of the intrinsic layer due to the doping of the layers. Because in a solar cell these layers are thin compared to the intrinsic layer, changes in the resistivity of the doped layers will not have a significant influence on the solar-cell performance. More important for the solar-cell performance is the activation energy of the doped layers, which is a good indication of the location of the Fermi level in the bandgap in that layer and related to that the active doping concentration. The Fermi-level position in the p- and n-layer determines to a large extent the built-in voltage of the p-i-n diode or solar cell, which is in turn linked to open-circuit voltage. In case of an ideal i-layer in the solar cell, the open-circuit voltage is just the difference between the Fermi-levels of the n- and p-layer [54]. The activation energy of dark conductivity of the doped layers was determined from the slope of the dark conductivity between 60 °C to 90 °C in an Arrhenius plot. This small temperature range was chosen in order to prevent significant annealing of the irradiated samples, although annealing effects were observed during the measurements.

Figure 2.5 shows the activation energy of the n- and p-doped layers following electron-beam irradiation. In case of the n-doped layer, the activation energy represents the energy difference between the Fermi-level and the bottom of the conduction band, whereas for the p-doped material this is difference between

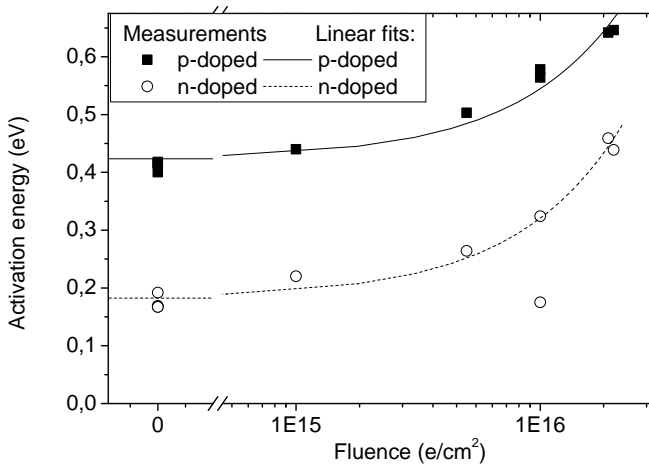


**Figure 2.5:** The activation energy of p-doped a-SiC:H (closed squares) and n-doped a-Si:H (open circles) as a function of the electron-beam irradiation fluence. The lines are linear fits to the data.

the Fermi-level and the top of the valence band. Overall we see an increase in the activation energy. After the highest fluence the activation energy of the n- and p-layer increased by 0.25 eV and 0.2 eV, respectively. These observations indicate that the Fermi level for both layers shifts toward midgap. The activation energy seems to vary linearly with the irradiation fluence. Similar increases in the activation energy of doped a-Si:H and was observed by Neitzert et al. following 1.7 MeV proton beam irradiation [33] or by Babras et al. [31] and Scholz et al. [32] with keV electron irradiation. In addition, Scholz et al. [32] suggested that this increase in activation energy is related to an increase in the dangling bond concentration and heavier doping will lessen the degradation of the doped layers.

## 2.3 Time-resolved microwave-conductivity spectroscopy

### 2.3.1 Introducing TRMC

With the measurement techniques used so far the effect of electron-beam irradiation on recombination processes in a-Si:H could not or only indirectly be investigated. In addition, the measurement techniques need electrical contacts on the a-Si:H and the analysis is performed ex-situ of the electron accelerator. Time-Resolved Microwave Conductivity (TRMC) is a valuable addition to the techniques discussed so far to study degradation by electron-beam irradiation of a-Si:H, because it measures directly changes in conductivity of a-Si:H in-situ and without the use of contacts. In addition, the electron mobility in a-Si:H may be monitored during the irradiation. With TRMC the change in the electrical conductivity of material is monitored as a function of time by measuring the change in microwave absorption following a probe-beam pulse [55] to generate excess charge carriers in the material. Typically either a laser or a high-energy electron pulse is used. In our case a high-energy electron pulse is favorable because this provides a uniform electron-hole (e-h) generation rate across the whole layer, and this probe beam can be utilized for the degradation of the samples as well. The induced conductivity change of the material is proportional to the product of the density of the excess charge carriers generated by the probe-beam pulse and their respective mobilities.

The degradation of a-Si:H is performed with the same electron beam as used for the probe-beam pulse, in this case a 3-MeV electron-beam will be used. Compared to 1-MeV electrons, the Constant-Stopping-Derivation-Approach (CSDA) stopping range is now a little higher, while the ionizing energy deposition rate is lower. However, 3-MeV electrons may transfer more energy to an Si-atom during a direct collision and the chance of a displacement event is increased.

In section 2.3.2 we will first briefly describe the TRMC technique and setup in more detail. Then we show in section 2.3.3 the computer model used to obtain the defect density of states from a given TRMC transient. Finally, we present the results derived from the TRMC measurements on as-deposited and electron-irradiated a-Si:H layers (section 2.3.4). Our aim is to find a relationship between the irradiation fluence and the defect density in the material.

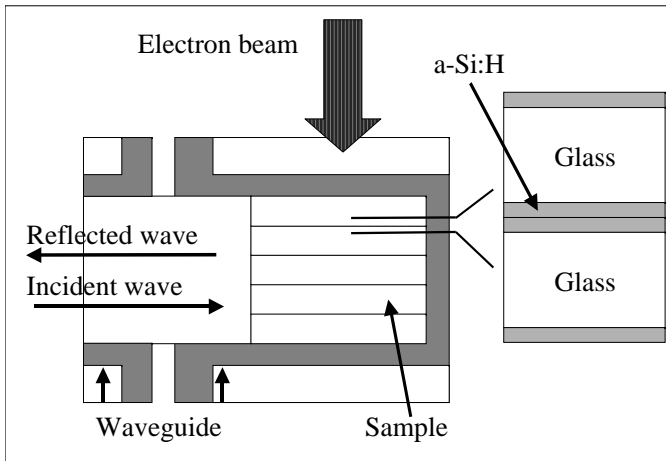


**Figure 2.6:** Principle of the set-up with the microwave cell containing amorphous silicon films deposited on glass.

### 2.3.2 Experimental details

TRMC measurements were carried out on a-Si:H layers deposited on Corning 1737 glass. 700-nm thick layers were deposited on both sides of the glass to increase the amount of material for the TRMC measurements. Five of these a-Si:H-on-glass samples were then stacked inside a cell which carries the  $K_a$ -band (Kurtz-above band, 26.5-42 GHz); the internal dimensions of the waveguide are 3.55 mm  $\times$  7.11 mm.

In the following we will refer to the electron beam for TRMC measurements as the ‘probe beam’. On the other hand, when the electron beam is used for sample irradiation (i.e., for degradation) we will refer to this process as ‘electron irradiation’. In both cases a 3-MeV Van de Graaff accelerator generates the electron beam.

The principle of TRMC is shown in figure 2.6. Excess e-h pairs in the material are generated by a short ( $< 10$  ns) electron-beam probe pulse. During and after the pulse the decay of the conductivity change is monitored by measuring the change in microwave reflection as a function of time. The probe-beam dose used was varied between 4 and 40 nC. The energy dissipated in the material,  $E_{dis}$ , was

measured to be  $2100 \text{ J nC}^{-1} \text{ m}^{-3}$  [56]. Given the formation energy of e-h pairs by high-energy electrons,  $E_{e-h \text{ form}}$ , of 5.1 eV [57], the e-h pair density,  $n$ , generated by a given pulse dose can be calculated. Here, the formation energy is defined as the average amount of energy the electron beam loses per e-h pair generated. From the change in conductivity,  $\Delta\sigma$ , shortly after the probe pulse, the mobility of the dominant charge carrier,  $\mu$ , can be obtained, if the recombination of the charge carriers during the probe pulse is ignored:

$$\Delta\sigma = q\mu n. \quad (2.1)$$

The changes in conductivity due to this probe-beam pulse were obtained by measuring the change in microwave radiation absorption. The full apparatus to measure the changes in the absorbed power has been extensively described by Infelta et al. [58]. This absorbed microwave power can be correlated to a change in the conductivity with the method as described by Warman et al. [55].

The samples were analyzed as-deposited and after six different electron-beam irradiation fluences steps. The samples were irradiated in-situ, with 80-nC, 20-ns pulses. To reach the final fluence the material was subjected to 32000 80-nC pulses, far more than used to analyze the material using TRMC. This radiation dose of 32000 80-nC pulses is equivalent to a fluence of approximately  $1 \times 10^{16}$  electrons/cm<sup>2</sup>. After each irradiation step, the samples were analyzed with four different probe-pulse doses,  $Q$ ; 4.3, 7.3, 20, and 40 nC, each with a different probe-pulse lengths,  $\tau$ , of 1, 2, 5 and 10 ns, respectively. For each probe-pulse dose two transients were measured: one where the change in conductivity is sampled every 0.8 ns over a time window of 180 ns, and one that samples every 4 ns over a time window of 900 ns. Afterwards these two transients were appended to each other, ignoring the first 180 ns of the 900-ns transient.

It was found that not only the a-Si:H contributes to the TRMC transients, but that the glass gives a relatively small signal as well. To correct for this effect, TRMC transients were also measured for uncoated glass samples. The glass signal is later subtracted from the measured transients of the glass/a-Si:H stack and then only the signal from a-Si:H remains.

### 2.3.3 Model description

To obtain the defect density-of-states from a measured TRMC transient a model was developed based on the continuity equations in which only generation and

recombination terms are included. Two types of recombination processes are considered: bi-molecular recombination and Shockley-Read-Hall (SRH) recombination [59]. With bi-molecular recombination, an electron in the conduction band will recombine directly with a hole in the valence band and this process has a capture-cross section  $\sigma_{bm}$ , while with SRH the recombination is facilitated by defect states in the mobility gap. With SRH recombination capture and emission processes are considered between localized states in the mobility gap and the extended states. The extended states are described as a single state with an effective density of states. The continuity equations for the changes in the density of excess electrons,  $n$ , and excess holes,  $p$ , in the extended states as a function of time,  $t$ , during the transient are then given by:

$$\frac{dn}{dt} = g(t) - \sigma_{bm} \cdot n \cdot p - \sum_E r_n(E, t) \quad (2.2)$$

and

$$\frac{dp}{dt} = g(t) - \sigma_{bm} \cdot n \cdot p - \sum_E r_p(E, t), \quad (2.3)$$

where  $g(t)$  is the charge-carrier generation rate (only during the probe-beam pulse),  $r_n$  is the net electron capture and emission rate and  $r_p$  the net hole capture and emission rate for a trap of given energy level,  $E$ , in the mobility gap. The e-h pair generation rate is calculated as described in subsection 2.3.2, and is given by:

$$g(t) = \frac{Q}{\tau} \frac{E_{dis}}{E_{e-h \text{ form}}} \text{ if } t < \tau. \quad (2.4)$$

The individual emission and capture equations for both electrons and holes processes are given in table 2.1, where  $v_{th}$  is the thermal velocity,  $\sigma_n$  ( $\sigma_p$ ) the capture cross section for electrons (holes), and  $f(E)$  the occupation function, which determines the ratio between the electron and hole density at a given energy level in the DOS. The change in occupation function,  $\Delta f(E)$ , and the net hole and electron capture and emission functions are given by:

$$r_n = r_1 - r_2 \quad (2.5)$$

$$r_p = r_3 - r_4 \quad (2.6)$$

$$\Delta f(E) = \frac{r_1 - r_2 - (r_3 - r_4)}{DOS} \quad (2.7)$$

The distribution and density of energy states in the mobility gap of a-Si:H is described with a basic density-of-states model [50]. We assume that the conduction-

**Table 2.1:** Rate equations for the trapping and emission processes for traps.

Process		Rate function
Electron capture	$r_1$	$n \cdot v_{th} \cdot \sigma_n \cdot DOS \cdot (1 - f)$
Electron emission	$r_2$	$v_{th} \cdot DOS \cdot f \cdot \sigma_n \cdot N_c \cdot \exp(\frac{E - E_c}{kT})$
Hole capture	$r_3$	$p \cdot v_{th} \cdot \sigma_p \cdot DOS \cdot f$
Hole emission	$r_4$	$v_{th} \cdot DOS \cdot f \cdot \sigma_p \cdot N_v \cdot \exp(\frac{E_v - E}{kT})$

and valence-band-tail states vary exponentially with energy. The conduction-band tail is defined by its density-of-states at the mobility edge,  $N_{0c}$ , and the characteristic energy,  $E_{cc}$ , which defines the exponential slope of the band. Further, we define the hole-,  $\sigma_{pc}$ , and electron-capture-cross section,  $\sigma_{nc}$  for the conduction-band-tail states. Similarly,  $N_{0v}$ ,  $E_{cv}$ ,  $\sigma_{pv}$ , and  $\sigma_{nv}$  are defined for the valence-band tail. Finally, the defect density-of-states in the gap,  $N_d$ , having a hole-,  $\sigma_{pd}$ , and an electron-capture-cross section,  $\sigma_{nd}$  are assumed to be uniformly distributed throughout the mobility gap as observed for as-deposited a-Si:H. Although it is expected that the defect density of states distribution will become non-uniform following degradation, this effect is not included in the simulations.

At the start of the simulation it is assumed that the material is in thermal equilibrium: there are no excess charge carriers. The intrinsic carrier concentration is neglected, because this concentration is orders of magnitude lower than the induced excess carrier concentration during the measurement. Further, the occupation function for the density of states in the mobility gap is given by the Fermi-Dirac occupation function, where the temperature is chosen to be 300 K.

### 2.3.4 Results and discussion

Figure 2.7 shows measured TRMC transients of as-deposited a-Si:H for different probe-beam pulses. The time is measured with respect to the start of the probe-beam pulse. As expected, a higher maximum conductivity change is observed for higher probe-beam pulses and the conductivity is sustained for longer. Also included in figure 2.7 are the corresponding simulations of the transients for as-deposited a-Si:H for the four probe-beam doses used. The parameters used to obtain these transients are given in Table 2.2. Only the probe-beam dose and length were changed for these simulations. A good match between the measured and the simulated transients is obtained over the investigated time range for all the

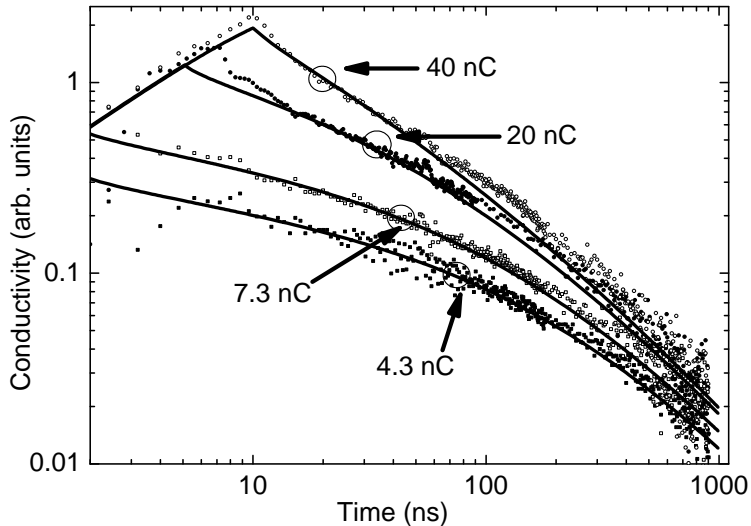


**Figure 2.7:** Measured TRMC transients (markers) of as-deposited a-Si:H for various probe-beam doses with the corresponding simulation (lines) for each beam dose used.

probe-beam doses used. However, some small discrepancies can be seen, mostly during the probe-beam pulse and at the end of the transient. We believe that these discrepancies can be attributed to the glass, i.e., the glass signal was not properly subtracted from the transient.

With the simulations a better understanding of the processes during the transient can be acquired. Figure 2.8 shows the time evolution of major charge-carrier trapping, emission and recombination processes during the measurement. During the probe-beam pulse excess e-h pairs are generated. The simulations reveal that most holes are then either trapped in the valence-band tails, or recombine with an electron via a defect (SRH recombination). As a result the density of free excess holes is low, compared to the density of free excess electrons. After the probe-beam pulse, the trapped holes are slowly re-emitted into the valence band. Once in the valence band, the holes can contribute again to the SRH recombination. In the simulations at longer times the hole-emission decay rate is nearly equal to the SRH-recombination rate. Therefore it may be concluded that this hole-emission process is the driving force of the e-h recombination rate after the probe-beam pulse. Simulations (not shown here) showed that in case holes were not trapped, the excess charge carrier decay would be much faster. Bi-molecular recombination

**Table 2.2:** Parameters used in computer simulations to describe as-deposited a-Si:H

Valence band tail states		Conduction band tail states	
$N_{0v}$	$5 \times 10^{27} \text{ eV}^{-1} \text{ m}^{-3}$	$N_{0c}$	$5 \times 10^{27} \text{ eV}^{-1} \text{ m}^{-3}$
$E_{cv}$	43 meV	$E_{cc}$	30 meV
$\sigma_{nv}$	$1 \times 10^{-21} \text{ m}^{-2}$	$\sigma_{nc}$	$1 \times 10^{-21} \text{ m}^{-2}$
$\sigma_{pv}$	$1 \times 10^{-21} \text{ m}^{-2}$	$\sigma_{pc}$	$1 \times 10^{-21} \text{ m}^{-2}$
Defect states		Extended states	
$N_d$	$3.5 \times 10^{21} \text{ eV}^{-1} \text{ m}^{-3}$	$N_v$	$2.0 \times 10^{20} \text{ m}^{-3}$
		$N_c$	$1.5 \times 10^{20} \text{ m}^{-3}$
$\sigma_{nd}$	$1.5 \times 10^{-19} \text{ m}^{-2}$	$\mu_n$	$2.4 \text{ cm}^2 \text{ V}^{-1} \text{ s}^{-1}$
$\sigma_{pd}$	$1.5 \times 10^{-19} \text{ m}^{-2}$	$\mu_p$	$0.5 \text{ cm}^2 \text{ V}^{-1} \text{ s}^{-1}$

is only significant for the higher probe beam doses, and only during and shortly after the probe-beam pulse, because the hole concentration in the valence band is then highest. SRH recombination can be seen throughout the whole transient.

Figure 2.9 shows transients obtained with the 20-nC probe-beam pulse for various irradiation fluences. The observed maximum peak height is within 15% the same as for the as-deposited sample, suggesting that the electron mobility and the e-h generation are not significantly altered by the irradiation. The excess-carrier-decay rate, however, is increased following the irradiation, indicating an increase in recombination rate in the a-Si:H. It should be noted that after degradation the noise disturbs the measurements sooner, because the signal drops faster. Therefore a smaller part of the transients can be used to study the material. The transients obtained with the other probe-beam pulse doses show similar trends, although the signal-to-noise ratio is lower because of the lower signals. Also shown in figure 2.9 are the corresponding simulated transients. We found that we can obtain good fits for all irradiation doses and all probe-beam pulse doses by adjusting only the defect density-of-states in the mobility gap. The defect density-of-states varies between  $3.5 \times 10^{21} \text{ eV}^{-1} \text{ m}^{-3}$  as-deposited and  $2.5 \times 10^{22} \text{ eV}^{-1} \text{ m}^{-3}$  after 32000 80-nC irradiation pulses.

Figure 2.10 shows the defect density-of-states used in the simulations as a function of the irradiation fluences. We note that the defect density seems to have a  $F^{1/2}$  dependence, similar to time dependence of light-soaking experiments using a pulsed laser [60]. This observation suggests that the initiation of defect creation in high-energy electron-irradiated a-Si:H is similar to that in light-soaked

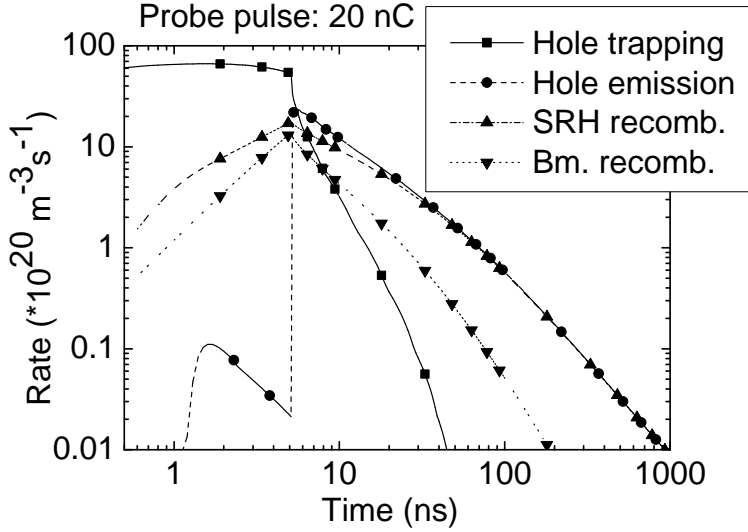


**Figure 2.8:** The rate of major charge-carrier trapping, emission and recombination processes as a function of time during the TRMC measurement as obtained from computer simulations.

a-Si:H, which was also suggested by Danesh et al. [41]. The fluence dependence reported here is different from the results obtained by Schneider et al. with low-energy electron-beam irradiation of a-Si:H who found a linear dependence of the defect density on the fluence [61]. In addition, in chapter 5 also a linear dependence of the defect density on the fluence is found for high-energy electron-beam irradiation. However, in our TRMC measurements during the probe pulse the e-h pair generation rate is very high as compared to other electron-beam irradiation experiments:  $1 \times 10^{31} \text{ m}^{-3} \text{ s}^{-1}$ . Similarly, the e-h pair generation rate here is also a few orders of magnitude higher than under light-soaking conditions using 1 sun. Because of this high generation rate and subsequently high recombination rate, it is not unlikely that when using 80-nC, 20-ns pulses to irradiate a-Si:H the degradation is dominated by defect-creation processes linked to recombination events, similar to light soaking.

Finally, the samples were annealed in-situ at 150°C for 30 minutes. After annealing, the transients were found to be identical to those prior to irradiation. It was concluded that the material fully recovered by the anneal step.

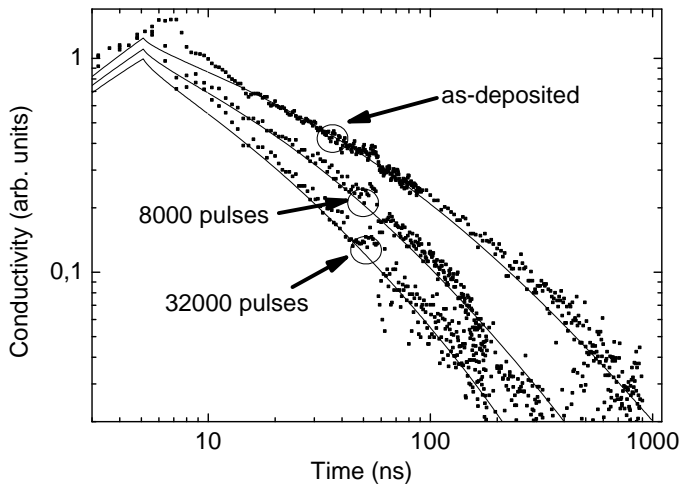


**Figure 2.9:** Measured TRMC transients (markers) obtained with a 20-nC probe-beam pulse for various accumulated radiation fluences with their corresponding simulations (lines).

## 2.4 Conclusions

Intrinsic, n- and p-doped a-Si:H, and CMZ glass samples have been subjected to 1-MeV electron beam irradiation in order to study the changes in opto-electronic material properties qualitatively and quantitatively. This information is used to build the model as presented in chapter 3 to simulate the degradation of a-Si:H solar cells due to high-energy charged-particle irradiation.

Both investigated glass types exhibit reduction of the transmission following irradiation, which, as we will show later, will lead primarily to a change in the  $J_{sc}$  of degraded solar cells. As expected, CMZ glass shows better radiation tolerance than Corning 1737, although the initial absorption in the CMZ glass is higher at shorter wavelengths. For intrinsic a-Si:H the dark-, photoconductivity and the sub-bandgap absorption results suggest an increase in defect density of more than an order of magnitude following irradiation using a fluence of  $2 \times 10^{16}$  electrons/cm<sup>2</sup>. This increase in defect density indicates that electron-beam irradiation will likely lead to a decrease in solar cell performance, especially in the  $J_{sc}$  and  $FF$ . The dark-conductivity activation energy of the p- and n-doped layers is

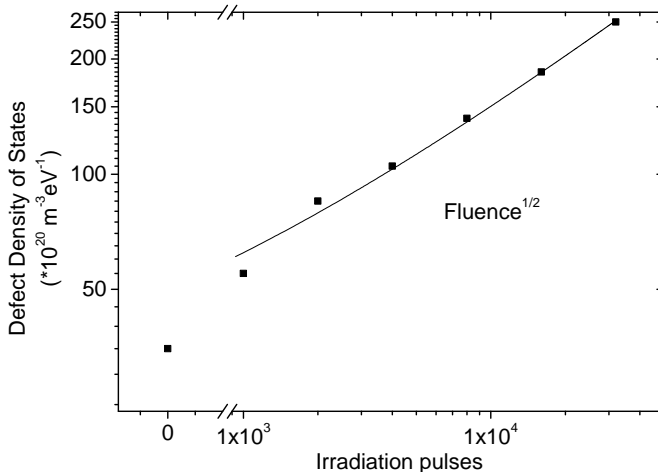


**Figure 2.10:** The defect density obtained from the simulations of the measured TRMC transients as a function of the irradiation fluence.

increased following irradiation, which we think is due to a lowering of the effective doping efficiency. It is expected that this decrease in activation energy will lower the  $V_{oc}$  of a-Si:H solar cells following irradiation. The RT and DBP data show that the bandgap and Urbach energy remain constant during irradiation, and no changes in the optical models are needed to simulate the degradation of a-Si:H solar cells.

The increase in defect density in intrinsic a-Si:H has been studied more extensively using TRMC analysis. It was found that the defect density increase approximately an order of magnitude after  $1 \times 10^{16}$  electrons/cm<sup>2</sup>. The fluence dependence of the defect density obtained from the TRMC measurements suggests that e-h pair recombination initiates the defect creation in electron-beam irradiated a-Si:H. We will show in chapter 5 that no such correlation between the defect density and the recombination rate is found in the degradation of a-Si:H solar cells. This discrepancy may be explained by the very high electron-hole pair generation rate during the irradiation in the TRMC experiments, which is more than an order higher than the generation rate under 1-sun illumination. Finally, the TRMC results showed that the electron mobility is not influenced by the irradiation.

## Chapter 3

# Computer modeling of degraded amorphous silicon solar cells

### 3.1 Introduction

During degradation of a-Si:H solar cells some material properties of the cell are altered. In chapter 2 major components in the degradation of a-Si:H solar cells following electron irradiation have been identified: a change in the defect density of intrinsic a-Si:H, an increase of the activation energy of the doped layers, and finally an increase in the absorption of the glass substrates. Degradation by light-soaking and current injection is ascribed largely to changes in the defect density of states. However, it is difficult to assess quantitatively how each degradation component affects the solar-cell performance.

Computer simulations is a valuable aid to study the degradation of a-Si:H solar cells quantitatively based on changes in the material properties. In this chapter we introduce a procedure with which we can simulate the performance degradation of a-Si:H solar cells by high-energy electron and proton beam as well as by light-soaking. With this procedure a model may be constructed to predict the End-Of-Life (EOL) efficiency of a-Si:H solar cells for a particular space mission, based on changes in material properties. In future development computer modeling might be useful in the optimization of solar cells for a particular mission.

In addition, with these computer simulations further insight is obtained in the processes involved in the degradation. In particular, we focus on the correlation of the degradation with changes in the internal electric field and recombination rate density.

Computer simulations have already been utilized to study the degradation of a-Si:H layers and solar cells by light-soaking, current-injection, and charged-particle irradiation. Meytin et al. [62] performed computer simulations of the dark- and photoconductivity to study the energy position of light-induced defects in the band gap. They concluded that the dark-conductivity degradation was mainly determined by the shift in peak position of the positively-charged/neutral defect-state peak of the defect density of states (DDOS) and the photoconductivity by the total defect density. Caputo et al. [63] presented simulation results of the performance of light-soaked solar cells and investigated the influence of the laser wavelength on the degradation. They demonstrated that the performance degradation could be reproduced by increasing the defect density in the intrinsic layer and this increase was profiled using the spatial distribution of the electron and hole densities. Caputo et al. [64] also applied their model to simulate the degradation by current injection arriving at similar conclusions. Dutta et al. [65] showed simulations of the degradation of a-Si:H solar cells by current injection. In their results they noted that the increase in defect density due to current injection seems to be correlated to the recombination rate during the degradation, although this correlation was not studied in more detail. Lord et al. [66] presented simulations of a-Si:H solar cells irradiated with 40-keV electrons to extract the defect-density changes. They matched experimental results of the dark  $J$ - $V$  curve following two irradiation fluences with simulations and only assumed changes in defect density. Here, an increase in defect density of a factor 200 was found following the highest fluence of  $1 \times 10^{17}$  electrons/cm<sup>2</sup>.

In this chapter we will first introduce briefly the device simulator *Advanced Semiconductor Analysis* (ASA) in section 3.2, which we have used for the simulation of the solar-cell performance. We will then present in section 3.3 our procedure to describe the changes in material properties of the individual layers. These changes are either based on experimental results on a-Si:H following high-energy particle irradiation or on the recombination characteristics of solar cells. We will explain our procedure to simulate the degradation of a-Si:H solar cells by using these changed material properties as input for the device simulator ASA to calculate the degraded performance of the solar cells. Furthermore, a sensitivity

study of this procedure will be presented. For this study we will first investigate in section 3.4.2 the effect of an increase in activation energy of the doped layers and increases in the defect density on the solar-cell performance. Later, in section 3.4.3 the influence of the depth profile of the induced defect states on the degradation is evaluated together with the energy location of the induced states. Finally, in section 3.6 the main conclusions of this chapter are drawn.

## 3.2 The ASA device simulator

The procedure presented in section 3.3 to calculate the EOL performance of solar cells subjected to electrons, protons or light soaking is built around the device simulator ASA, which has been developed at the Delft University of Technology [67]. This program is a two-terminal, steady-state device simulator in which various models for describing the a-Si:H defect density of states (DDOS) are included and in which appropriate recombination-generation statistics are used. It is based on the adapted drift-diffusion model and solves the Poisson equation together with the continuity equations for electrons and holes. For a detailed description of ASA and the models that are included we refer to Ref. [68]. In this section we will briefly describe the most important features.

In ASA the free electron,  $n$ , and hole concentration,  $p$ , as well as the electrostatic potential,  $\Psi$ , are taken as independent variables. For steady-state conditions the Poisson and continuity equations reduce to:

$$\nabla \cdot (\epsilon \nabla \Psi) = -\rho \quad (3.1)$$

$$\frac{\partial n}{\partial t} = \frac{1}{q} \nabla \cdot \vec{J}_n + G - R = 0 \quad (3.2)$$

$$\frac{\partial p}{\partial t} = -\frac{1}{q} \nabla \cdot \vec{J}_p + G - R = 0, \quad (3.3)$$

where  $G$  is the generation rate,  $R$  the recombination rate,  $\epsilon$  the dielectrical constant,  $\rho$  the space-charge density,  $q$  the elementary charge,  $\vec{J}$  the current density, and  $t$  the time. The generation rate is obtained from the optical simulations of the solar cells and is discussed in more detail in the section 3.2.2, while the recombination rate is discussed in 3.2.1. The  $\nabla \cdot \vec{J}_n$  and  $\nabla \cdot \vec{J}_p$  terms include the diffusion and drift terms of the free charge carriers and are dependent on  $n$ ,  $p$ , and  $\Psi$ . Finally,  $\rho$  is the net charge density at a given location in the cell and is

determined by the free charge in the conduction and valence band, trapped charge in the mobility gap, and the donor and acceptor ions in the a-Si:H.

From this set of equations and the relevant electrical and optical properties of all layers in the cell, ASA is able to simulate solar-cell characteristics. In this thesis we use ASA particularly to calculate the external parameters of the solar cells and the quantum efficiency (QE). This computer program has been successfully applied to study several types of solar cells: a-Si:H [69], a-SiGe:H [70, 71], a-Si:H/a-SiGe:H tandem cells [67], transverse-junction [72, 73], and microcrystalline silicon [74] cells. In addition, it was utilized to investigate light-degraded a-Si:H [62] and a-Si:H solar cells [75].

#### 3.2.1 Recombination statistics

Defect states in the mobility gap may act as trapping and recombination centers, reducing the performance of the solar cell. To calculate the recombination and trapping rates in the solar cell, the density of states (DOS) must be provided. In this work, the DOS in as-deposited a-Si:H solar cells is modeled in the following way: The valence and conduction bands are described using the effective state density approach [50]. We assume that the valence- and conduction-band tails vary exponentially with energy in the band gap. In order to calculate the as-deposited defect density-of-states (DDOS) profile in the solar cell we have used the defect-pool model [76]. In this model the DDOS energy distribution is dependent on the local weak-bond density and the location of the Fermi-level in the band gap. The defect states in a-Si:H, which are related to dangling bonds in the material, have a so-called amphoteric character, meaning that the defects can show simultaneously a donor-like and acceptor-like behavior. For this reason we identify three defect states:  $D_h$  defect states (positively-charged defects) near the conduction band tail,  $D_z$  defect states (neutral defects) in the middle of the bandgap, and  $D_e$  defect states (negatively-charged defects) near the valence band tail.

As defect states in a-Si:H are amphoteric, the recombination rate,  $R$ , is calculated using the model of Sah and Shockley [68, 77]. In this model  $R$  scales with the  $np$ -product and increases when more electron-hole pairs are generated in the a-Si:H solar cells. Thus the rate of recombination events involving defect states is strongly linked to the local generation rate and the internal electric field. The recombination rate is mainly determined by defect states in between the quasi-

Fermi levels, implying that defect states in the middle of the band gap contribute most to the recombination rate.

#### 3.2.2 Optical simulations

In a-Si:H solar cells the charge-carrier generation rate at a specific location,  $G$ , is directly related to the generation-rate profile, which in turn is calculated using the light absorption of all layers in the solar cell. Here, it is assumed that every absorption event in a-Si:H leads to the creation of an excess electron-hole pair. In the a-Si:H solar cells used in this work both interference and light-scattering effects play a role in the optical absorption. Interference effects lead to the sequential constructive and de-constructive interference peaks in the QE (see for example figure 4.1 in chapter 4), whereas light-scattering at interfaces between the layers results in an increase in optical path length of the light traveling through the solar cell, increasing the absorption.

The absorption profile and consequently the generation rate is calculated using the *Genpro3* routine in ASA. This routine includes both coherent and incoherent models to simulate interference and light-scattering events, respectively. In the coherent model only the complex refractive index and thickness of each layer in the solar cell are needed as input parameters [78, 79]. In order to include the effect of light-scattering on rough interfaces, at each interface haze values and angular distribution functions (ADF) may be defined. The haze value defines the fraction of light which is transmitted (or reflected) incoherently at the interface and the ADF defines what fraction of the light is scattered at a specific angle [80, 81].

### 3.3 Procedure to simulate degraded solar-cell performance

The flowchart of our procedure to simulate the degradation of a-Si:H solar cells is presented in figure 3.1. From the as-deposited parameter set the performance of the as-deposited solar cells is calculated using ASA. In order to obtain the parameter set related to the degraded state of the solar cell, the changes in the parameter set between the as-deposited and degraded state are determined. These changes may be linked to the internal parameters of the solar cells as calculated by ASA, like the recombination rate, or the effect of external influences, like high-energy particle irradiation. Finally, using the adjusted parameter set ASA

### 3. Computer modeling of degraded amorphous silicon solar cells

---

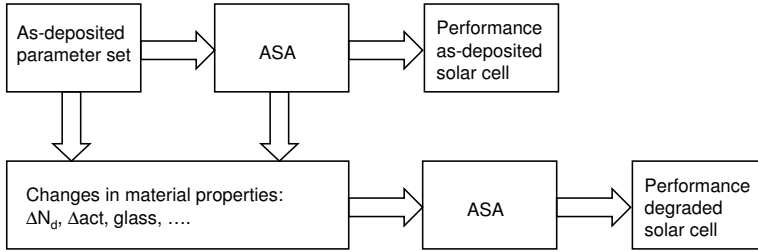


**Figure 3.1:** Flowchart of our procedure to simulate degraded a-Si:H solar cells. From the as-deposited parameter set the performance of the as-deposited solar cells is calculated using ASA. The as-deposited parameter set is then adjusted in accordance with the properties of the degraded state. The change in the parameter set may be based on the internal parameters of the as-deposited cells as determined by ASA or on the effect of external influences. Finally, ASA is invoked again to calculate the performance of the degraded solar cell.

is invoked to determine the performance of the degraded state. In principle, the performance of the degraded state can be used as input for the next iteration step in which the effect of further degradation is simulated. However, for the simulation results presented in this thesis the degraded state was always directly simulated from the as-deposited state and no iteration procedure was used.

First, the as-deposited parameter set needs to be determined, for which we have used the procedure as reported by Zeman et al. [69]. In this procedure various measurement results on single layers and solar cells are matched with simulation results in order to extract a parameter set. Then, using ASA the solar cell performance is calculated from which the external parameters are extracted as well as the internal parameters like the as-deposited defect density profile,  $N_{\text{as-deposited}}$ , recombination rate profile,  $R(x)$ , and internal electric field.

After the as-deposited parameter set has been established, the changes in material properties related to the degradation must be determined. In our procedure we assume that the solar-cell performance degradation after irradiation or light soaking is the result of three possible effects (see chapter 2 and chapter 4): (i) an increase of the activation energy of the doped layers, (ii) an increase of the absorption in the glass, and (iii) an increase of the defect density and corresponding changes in the defect density-of-state distribution. In principle, the procedure can be extended easily to include more degradation effects. In order to incorporate

the increase in activation energy of the doped layers, the corresponding ASA parameter is altered. The increase of the absorption by the glass substrates is taken into account by replacing in the optical simulations the complex refractive index of the pristine glass with that of the degraded glass.

To incorporate the increase in defect density following degradation in our procedure the DDOS profile related to the degraded state,  $N(x, E)_{\text{degraded state}}$ , needs to be determined. The profile of the degraded state is related to the as-deposited profile,  $N(x, E)_{\text{as-deposited}}$ , by the expression

$$N(x, E)_{\text{degraded state}} = N(x, E)_{\text{as-deposited}} + \Delta N(x, E)_{\text{induced}}, \quad (3.4)$$

where  $x$  is the position in the solar cell,  $E$  the energy position in the band gap, and  $\Delta N(x, E)_{\text{induced}}$  the induced change in the DDOS by irradiation or light soaking. Thus both the energy distribution and the depth profile of the induced defect states need to be determined, for which we use the following expression

$$\Delta N(x, E)_{\text{induced}} = \sum_{n=e,z,h} (C_n - 1) \cdot P(x) \cdot N_n(\text{ref}, E), \quad (3.5)$$

where ‘*ref*’ denotes an arbitrarily chosen position in the solar cell, and the subscripts ‘*e*’, ‘*z*’, and ‘*h*’ denote the as-deposited defects  $N_n(\text{ref}, E)$  having a negative, neutral, and positive charge state, respectively. The negatively charged states are located near the conduction band, the neutral charge states in the middle of the band gap, and the positively charged defect states near the valence band. In this way we can control in which part of the band gap defect states are induced. For instance, if only  $C_z$  is used in the simulations, all defects are induced in the middle of the band gap at the same energy position as the dangling bonds. Similarly,  $C_e$  creates defects states near the valence band, while  $C_h$  creates states near the conduction band. In equation 3.5,  $P(x)$  provides the depth profile of the induced defects and equals unity at the ‘*ref*’ position. In section 3.4.3 we will investigate three possible depth profiles: a uniform profile, a profile calculated using the total recombination rate, and a profile obtained using the recombination rate involving only valence band tail states. For these three depth profile we have:

$$P(x) = 1, P(x) = \frac{R(x)}{R(\text{ref})} \text{ or } P(x) = \frac{R_{vb}(x)}{R_{vb}(\text{ref})}. \quad (3.6)$$

After the changes in the parameters have been determined, the parameter set related to the degraded state is obtained and ASA is used to calculate the degraded solar-cell performance.

### 3.4 Sensitivity study of simulation procedure

An important advantage of computer simulations is that the influence of each degradation effect on the solar-cell performance can be investigated separately. Such an investigation will provide valuable insight in the sensitivity of the solar-cell performance to these effects. In this section we will investigate the influence of three degradation profiles on the solar cell performance. In the remainder of this chapter we will use the parameters given in table 3.1 for the description of the as-deposited state. This parameter set is equal to the set used in chapter 4. The thickness of the solar cells is varied to discern the effect the as-deposited recombination rate and the internal electric field have on the solar cell performance degradation.

#### 3.4.1 Increase of light absorption in glass substrates

In section 2.2.1 it was shown by using reflection-transmission measurements that light absorption of the glass substrates increased following electron-beam irradiation. In order to take this effect into account, the refractive index as obtained from the reflection-transmission measurements of the irradiated glass is used in the optical simulations. This effect leads to a lower electron-hole pair generation rate in the solar cell and reduces mainly the  $J_{sc}$ .

Using our procedure, we conclude that the increase of the absorption of the CMZ glass substrates as observed in section 2.2.1 will only result in a  $J_{sc}$  reduction of 13 to 14 A/m<sup>2</sup> at most. The QE is decreased for wavelengths below 600 nm. The  $V_{oc}$  and  $FF$  only change less than 1% .

#### 3.4.2 Changes in activation energy doped a-Si:H and defect density intrinsic a-Si:H

The properties of n- and p-type doped layers in a-Si:H solar cells are not much affected by light soaking [82]. However, irradiation by high-energy charged-particles will lead to significant changes in the activation energy of doped a-Si:H layers (see section 2.2.4). We found an increase of up to 0.2 and 0.25 eV after a fluence of  $1.9 \times 10^{16}$  1-MeV electrons/cm<sup>2</sup> in 500-nm thick p-doped a-SiC:H and n-doped a-Si:H layers, respectively. Such an increase in activation energy of doped a-Si:H will have a profound effect on the solar-cell performance, in particular on the  $V_{oc}$ . The defect density in the intrinsic layer, however, is affected both by light soaking

**Table 3.1:** Input parameters used for the electrical simulations of the a-Si:H solar cells for the as-deposited state.

Doped layers	
Activation energy p-layer	0.55 eV
Activation energy n-layer	0.35 eV
Intrinsic layer	
Mobility gap	1.75 eV
Effective DOS valence band	$4 \times 10^{26} \text{ m}^{-3}$
Effective DOS conduction band	$4 \times 10^{26} \text{ m}^{-3}$
DOS at valence band edge	$2 \times 10^{27} \text{ m}^{-3} \text{ eV}^{-1}$
Characteristic energy valence band tail	0.045 eV
Hydrogen concentration	$5 \times 10^{27} \text{ m}^{-3}$
Si-Si bond concentration	$2 \times 10^{29} \text{ m}^{-3}$
Width of defect pool	0.185 eV
Position of defect pool (relative to valence band)	1.20 eV
Electron mobility	$28 \times 10^{-4} \text{ m}^2 \text{ V}^{-1} \text{ s}^{-1}$
Hole mobility	$8 \times 10^{-4} \text{ m}^2 \text{ V}^{-1} \text{ s}^{-1}$

and high-energy charged particle irradiation. This increase in defect density may mainly lead to lowering of the  $FF$  and  $J_{sc}$ . In this section we investigate the effect of changes in the activation energy on the external parameters and QE and show how this effect differs from increases in the defect density in the solar cell.

The effect of changes in activation energy of the doped layers and increases in the defect density will be illustrated using three simulations. In the first simulation (A1) only the activation energy of both doped layers is increased by 0.2 eV, while keeping the other parameters in the simulation constant. In the second simulation (A2) only the defect density in the middle of the bandgap is increased. For  $C_z$  in equation 3.5 a value of 200 was chosen, while  $C_e = C_h = 1$ , comparable to values used in chapters 4 and 5 to simulate the degraded state of the light-soaked or electron-beam irradiated solar cells. For A2, a uniform profile is used,  $P(x) = 1$ . Finally, both effects are combined creating parameter set (A3). These simulations are compared to results obtained with the parameter set for the as-deposited state (A0).

Table 3.2 shows the results for the external parameter simulations of the above-described test simulations. When increasing the activation energy of (A1), the

### 3. Computer modeling of degraded amorphous silicon solar cells

---

**Table 3.2:** External parameter simulations (Sim.) of the as-deposited cells, A0, in which only the activation energy of the doped layers is increased, A1, in which only extra  $D_z$ -defect states are generated throughout the solar cells, A2, and in which both degradation effects are combined, A3.

Sim.	deg. effect	ext.	150 nm	450 nm	900 nm
A0	as-depo.	$J_{sc}$ (A/m <sup>2</sup> )	123.3	148.9	154.6
A0	as-depo.	$V_{oc}$ (V)	0.855	0.860	0.860
A0	as-depo.	$FF$ (-)	0.735	0.704	0.677
A1	act.	$J_{sc}$ (A/m <sup>2</sup> )	126.4	149.0	152.2
A1	act.	$V_{oc}$ (V)	0.812	0.818	0.820
A1	act.	$FF$ (-)	0.682	0.658	0.669
A2	defects	$J_{sc}$ (A/m <sup>2</sup> )	124.2	138.4	128.9
A2	defects	$V_{oc}$ (V)	0.849	0.847	0.842
A2	defects	$FF$ (-)	0.699	0.610	0.508
A3	act. + defects	$J_{sc}$ (A/m <sup>2</sup> )	126.5	137.2	127.3
A3	act. + defects	$V_{oc}$ (V)	0.802	0.804	0.800
A3	act. + defects	$FF$ (-)	0.632	0.582	0.456

$V_{oc}$  decrease for each solar-cell thickness is similar. The  $J_{sc}$  even increases for thin solar cells, while a small drop is observed for the 900-nm thick solar cell. The  $FF$  of the 900-nm cell is least affected by the increase in activation energy of the doped layers, while the 150-nm cell shows most  $FF$  degradation.

When only additional defects are introduced in the intrinsic layer (A2), most degradation is observed in the  $J_{sc}$  and  $FF$ . The  $V_{oc}$  is also affected, but not as much as for simulation A1, because the intrinsic layer properties only weakly affect the  $V_{oc}$  [54]. Both the  $FF$  and  $J_{sc}$  degradation are more pronounced for solar cells with thicker intrinsic layers.

If both degradation effects are taken into account (A3), it is clear that both influence the performance. The combined effects may even have a stronger influence, especially on the  $FF$ . When comparing simulation A1 to A0 for the 900-nm cell, only a small decrease in  $FF$  was observed. However, when only defects are introduced in the intrinsic layer (simulation A2) the  $FF$  is much more affected. Combining A1 and A2 (simulation A3) leads to an even more pronounced effect on the  $FF$ , so the effect of increasing the activation energy of the doped layers is much stronger in case the defect density is high. The  $V_{oc}$  degradation is dependent

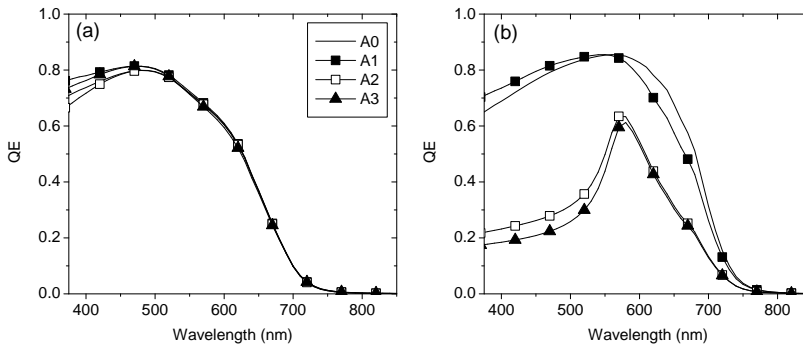


**Figure 3.2:** QE of the (a) 150-nm and (b) 900-nm solar cells for simulations A0 to A3.

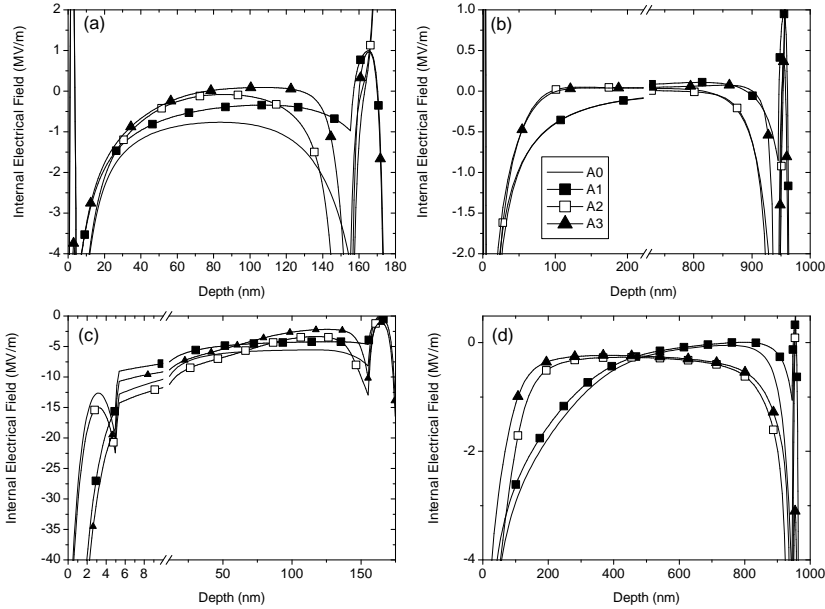
on both the changes in activation energy of the doped layers, and defect density in the intrinsic layer; the results suggest that the  $V_{oc}$  change in simulation A3 is the sum of the changes in simulation A1 and A2. The  $J_{sc}$  is mainly affected by the increase in defect density in the intrinsic layer. For the 150-nm cell, both the  $FF$  and  $V_{oc}$  degrade more when both effects are combined. The slight increase in  $J_{sc}$  found here is largely similar to the increase in  $J_{sc}$  when only changes the the activation energy of the doped layers are assumed.

Figure 3.2(a) and (b) shows the QE of the 150-nm and the 900-nm thick solar cell, respectively, for simulations A0 to A3. In case of the 150-nm thick cell, the change in QE in each simulation is observed mainly in the short-wavelength range, below 550 nm. For A1 and A3 the QE increases in this wavelength range, but when only the defect density is increased (A2) the QE is reduced in this wavelength range. We note, however, that  $J_{sc}$  of the 150-nm cell increased slightly in simulation A2 compared to the as-deposited state and this is due to a slightly higher QE above 500 nm for A2.

For the 900-nm cell a change in QE is observed when only increasing the activation energy of the doped layers (A1). For shorter wavelengths an increased QE is found, while above 550 nm the QE is lowered. Increasing the defect density leads to significant reduction of the QE and a distinct peak around 570 nm is observed. Combining both effects (A3) slightly more degradation is observed as compared to A2, mainly at shorter wavelengths.

The trends in external parameters and QE for simulations A0 to A3 may be clarified when studying the effect of changes in material properties on the internal electric field of the a-Si:H solar cells. The internal electric field plays a major role

### 3. Computer modeling of degraded amorphous silicon solar cells



**Figure 3.3:** Internal electrical field of (a) the 150-nm cell and (b) the 900-nm cell under open-circuit conditions, and (c) the 150-nm cell and (d) the 900-nm under short-circuit conditions for simulations A0 to A4.

in the current collection and thus determines to a large extent the  $FF$  and  $J_{sc}$ . The  $V_{oc}$  is even directly related to internal electric field at open-circuit condition by Poisson's equation. Both increases in defect density and activation energy lead to changes in space charge profile over the solar cell, which in turn will alter the electric field profile. An increase in defect density in the intrinsic layer, especially near the p-i interface, typically leads to an increased accumulation of space charge at that location, which will result in band-bending and a lower internal electric field deeper in the solar cell. The changes in activation energy will result in a decrease in the voltage drop over the cell, which must lead to lowering of the electric field as well. In figure 3.3 the internal electric field of the 150-nm and 900-nm cell at open-circuit and short-circuit conditions is plotted for simulations A0 to A3, to highlight the role of the electrical field in the external parameter degradation.

The internal electric field of the 150-nm cell under open-circuit conditions is shown in figure 3.3(a). Following degradation a decrease in the electric field

strength is observed in the intrinsic layer, except for simulation A2, for which the electric field strength increases at the back of the solar cell. Therefore, the  $V_{oc}$  decreased most in simulation A1 and A3. Figure 3.3 also indicates that the reduction of the electric field strength across the intrinsic layer is an important contributor to the lowering of the  $FF$ , as this results in an increased recombination rate.

Under short-circuit condition a high internal electric field in excess of 2.5 MV/m (see figure 3.3(c)) is obtained in each simulation of the 150-nm cell. In the intrinsic layer of the degraded solar cells the electric field strength is lower compared to the as-deposited cell, except for simulation A2 in which a stronger electric field strength is obtained in the front of the cell compared to simulation A0. Based on this observation a lower  $J_{sc}$  is expected for the degraded 150-nm cells, which is not found in the external parameter simulations. It may be assumed that the internal electric field in the intrinsic layer is high enough to sweep almost all charge carriers to the doped layers. However, when increasing the defect density and especially the activation energy of the doped layers, a much higher electric field in the p-doped layer is found. This higher electric field leads to a lowering of the recombination rate in the p-doped layer, resulting in an increase in the  $J_{sc}$ .

The internal electric field of the open-circuit-degraded 900-nm cell is always equal or lower in the intrinsic layer when compared to the as-deposited cell; simulation A3 has the lowest electric field (see figure 3.3(b)), resulting in the lowest  $V_{oc}$ . For simulation A1 the electric field is high near the p-i interface giving rise to the high  $V_{oc}$  stability. A similar reason may be applicable to the reasonably higher  $FF$  stability for A1, as compared to A2, or A3, because in simulation A1 the electric field is highest in the region where the electron-hole pair generation rate is highest.

The internal electric field of the degraded 900-nm cell at short-circuit condition is shown in figure 3.3(d). When only the activation energy of the doped layers is increased (A1), a small reduction of the internal electric field in the intrinsic layer is observed, resulting in a  $J_{sc}$  comparable to that of the as-deposited solar cell. When more defect states are introduced, band bending in the intrinsic layer near the p-i interface is found. This in turn lowers the internal electric field over first 500 nm of the intrinsic layer where most electron-hole pairs are generated, and a lower  $J_{sc}$  is obtained.

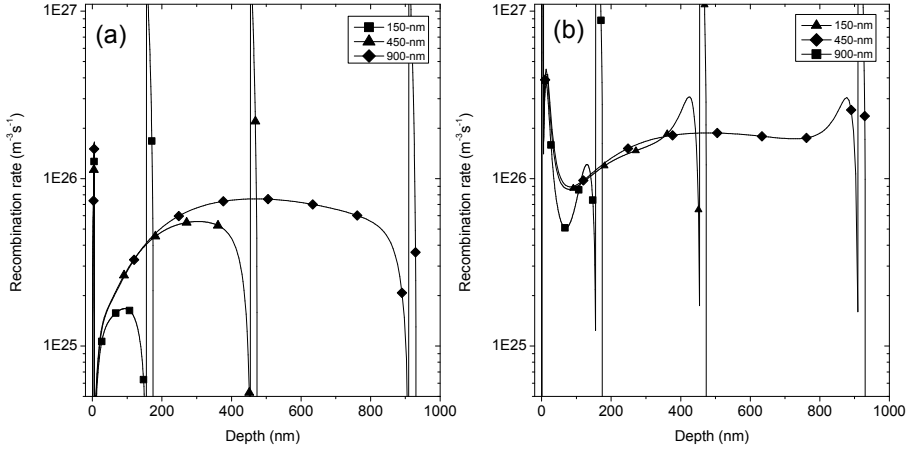


**Figure 3.4:** The depth profiles of (a) the recombination rate involving valence-band-tail states and (b) the total recombination rate for solar cells with a varying intrinsic layer thickness under AM 1.5 illumination.

### 3.4.3 Defect creation depth profile

It has been shown extensively that electron-beam irradiation and light soaking introduce defect states in a-Si:H [61], and these defects will affect the performance of the solar cells (see chapter 5 and 4). For light soaking it is generally accepted that the defect creation is triggered by recombination events [60]. However, for electron-beam irradiation the nature of the induced defects and the underlying defect-creation mechanism is still under discussion. For the simulation of the degraded solar-cell performance the depth profile of the induced defects, which is to a large extent related to the degradation mechanism, is important. In this section we study the effect of different defect creation depth profiles (DCDP) on the external parameters and the QE of a thickness series of solar cells by means of computer simulations. Both the depth profile and the energy position of the induced defect states in the band gap are investigated.

Three depth profiles,  $P(x)$ , as described by equation 3.6, are used in the simulations presented here to study the effect on the external parameters following degradation. In simulation B1 the defects are created uniformly over the whole solar cell,  $P(x) = 1$ , and the defects are created in the middle of the bandgap. For  $C_z$  a value of 200 was chosen while  $C_e = C_h = 1$ . Note that simulation B1 is the same as simulation A2 in section 3.4.2. In simulation B2 the degradation

is linked to the total recombination rate in the cell during degradation,  $P(x) = R(x)/R(ref)$ . We define the total recombination rate at a particular position as the rate obtained by taking into account all recombination events at that position. In order to have similar  $FF$  degradation for the 450-nm thick solar cell as in simulation B1,  $C_z$  was decreased to 165 in this simulation. A depth profile related to the recombination events involving the valence band tail,  $P(x) = R_{vb}(x)/R_{vb}(ref)$  is used in simulation B3. In this case  $C_z$  was increased to 220.

The effect of the energy position in the bandgap of the induced defect states is investigated in simulations C1 and C2. Here, simulation C1 is the same as simulation B1 (which in turn is the same as simulation A2) and the defects are created in the middle of the bandgap with  $P(x) = 1$ . In C2 the defects are created near the valence band tail. In this case an  $C_e$  value of 72 was chosen, while  $C_z = C_h = 1$ . Again a uniform depth profile is assumed. Simulations B0 and C0 are the same as simulation A0 and correspond to the simulation of the as-deposited state.

Figures 3.4(a) and (b) show the total recombination rate density profiles and the recombination rate density profile involving states in the valence-band tail,  $R_{vb}$ , respectively, in solar cells under AM 1.5 illumination and open-circuit condition. The recombination through valence-band-tail states gives a significant contribution to the total recombination rate. In both cases there is a large peak in the recombination rate in the p- and n-layer, due to the high defect density in those layers. In the intrinsic layer the  $R_{vb}$  shows a maximum in the middle and towards the doped layers the recombination rate drops off. In contrast the total recombination rate shows a peak near the i-n interface. In all cases the recombination rate is higher for the thicker solar cells.

The low recombination rate near the p-i interface is related to the low local electron density. The high recombination rate for electrons in the p-layer leads to a diffusion current of electrons towards the p-layer. Because of the high electron mobility of this effect extends up to 500 nm into the intrinsic layer. For the holes near the n-layer a similar effect is noted, but it will only extend about 50 nm into the intrinsic layer, because of the lower hole mobility. The peak in the total recombination rate profile near the i-n interface is associated to a local higher defect density relative to the middle of the intrinsic layer.

Using the above recombination profiles, simulation B2 and B3 are calculated. Table 3.3 shows the external parameters for the simulations B0 to B3 and C0 to C2. Note that the  $FF$  of the degraded 450-nm cells was chosen to be equal for

### 3. Computer modeling of degraded amorphous silicon solar cells

---

**Table 3.3:** Simulation results of the external parameters (ext.) of the 150-nm, 450-nm and 900-nm thick solar cell for the as-deposited and degraded state, in which different depth profiles are tested. The simulations are described in the text.

Sim.	Deg. effect	ext.	150 nm	450 nm	900 nm
A0	as-depo.	$J_{sc}$ (A/m <sup>2</sup> )	123.3	148.9	154.6
B0		$V_{oc}$ (V)	0.855	0.860	0.860
C0		$FF$ (-)	0.735	0.704	0.677
A2	Uniform	$J_{sc}$ (A/m <sup>2</sup> )	124.2	138.4	128.9
B1	$C_z$	$V_{oc}$ (V)	0.849	0.847	0.842
C1		$FF$ (-)	0.699	0.610	0.508
B2	Rec.	$J_{sc}$ (A/m <sup>2</sup> )	122.9	141.6	132.7
	$C_z$	$V_{oc}$ (V)	0.846	0.849	0.841
		$FF$ (-)	0.692	0.610	0.513
B3	Rec.vb	$J_{sc}$ (A/m <sup>2</sup> )	122.6	140.5	128.0
	$C_z$	$V_{oc}$ (V)	0.850	0.848	0.842
		$FF$ (-)	0.700	0.610	0.495
C2	Uniform	$J_{sc}$ (A/m <sup>2</sup> )	123.8	143.7	127.7
	$C_e$	$V_{oc}$ (V)	0.845	0.849	0.845
		$FF$ (-)	0.710	0.610	0.535

each simulation. The thickness variation of the degraded  $FF$  is highest for solar cells profiled using  $R_{vb}$ . The cells profiled using the total recombination rate show a smaller thickness variation of the degraded  $FF$ . This difference in the thickness dependence of the  $FF$  degradation between simulations B1, B2 and B3 is directly related to the total amount of defects generated in the solar cells. In simulation B3 approximately 5 times more defect states are induced per unit depth in the 900-nm thick cell than in the 150-nm cell. In simulation B1, an equal amount of defect states is induced per unit depth for each solar cell, while in simulation B2 more defect states per unit depth are induced in the 150-nm cell than in the 900-nm cell. This last effect is due to the fact that the recombination in the p- and n-layer contributes relatively more to the total recombination in the 150-nm thick solar cell. The position in the cell at which the defect states are induced does not play a major role in the  $FF$  degradation. The  $J_{sc}$  degradation is only influenced a little by the DCDP. In all cases, as expected from the previous simulations, the  $V_{oc}$  is not altered significantly by the DCDP, although the obtained  $V_{oc}$  degradation

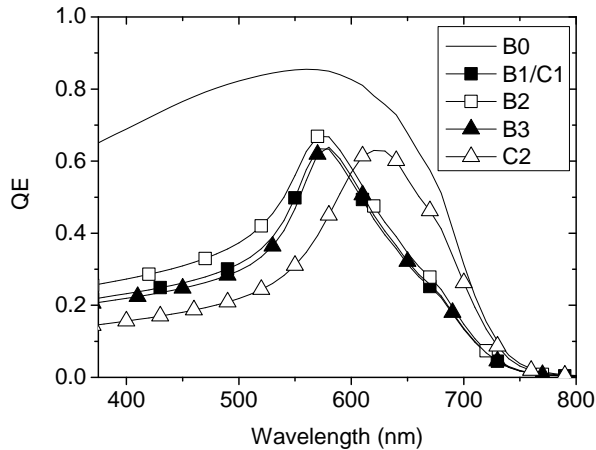


**Figure 3.5:** Effect of various DCDPs on the QE of the 900-nm thick solar cell.

is highest for the thickest cells.

The energy location in the bandgap of the induced defect states has a major effect on the degradation. If defect states are induced more towards the valence-band tail in the band gap (C2) the  $FF$  does not decrease as much for the 150-nm and 900-nm thick cells as compared to the other simulations. This effect is due to a lower recombination efficiency (defined as  $R/N_t$ , in which  $N_t$  is the defect density) of defect states in the bottom of the band gap. The  $J_{sc}$  and  $V_{oc}$  degradation is similar to simulation C1.

Because the defects are created at different positions in the cell between the different simulations, it is expected that the QE should be sensitive to these changes in DCDP. In case of a uniform defect-creation profile, on average more defects are generated near the p-i interface as compared to the DCDP calculated from the recombination rate density or the recombination rate involving valence band tail states. The QE simulations for the 900-nm solar cells for various DCDPs and different defect states are plotted and compared to the as-deposited QE in figure 3.5. For all simulations a distinct narrow peak in the QE is observed. For the simulations in which the defects are induced in the middle of the bandgap this peak is located at 570 nm, while this narrow peak is observed around 620 nm when the defect states are created near the valence band tail. This peak also seems to widen in this latter case. Even though B2 and B1 show relatively more induced defect states near the p-i interface as compared to B3, B3 degrades more

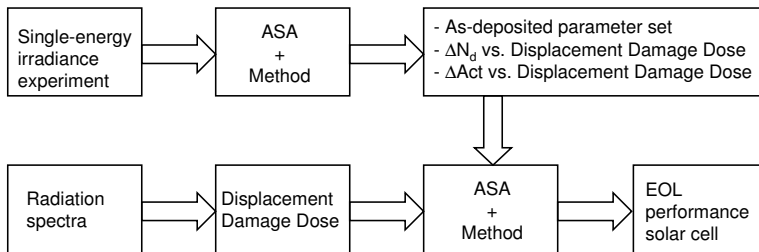


**Figure 3.6:** Flowchart to predict EOL performance of a-Si:H solar cells using our methodology.

in the shorter wavelength range than B1 and B2. We conclude that there is no clear effect of  $P(x)$  (see equation 3.6, i.e., the location in the cell where the defect states are induced) on the QE; a clear effect is found when the energy location of the defect states is varied.

### 3.5 Procedure to predict the EOL performance

The aim of the thesis is to create a model to predict the end-of-life (EOL) performance of a-Si:H solar cells for a given space mission due to high-energy charged-particle irradiation. Figure 3.6 depicts a flowchart of the procedure we envisage to predict the EOL performance. First, a charged-particle irradiation experiment is performed using single-energy particle irradiation, either electrons or protons, and the performance versus the fluence is recorded. Using the method as presented in section 3.3 of this chapter the as-deposited parameter set and the changes in material properties may be extracted. As an example we present simulations of the 1-MeV electron-beam degradation of a-Si:H solar cells in section 5.4.2, where the increase in defect density following irradiation shows a linear dependence on the fluence. The results of the single-energy beam irradiation need to be extrapolated in order to relate these results to the degradation in the space environment, which is required in order to be able to predict the EOL performance.

AP8 proton [83] and AE8 electron [84] environment models may be used to calculate the differential proton,  $d\Phi_p/dK$ , and electron spectra,  $d\Phi_n/dK$ , incident on the solar cells during the space mission. To correlate the degradation caused by the incident particles of different energies and type, we propose to use the so-called NRL approach [85]. In this approach it is assumed that the perfor-

mance degradation is a function of the total non-ionizing energy loss (NIEL) of the incident particles. For this approach a NIEL function for both protons and electrons incident on a-Si:H needs to be calculated using numerical simulations. This function has already been determined for crystalline silicon solar cells (see figure 1.1), but we think that this function is not directly applicable to a-Si:H solar cells, as we will explain in chapter 6.

The NIEL function is used to calculate the displacement damage dose,  $D_d$ , i.e., the amount of energy used to induce defects in the material. The conversion of the radiation spectra to the displacement damage dose is as follows:

$$D_d = \int \frac{d\Phi_n}{dK} NIEL(K)_n dK + \int \frac{d\Phi_p}{dE} NIEL(K)_p dK. \quad (3.7)$$

If  $D_d$  induced in the cell for the mission is known, using the results obtained from the 1-MeV electron beam irradiation experiments, the increase in defect density and activation energy at the end of the mission may be estimated. Using ASA the EOL performance of the solar cells is calculated with the parameter set for the degraded material. With this approach slowing down of particles in the cell leading to a non-uniform energy deposition profile is not incorporated, but it may be easily extended to correct for these events.

## 3.6 Conclusions

A procedure to simulate degraded solar cells using the ASA device simulator program is developed. In the simulations in this thesis only three changes in the material properties of the solar cells due to the irradiation are taken into account: reduction in the transmission of the glass substrates, increases in activation energy of doped a-Si:H, and changes in the defect density of states in the band gap of intrinsic a-Si:H. Changes in other material properties, for instance a change in the valence-band-tail width, are not taken into account here, but most are easy to include in the model if required.

The reduction in transmission of the glass leads mainly to an decrease in  $J_{sc}$ , while other external parameters are hardly affected. Changes in the activation energy of the doped layers will mainly lead to a lowering of the  $V_{oc}$  and  $FF$  while the  $J_{sc}$  is hardly affected or may even increase. Increasing the defect density of states will result in  $FF$  and  $J_{sc}$  degradation, while the  $V_{oc}$  only changes slightly. When combining both the increase in activation energy of the doped layers with

the increase in defect density, an enhancement in  $FF$  degradation is observed. In addition, thicker solar cells show typically more degradation in all external parameters as compared to the thinner cells. Similar to the  $J_{sc}$  the QE is mainly sensitive to changes in the defect density and not to the activation energy of the doped layers. When more defect states are induced in the intrinsic layer, the QE of 900-nm cells shows a narrow peak around 570 nm.

In the simulations where the depth profile of the induced defect states was varied it was found that the degradation is mainly dependent on the amount of defects induced and not on the depth location in the intrinsic layer. The depth profile does play a major role to determine the degradation difference between the solar cells with a different thickness. For instance, if the DCDP is profiled using the recombination rate involving the valence-band-tail states, the thickness dependence of the degradation is increased.

When the energy position of the induced defects states is not near midgap, but more towards the valence band tail, the difference in  $FF$  degradation rate between the 150-nm and 900-nm is reduced. In addition the QE peak following degradation is shifted to longer wavelengths as compared to simulations where the defects states are generated in the midgap.

Finally, we have presented the model how the EOL performance of a solar cell may be estimated for a particular space mission. The model is based on our method to simulate degraded a-Si:H solar cells using ASA. It provides a method to extrapolate the results obtained from a single-energy charged-particle irradiation experiment to the degradation as expected in a space mission, due to charged particles with varying energies.

## Chapter 4

# Degradation of solar cells by light soaking

### 4.1 Introduction

In 1977 changes in the light and dark conductivity of a-Si:H due to light soaking were reported for the first time by Staebler and Wronski [12] and the meta-stability of a-Si:H, since then called the Staebler-Wronski effect, has been a research topic ever since. The degradation is often attributed to an increase in dangling-bond related spin density, as revealed by ESR-measurements [86, 87], although nowadays more types of defects are assumed to play a role in the Staebler-Wronski effect, like floating bonds [88, 89] or hydrogen complexes [90]. As a result of this effect, the performance of a-Si:H solar cells degrades following prolonged illumination.

Various models have been developed to explain the metastability of a-Si:H, like the hydrogen-collision model of Branz et al. [91] and the network-rebonding model of Biswas et al. [89]. In the hydrogen-collision model, pairs of mobile hydrogen and dangling bonds are generated by, e.g., recombination processes of electron-hole pairs on weak bonds. When two mobile hydrogen atoms ‘collide’, a metastable complex containing two Si-H bonds is formed together with two dangling-bond defects. In the network-rebonding model two defect types are assumed: dangling bonds and floating bonds. In this model electron-hole pair recombination on a weak bond generates a pair consisting of a floating bond and a dangling bond. The floating bond is then allowed to move through the material,

where it can interact with other dangling bonds, floating bonds, or hydrogen in the a-Si:H structure, whereas the dangling bond remains stationary. In both models the defect-creation mechanism can be initiated by electron-hole recombination on weak-bonds. Using simulations it was concluded that the dangling bond is the major defect configuration that is created in a-Si:H following light soaking. Nádaždy et al. [90] suggested an additional defect type: a hydrogen-molecule complex. In contrast to other defect types, this type is annihilated during light soaking and supplies mobile hydrogen which in turn may interact with floating bonds forming electronically-inactive local configurations.

Various workers [92–94] have reported on the thickness dependence of light-induced degradation in a-Si:H solar cells and concluded that the observed effects are strongly linked to the internal electric field in the solar cell. Meytin et al. [62] investigated the light degradation of the dark and photoconductivity of a-Si:H using computer simulations. Only changes in the defect density of states (DDOS) were assumed in these simulations and the DDOS was simulated by two Gaussian distributions. It was concluded that the dark-conductivity degradation was mainly determined by the shift in peak position of the positively-charged/neutral defect-state peak of the DDOS and the photoconductivity by the total defect density. Computer simulations of the performance degradation of light-soaked solar cells were reported by several workers. Using four different profiles for the defect creation in the intrinsic layer Block [95] showed that the best results were obtained starting with a defect distribution as predicted by the defect-pool model and modeling the degradation using spatially homogeneous created defects. Caputo et al. [63] presented computer-simulation results of the performance of light-soaked solar cells. They demonstrated that the degradation of the performance could be reproduced by increasing the defect density in the intrinsic layer and this increase was profiled using the spatial distribution of the electron and hole densities. The electron and hole densities during light soaking were varied by altering the wavelength of the incident light. Dutta et al. [65] showed simulations of the degradation of a-Si:H solar cells by current injection. In their results they found that the increase in defect density due to the current injection is correlated to the recombination rate during the degradation, although this correlation was not studied in full detail.

In this chapter we study the performance degradation of a-Si:H solar cells due to light soaking with a high-intensity laser having a photon energy slightly above the band gap of a-Si:H and compare the findings to results of computer simula-

tions. According to literature reports light soaking mainly leads to a change in the defect density of a-Si:H and the creation of defects is initiated by recombination events in the intrinsic layer of the device (e.g., [89]). In the simulations that we will present in this article the degradation will be linked to the recombination profile in the solar cell. In order to verify our simulation results, we have opted to light soak the cells under both open- and short-circuit conditions with the objective to alter the recombination profile substantially in the cells. The dependence of light-induced performance degradation on applied bias was already reported before [96, 97]. The aim of this chapter is to develop a model in which the performance degradation of a thickness series of a-Si:H solar cells is related to the recombination profile in the devices.

In this article we will first explain the experimental procedures that we have used. We will then present in section 4.3.1 the performance of the as-deposited solar cells used in the light soaking experiment. In section 4.3.2 the experimental results of the degradation of the solar cells following light soaking are shown for both open- and short-circuit conditions. We will then explain how we have simulated the Staebler-Wronski effect in the solar cells. Simulations of the as-deposited state are presented in section 4.5.1 and compared to the experimental results. Subsequently, we show the results of the degradation simulations in section 4.5.2, in which degradation under open- and short-circuit conditions is simulated simultaneously by linking the defect-creation mechanism to electron-hole recombination events. Here, the defect density following light soaking versus the illumination time is extracted from the simulations. Finally, in section 4.6 we give the main conclusions of this article.

## 4.2 Experimental details

For the light-soaking experiments single junction a-Si:H solar cells deposited on Asahi U-type substrates were used. The following solar-cell structure was used: 9-nm thick p-doped a-SiC:H layer, 15-nm thick a-SiC:H buffer layer, a-Si:H i-layer with varying thickness, 15-nm thick n-doped a-Si:H layer, and a 300-nm thick aluminum layer. In order to study the defect-creation-depth profile following light soaking, the i-layer thickness ranged from 150 nm to 900 nm [98]. We used an Al back-reflector in order to minimize changes in the reflectance of this contact due to some heating during the light soaking [99]. The cells were characterized by their external parameters and the quantum efficiency (QE). The QE has been

measured using a bias of 0 V and no bias light was used. The cell area is 4 mm  $\times$  4 mm.

For the light-soaking experiments a semiconductor laser was used with a wavelength of 635 nm. At this wavelength the absorption of intrinsic a-Si:H is approximately  $1 \mu\text{m}^{-1}$ , corresponding to a penetration depth of 1000 nm, which implies that the electron-hole pair generation profile is non-uniform for the thicker solar cells. The power density was 3.4 kW/m<sup>2</sup>. In order to investigate the defect-creation-depth profile and the effect of the recombination profile on the degradation of the solar cells, one cell was degraded under short-circuit conditions and the other under open-voltage conditions. In this way the recombination rate profile can be changed substantially. The cells were short-circuited by connecting them to a current meter; a contact resistance of less than 4  $\Omega$  was achieved. The initial current measured at the beginning of the light-soaking experiment was in between 9.2 mA and 12.5 mA depending on the thickness. The substrates were not actively cooled during the light soaking and an increase in temperature to about 35  $^{\circ}\text{C}$  was noted, which means that some thermal annealing during the light soaking cannot be excluded. At predetermined illumination times the cells were taken out of the laser-irradiation setup to measure  $J$ - $V$  under AM 1.5 illumination and QE. We remark that the differences between recombination profiles using AM 1.5 and monochromatic light at 635 nm are not very large. Using monochromatic light at 635 nm the electron-hole pair generation rate is more uniform and as a result the recombination rate is more dependent on the intrinsic layer thickness.

For the results presented in the following sections, two solar cells with similar performance were selected for each thickness. Throughout this chapter we will show the results of these two cells.

## 4.3 Experimental results

### 4.3.1 Experimental results for the as-deposited solar cells

Table 4.1 shows the external parameters of the solar cells used in the light-soaking experiment in their as-deposited state. The values are the average of the two selected solar cells. This table shows that conversion efficiencies range from 7.3% to 8.8%, the short-circuit current density,  $J_{\text{sc}}$ , from 113 to 157 A/m<sup>2</sup>, the open-circuit voltage,  $V_{\text{oc}}$ , from 0.88 to 0.84 V, and finally the fill factor,  $FF$ , from 0.734 to 0.677. The results show that the  $FF$  and  $V_{\text{oc}}$  decrease when the i-layer thickness

**Table 4.1:** Measured and simulated external parameters under AM1.5 for the as-deposited solar cell thickness series used in the light-soaking experiments. In this table 'exp' refers experimentally obtained results on solar cells and 'sim' to results obtained using the computer program ASA.

thickness (nm)	type	$V_{oc}$ (V)	$J_{sc}$ (A/m <sup>2</sup> )	$FF$	efficiency (%)
150	exp	$0.88 \pm 0.01$	$113 \pm 2$	$0.73 \pm 0.01$	$7.26 \pm 0.06$
150	sim	0.86	123	0.734	7.70
300	exp	$0.85 \pm 0.01$	$140 \pm 1$	$0.713 \pm 0.01$	$8.53 \pm 0.02$
300	sim	0.86	140	0.728	8.72
450	exp	$0.86 \pm 0.01$	$143 \pm 2$	$0.683 \pm 0.03$	$8.44 \pm 0.5$
450	sim	0.86	148	0.704	9.00
600	exp	$0.86 \pm 0.01$	$149 \pm 2$	$0.685 \pm 0.01$	$8.76 \pm 0.03$
600	sim	0.86	152	0.686	9.00
900	exp	$0.84 \pm 0.01$	$157 \pm 2$	$0.637 \pm 0.01$	$8.36 \pm 0.02$
900	sim	0.86	154	0.677	8.97

is increased, whereas the  $J_{sc}$  is increased. When the i-layer is increased more is light absorbed in the solar cell, increasing the  $J_{sc}$ . However, the recombination rate is also increased due to a lowering of the internal electric field, which leads to a loss in  $FF$ . The  $V_{oc}$  is mostly dependent on the properties of the doped layers and not so much on the properties of the intrinsic layer [54], thus the  $V_{oc}$  shows only a weak dependence on the i-layer thickness (the  $V_{oc}$  decreases by about 0.04 V when the thickness is increased from 150 nm to 900 nm).

Figure 4.1 shows the QE of the cells in their as-deposited state. For each thickness a QE of at least 0.6 is obtained in the short-wavelength region. Between 500 nm and 600 nm the QE shows a maximum and at longer wavelengths the QE decreases again. The decrease at longer wavelengths is mainly related to the low absorption coefficient of a-Si:H and, consequently, the low generation rate. As already indicated by the obtained  $J_{sc}$  results, increasing the i-layer thickness results in higher QEs at longer wavelengths because of an increase in optical path length. This increase in thickness also shifts the maximum in the QE to longer wavelengths. At shorter wavelengths, increasing the i-layer thickness leads to a lower QE. This effect is probably related to a decrease in the internal electric field near the p-i interface, increasing the recombination and reducing the current-collection efficiency.

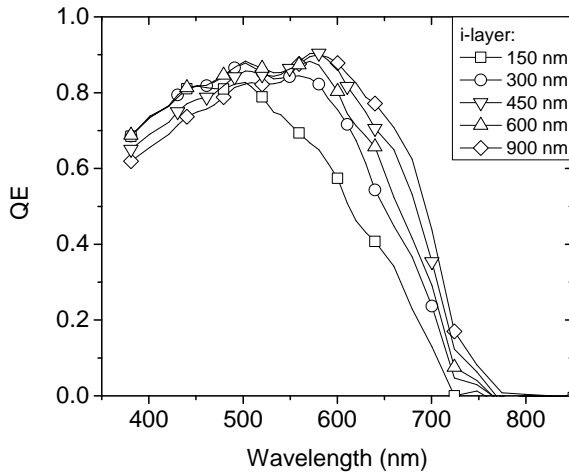


**Figure 4.1:** Quantum efficiency of the as-deposited series of solar cells on Asahi U-type substrates with a varying i-layer thickness.

Compared to the solar cells used in the electron-beam degradation experiments, presented in chapter 5, we found higher QE at shorter wavelengths due to the higher transmission of the Asahi U-type substrates with respect to the CMZ/ZnO substrates. At longer wavelengths the QE of the solar cells presented in Fig. 4.1 is lower compared to the cells used for the electron-beam degradation, which is due to the application of Al as back-contact material that has a lower reflectivity than Ag. Due to this lower reflectivity of the back contact, light with longer wavelengths is less likely to be reflected but absorbed at the back contact and thus the QE is reduced at higher wavelengths as compared with cells using an Ag-Al back-contact.

### 4.3.2 Degradation under open- versus short-circuit condition

Figure 4.2 shows the external parameters of the solar cells with different i-layer thickness following laser degradation under both open-circuit (open markers) and short-circuit conditions (closed markers). Following light soaking, the largest relative decrease is found in the  $FF$ . Under both conditions, the reduction of the  $FF$  is smallest for the thinner cells. For each thickness the  $FF$  degrades faster under open-circuit conditions than under short-circuit degradation. The 150-nm-

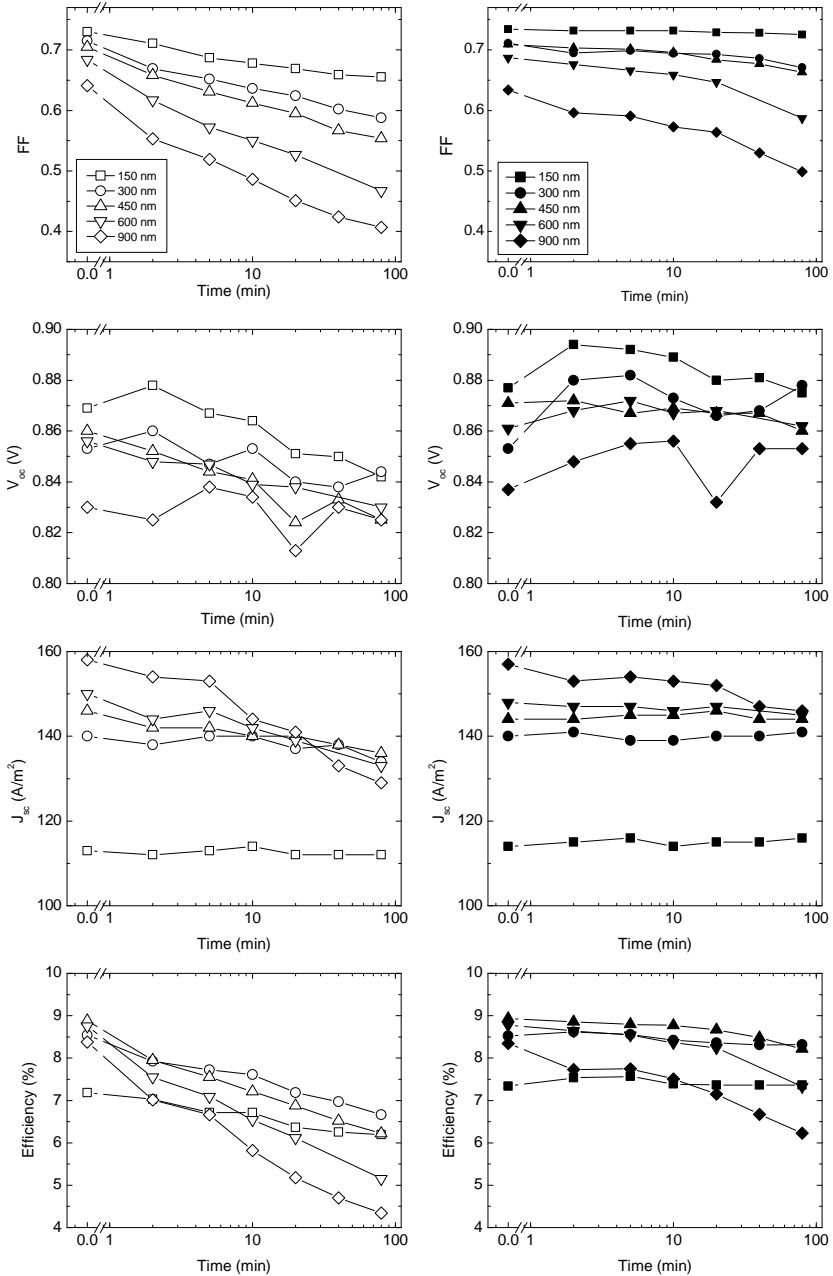


**Figure 4.2:** External parameters of solar cells with a varying i-layer thickness following laser degradation under short (closed markers) and open-circuit conditions (open markers).

thick cells had an initial  $FF$  of 0.74 and this value degrades to 0.68 ( $-8\%$ ) under open-circuit condition, while under short-circuit condition virtually no degradation is observed. The  $FF$  of the 900-nm thick solar cell drops under both open- and short-circuit conditions: the as-deposited  $FF$  was 0.64 and dropped to 0.4 ( $-38\%$ ) under open-circuit conditions and 0.5 ( $-22\%$ ) when the cells were short-circuited.

Almost no change is observed in the  $V_{oc}$  after degradation under both open- and short-circuit conditions, at most 5%. Due to the scatter in the data, it is difficult to extract the time dependence of the  $V_{oc}$ , although it seems that the short-circuited cells are more stable than the open-circuited cells. The  $V_{oc}$  of some cells degraded under short-circuit condition even increases slightly.

The effect on the degradation of changing the i-layer thickness and circuit condition is most apparent in the  $J_{sc}$ . For both short- and open-circuit conditions, almost no degradation (less than 5%) is observed for the 150-nm cells, while the thickest cell degraded more than 8% or 18% in short- and open-circuit condition, respectively. In fact,  $J_{sc}$  values of all solar cells except the 900-nm thick cell are hardly affected by degradation under short-circuit condition. For all thicknesses the  $J_{sc}$  appears to be more stable against light soaking for shorter illumination times when compared to the  $FF$ . For longer illumination times the degradation of the  $J_{sc}$  is comparable to the degradation in  $FF$ , especially for the thicker cells.

The decrease in efficiency following light soaking under open- and short-circuit condition is presented in figure 4.2. As expected from the results of the  $FF$  and  $J_{sc}$  degradation, the efficiency of the cells degrades much faster when illuminated under open-circuit condition. For the 150-nm thick cells after light soaking under short-circuit condition we even observe a small improvement of the conversion efficiency, mainly due to a small increase in  $J_{sc}$ . This effect might be ascribed to some annealing of the samples due to the elevated temperatures during the light soaking, though the effect is not very strong. Under open-circuit condition the 150-nm cell shows a relative decrease of 14% after 80 minutes of light soaking. For the 900-nm cell the relative decrease in efficiency is equal to 25% and 48%, under short- and open-circuit conditions, respectively.

Figure 4.3 shows the QE of the 900-nm cell following light soaking under open-circuit and short-circuit condition, respectively. In agreement with the  $J_{sc}$  degradation data, a larger decrease in QE for cells degraded under open-circuit condition is found, independently of the light-soaking conditions. However, the shape of the QE is similar, irrespective of the circuit condition under which the

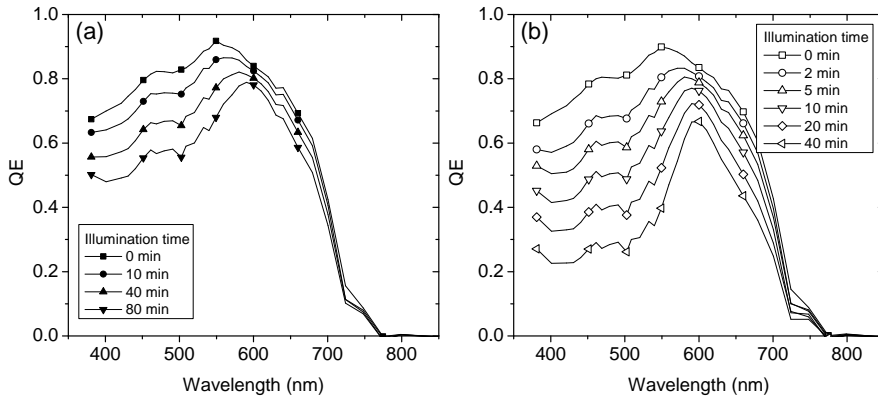


**Figure 4.3:** Quantum efficiency following light soaking under (a) short-circuit and (b) open-circuit condition for the 900-nm cell, respectively

cell has been degraded. For instance, the cell light soaked under open-circuit condition for 5 minutes is comparable within 5% over the whole wavelength range to the cell degraded under short-circuit condition for 80 minutes. For longer light-soaking times the QE shows a narrow peak around 600 nm. Similar trends are observed for the cells with other i-layer thickness, but these are less pronounced due to the fact that these cells do not degrade as much.

## 4.4 Simulation details

The experimental results for the external parameters and QE of the as-deposited cells as presented in section 4.3.1 have been matched to results of computer simulations in order to extract a baseline parameter set for the simulations of the light degradation of a-Si:H solar cells. The relevant parameters used in the electrical simulations of a-Si:H solar cells are given in table 4.2. The parameter set is in close agreement with the standard parameter set for p-i-n structures in the computer program ASA and this standard parameter set has been successfully applied in other simulations as well [75]. At first we used different values for the electron and hole mobility,  $10 \times 10^{-4} \text{ m}^3\text{V}^{-1}\text{s}^{-1}$  and  $5 \times 10^{-4} \text{ m}^3\text{V}^{-1}\text{s}^{-1}$ , respectively, however in that case the decay in  $J_{sc}$  could not be matched as will be explained in the next section.

In order to simulate the light-induced performance degradation of solar cells, the change in defect density as a function of illumination time as well as the profile

**Table 4.2:** Input parameters for electrical simulations corresponding to the as-deposited state of a-Si:H solar cells.

Doped layers	
Activation energy p-layer	0.55 eV
Activation energy n-layer	0.35 eV
Intrinsic layer	
Mobility gap	1.75 eV
Effective DOS valence band	$4 \times 10^{26} \text{ m}^{-3}$
Effective DOS conduction band	$4 \times 10^{26} \text{ m}^{-3}$
DOS at valence band edge	$1 \times 10^{27} \text{ m}^{-3} \text{ eV}^{-1}$
Characteristic energy valence band tail	0.045 eV
Hydrogen concentration	$5 \times 10^{27} \text{ m}^{-3}$
Si-Si bond concentration	$2 \times 10^{29} \text{ m}^{-3}$
Width of defect pool	0.185 eV
Position of defect pool (relative to valence band)	1.20 eV
Electron mobility	$25 \times 10^{-4} \text{ m}^2 \text{ V}^{-1} \text{ s}^{-1}$
Hole mobility	$3.5 \times 10^{-4} \text{ m}^2 \text{ V}^{-1} \text{ s}^{-1}$

describing where in the solar cell the defects (the so-called defect-creation-depth profile (DCDP)) are created, need to be determined. This process was carried out by matching the simulation to experimental results and details of the procedure will be given in the next section. In the simulations we assume that the electron drift mobility in the extended states does not change as a result of light soaking in analogy to Wyrsh et al. [100] and Hotling et al. [101]. Further, as no changes in the valence-band tail and in the width and peak position of the defect pool have been reported [102, 103], these quantities were not changed in the simulations. We also assumed that the small changes observed in the  $V_{oc}$  can be modeled by increasing the defect density in the intrinsic layer. This assumption is based on the fact that the  $V_{oc}$  is almost unaffected by the light soaking, which rules out substantial changes in the activation energy of the doped layers. Such changes would immediately lead to a decrease in the  $V_{oc}$  as suggested by Jiang et al. [54] and the simulations results obtained in chapter 3. Moreover, it has been noted by Wagner et al. [104] that the  $V_{oc}$  is slightly dependent on the defect density of the intrinsic layer .

In the last 20 years various microscopic models have been proposed to describe

the metastability of a-Si:H during light-soaking. Stutzmann et al. [87] linked the increases in defect density to non-radiative bi-molecular recombination events and proposed a weak-bond to dangling bond conversion process [105]. Biswas et al. [89] and Schumm et al. [106] suggested that recombination on weak bonds governs the defect creation. In contrast, Longeaud et al. [107] and Branz et al. [91] assume recombination on a Si-H site to initiate the defect creation. Irrespective of the details of the model, it is assumed that the defect creation is triggered by recombination events.

We will follow the reasoning of Biswas et al. [89] and Schumm et al. [106]. In the simulations we have linked the defect creation to the recombination-rate profile calculated by only taking into account the recombination path that involves states in the valence-band tail, which correspond to weak bonds in the a-Si:H [108, 109]. Another argument for considering only recombination events involving energy states in the valence-band tail is that the energy released in these events corresponds to the activation energy for defect creation, which has been found to be in between 1 and 2 eV [107, 110, 111]. We think that this energy cannot be provided by recombination through defect states situated in the middle of the band gap.

To simulate the DOS corresponding to the light-soaked state, the following procedure was used. First the density-of-states distribution as a function of energy,  $E$  and position,  $x$ , in the solar cell,  $N(x, E)_{\text{as-deposited}}$ , was calculated for the as-deposited state using the ASA simulation program. Subsequently, the change in the density of states,  $\Delta N(x, E)_{\text{induced}}$ , was determined and added to the as-deposited density of states to obtain the density of states in the degraded state:

$$N(x, E)_{\text{degraded state}} = N(x, E)_{\text{as-deposited}} + \Delta N(x, E)_{\text{induced}}, \quad (4.1)$$

where  $N(x, E)_{\text{degraded state}}$  is the defect density-of-states distribution. To calculate  $\Delta N(x, E)_{\text{induced}}$  the recombination rate density involving the valence band tail,  $R_{vb}$ , is used:

$$\Delta N(x, E)_{\text{induced}} = \sum_{n=e,z,h} (C_n - 1) \cdot \frac{R(x)_{vb}}{R(ref)_{vb}} \cdot N_n(ref, E), \quad (4.2)$$

where the subscripts ‘e’, ‘z’, and ‘h’ denote the as-deposited defects  $N_n(ref, E)$  having a negative, neutral and positive charge state, respectively. In Eq. 4.2  $C_n$  is the appropriate multiplication factor and ‘ref’ denotes a reference position in

the solar cells that is taken arbitrarily. As reference position, we have chosen the middle of the 600-nm cell and the  $C_n$  values correlate directly to the increase of the defect density at this position. From this reference point, the model then calculates the  $N(x, E)_{\text{induced}}$  throughout the intrinsic layer for each of the five solar cells. Using this method we can control in which energy range the defect states are created. For instance, if only  $C_z$  is used in the simulations, all defects are induced in the middle of the band gap at the same energy position as the dangling bonds.  $C_e$  creates defects states near the valence band tail, while  $C_h$  near the conduction band tail. In the simulations presented in this section only changes in the  $D_z$ -defect-state density in the middle of the the band gap are taken into account. This assumption is based on results of, e.g., Schumm et al. [106] and Nádaždy et al. [90], and on the simulations presented in chapter 3 where the observed, distinct QE peak of the 900-nm following light soaking could only be reproduced when assuming the creation of defects states in the middle of the bandgap.

The multiplication factors are obtained from careful matching of experimental and simulation results of the external parameters and the QE, and will be discussed in more detail below. We have matched on the  $J_{\text{sc}}$ ,  $V_{\text{oc}}$ , and  $FF$ , by reducing the difference between the experimental data and simulation results. If a reasonable match was obtained for the external parameters, the QE simulations were compared to the measurements. We stress that the degradation of all solar cells degraded under both circuit conditions were matched simultaneously by varying only  $C_z$ . Note that the  $C_z$  values are the same for both circuit conditions.

## 4.5 Simulation results

### 4.5.1 Simulations of the as-deposited solar cells

In the simulations presented in this section only the i-layer thickness was varied and all other parameters were kept constant. Using the parameter set presented in the previous section a reasonable good match is obtained between the simulations and the experimental results from section 4.3.1. In table 4.1 the simulation results of the external parameters of the cells in their as-deposited state are given for each i-layer thickness. The simulations show similar trends in the  $FF$  and  $J_{\text{sc}}$  with respect to the i-layer thickness as was observed in the experimental data. Increasing the i-layer thickness results in higher  $J_{\text{sc}}$  and lower  $FF$ . However, the

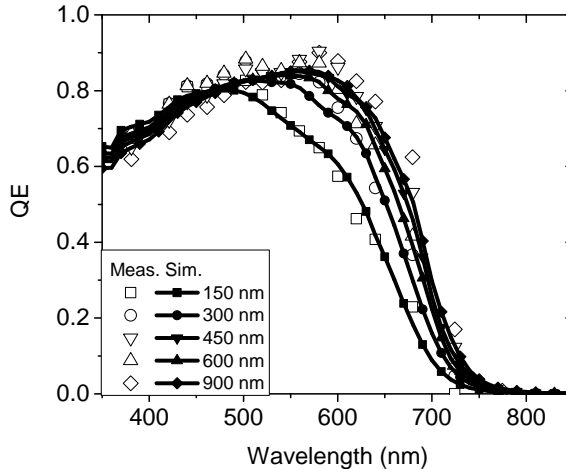


**Figure 4.4:** Measured (markers) and simulated (lines) QE for cells used in the light soaking experiments in the as-deposited state

simulations do not show a significant trend in the  $V_{oc}$ , whereas the experimental data suggested a small thickness dependence of the  $V_{oc}$ . Further we note that the simulations overestimate the  $J_{sc}$  for the 150-nm cell, and the  $FF$  for the 900-nm cell.

As remarked in the previous section, we used higher values for the electron and hole mobility in our simulations. These higher values were needed to reduce the  $J_{sc}$  degradation as compared to the  $FF$  degradation when increasing the defect density. Using the standard values of  $10 \times 10^{-4} \text{ m}^2 \text{ V}^{-1} \text{ s}^{-1}$  and  $5 \times 10^{-4} \text{ m}^2 \text{ V}^{-1} \text{ s}^{-1}$  for the electron and hole mobility, respectively, for the 900-nm cell, a  $J_{sc}$  of only  $20 \text{ A/m}^2$  in combination with a  $FF$  of 0.4 were obtained in the simulations of the degraded state, which is obviously not in agreement with our experimental observations. The parameter set used here is also in reasonable agreement to the set used by Dutta et al. [65] to simulate the as-deposited state for current-injection degradation simulations, including a higher mobility for the electrons and holes.

Figure 4.4 shows the results of the simulations (lines) for the QE and compares these results to the experimental data (markers). A good match is obtained between the experimental data and simulations for each i-layer thickness. For the entire investigated wavelength range the difference between the experimental and simulated QE is less than 0.1 and mostly less than 0.05. However, in the

experimental results the effect of interference is more pronounced than in the simulations, due to an underestimation of the fraction of coherent light transmitted through the TCO. The simulations show that the QE is lowered at shorter wavelengths when the i-layer thickness is increased, which is due to a lowering of the internal electrical field near the p-i interface for the thicker cells. This effect is much more pronounced in the experimental results. At longer wavelengths, higher QE is found when the i-layer thickness is increased. In this case, the simulations show similar trends as the experiments.

### 4.5.2 Simulation of light soaking of a-Si:H solar cells

In figure 4.5 the simulation results (lines with small markers) of the external parameters following light-soaking are compared with the measurements (large markers). Both the results of degradation under open- and short-circuit condition are presented. The trends observed in the experimental data are found in the simulated results as well. Compared to the other external parameters, the  $FF$  degrades most. The short-circuited cells are more stable against light soaking and increasing the i-layer thickness increases the amount of degradation. The difference in the  $FF$  between light soaking under the open- and short-circuit condition can be simulated well for the thicker cells, but is underestimated for the thin cells under open-circuit condition.

Compared to the  $FF$  and  $J_{sc}$ , the  $V_{oc}$  in the simulations is not very much affected by the increase of the defect density as seen in figure 4.5. A maximum drop of 0.05 V (6%) is found for the 900-nm thick solar cell following light soaking under open-circuit condition. In the simulations the  $V_{oc}$  of short-circuited cells seems to be less affected by the light soaking than of the open-circuited cells, which is more or less in agreement with the experimental data. However, we note that the trend in the  $V_{oc}$  as a function of the illumination time cannot be well simulated due to the large scatter in the experimental data.

The simulation results of the  $J_{sc}$  degradation are in reasonably good agreement with the experimental results (figure 4.5). However, in the simulations the decrease in  $J_{sc}$  is overestimated for the thicker solar cells, especially for the 900-nm thick solar cell both for open-circuit as for short-circuit conditions. Also in this case the short-circuited cells appear to be more stable against light soaking. The 150-nm thick cells show no degradation in the  $J_{sc}$  in agreement with the experimental results.

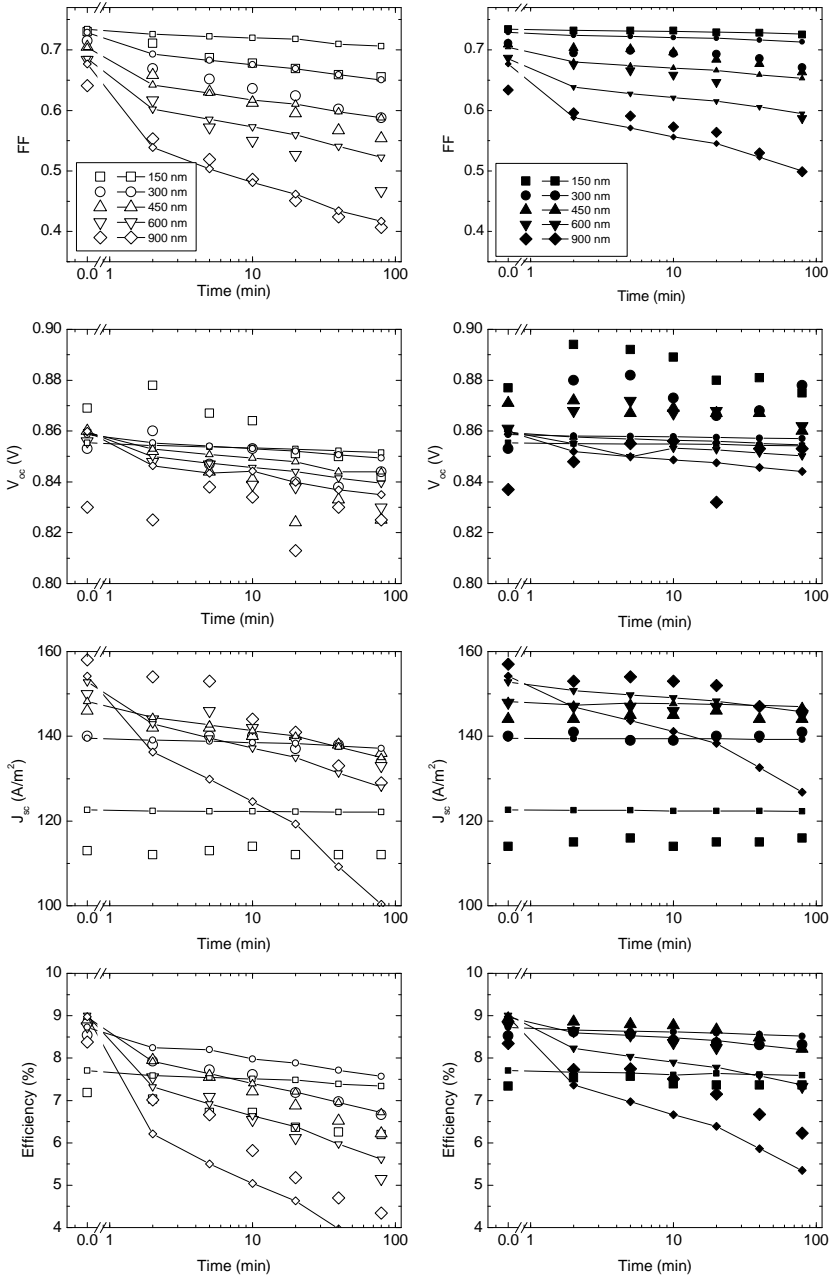


**Figure 4.5:** Simulation results (lines with small markers) of the external parameter degradation following light soaking under short-circuit (closed markers) and open-circuit (open markers) condition.

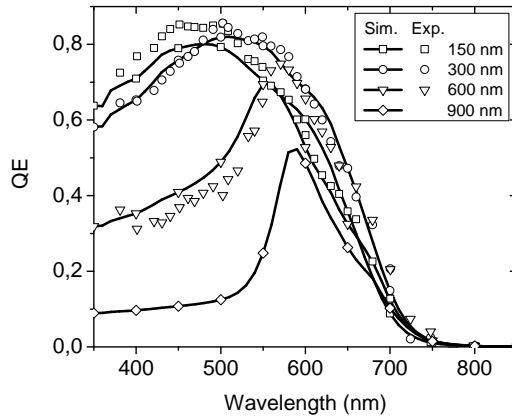


**Figure 4.6:** Simulations of QE degradation of the solar cells with a varying i-layer thickness following 80 minutes of light soaking under open-circuit condition.

Figure 4.6 shows simulations of the QE degradation of solar cells with a varying i-layer thickness during light soaking under open-circuit conditions. Similar trends are observed in the simulation results as in the measurement. The degradation in QE is mainly visible for the shorter wavelengths and the thicker cells are least tolerant to light-soaking. The simulations the QE degradation of the 900-nm cell displays the distinct shape typical for these cells as seen in figure 4.3.

In our model the induced defect density is assumed to be related to the recombination rate density in the solar cells. In that case differences in degradation rate of the solar cells with different i-layer thickness by light-soaking under both open- and short-circuit conditions is explained as follows. Figure 4.7 shows the recombination profiles during illumination in solar cells with different i-layer thickness for open- and short-circuit condition, respectively. The profiles were calculated using ASA for the as-deposited state of the cells and only the recombination events involving energy states in the valence-band tail have been taken into account. For all solar cells and irrespective of the circuit condition, the recombination rate is highest in the p- and n-layers, due to the high defect density in these doped layers. In the intrinsic layer, the recombination rate has a minimum near the p-i interface and the recombination rate increases when moving deeper into the cell, which is mainly due to differences between the mobility of holes and electrons.

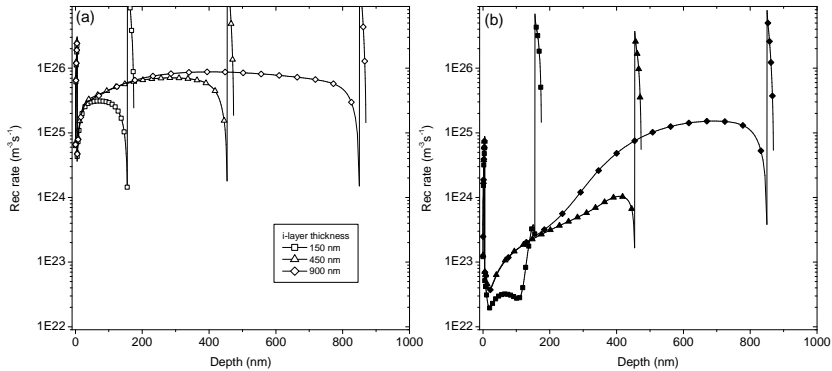


**Figure 4.7:** Recombination rate involving states in the valence-band tail during light soaking for solar cells with a different i-layer thickness under (a) open-circuit and (b) short-circuit condition.

Because of these differences in mobility, the charge-carrier concentration is higher in the back of the cell, leading to a higher recombination rate in this region. During light soaking the internal electric field over the intrinsic layer is higher in short-circuited solar cells than in open-circuited cells and therefore the charge-carrier collection is more efficient in the short-circuited cells, which implies that the recombination rate is lower. Furthermore, the thickness dependence of the recombination rate is stronger for short-circuited cells. In solar cells illuminated under open-voltage conditions there is about one order of magnitude difference in recombination rate between the 150-nm and 900-nm cells, whereas short-circuit conditions this difference is more than two orders of magnitude.

Figure 4.8 shows the multiplication factors used in the simulations as a function of the illumination time. The multiplication factors are obtained from careful matching of experimental and simulation results of solar cells degraded under both open-circuit and short-circuit conditions. The increase in defect density appears to follow a  $t^{1/3}$  dependence (with  $t$  the illumination time), as indicated by the fit in figure 4.8. This time dependence has been reported often for the increase in defect density during light soaking [89]. Noting the quality of the match between the experimental and simulation results at present moment, the parameter set used and models related to a-Si:H solar cells are not good enough to be able to distinguish with the model between the various recombination paths, either bimolecular, through valence band states or the total recombination rate,

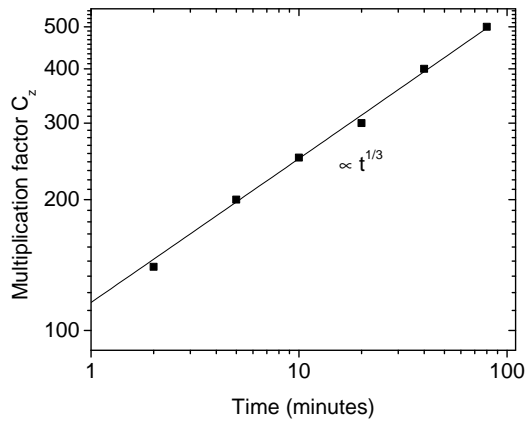


**Figure 4.8:** Multiplication factor to determine the DCDP in the simulations for each time.

because the difference between those recombination paths will lead to differences smaller than observed between the measurement and simulations (see chapter 3).

The multiplication factors determine the defect density following light soaking for each solar cell thickness under both open and short-circuit condition. Figure 4.9 compares the as-deposited defect density profile of the 150-nm and 900-nm cells with the profile following 80 minutes of light soaking under both open- and short-circuit conditions. The defect density profile of the 150-nm is only altered significantly for open-circuit degradation, especially in the middle of the i-layer addition defects are created. Here, the defect density increased approximately one order of magnitude. The defect density of the 900-nm solar cells shows an increase under both conditions, with the largest increase in the middle and back of the solar cell. However, under open-circuit degradation the increase in defect density is more pronounced over the whole thickness, up to two orders of magnitude.

## 4.6 Conclusions

In this chapter we have presented the results of light-soaking experiments on a-Si:H solar cells under both open- and short-circuit conditions, with the aim to develop a model in which the performance degradation of a thickness series

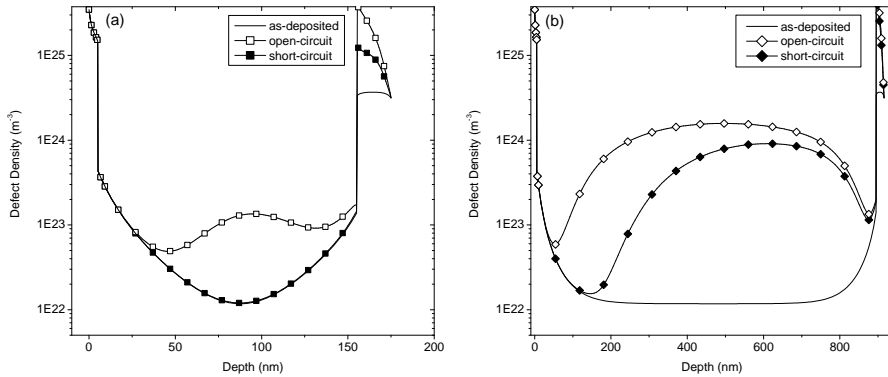


**Figure 4.9:** The simulated defect density before and after light soaking for 80 minutes under both open and short-circuit conditions for the 150-nm (left-hand figure) and 900-nm solar cells (right-hand figure).

of a-Si:H solar cells is related to the recombination profile in the device. Solar cells were degraded under open- and short-circuit conditions during light soaking, because in this way the recombination-rate profile in the cells could be changed substantially. The cells were characterized by measuring the external parameters and the QE at 0-V bias. The performance of thin solar cells is not so much affected by light soaking as for thick cells. Further, we observe that the performance of solar cells light soaked under short-circuit condition does not decrease as fast as for cells light soaked under open-circuit condition.

The experimental results of the degradation by light soaking have been matched to simulation results. In the simulations of the performance degradation, changes were only made to the defect density of states, more in particular the defect-state density in the middle of the band gap. If defect creation as a function of position in the solar cell is linked to the recombination rate profile of events involving energy states in the valence band tail, a reasonable good match of the degradation of the external parameters and the quantum efficiency due to light soaking under both open- and short-circuit conditions for each i-layer thickness is obtained. We stress that this match is obtained by adjusting only one parameter. The difference between the degradation of the external parameters under open- and short-circuit condition can be attributed to differences in the magnitude of the internal electric field in the solar cell and the subsequent recombination-rate profile. A  $t^{1/3}$  dependence has been found for the increase in defect density in the intrinsic layer

#### 4. Degradation of solar cells by light soaking

---

as a result of light soaking, in agreement to what has been reported in literature for light soaking of a-Si:H. To our knowledge it is the first time that light-induced degradation of the performance and the quantum efficiency of a thickness series of a-Si:H solar cells has been modeled at once using computer simulations.

## Chapter 5

# Degradation of solar cells by high-energy electrons

### 5.1 Introduction

Hydrogenated amorphous silicon (a-Si:H) solar cells are promising devices for electricity generation during space missions in which high radiation levels are expected. For the utilization of such solar cells it is necessary to be able to predict their End-Of-Life (EOL) performance for a given mission in which they are exposed to electron and proton irradiation having a wide range of kinetic energies. In this chapter we present results of our procedure to predict this EOL efficiency using computer simulations based on changes in the material properties of the layers. Therefore, knowledge about the degradation mechanisms in a-Si:H cells by the charged particle irradiation is needed. However, the degradation mechanism under charged-particle irradiation is still under debate [30].

High-energy charged particles moving through material can lose their energy by ionizing and non-ionizing events. Ionizing events lead to the creation of electron-hole pairs in the material, whereas with non-ionizing events either x-rays or phonons are generated, or atoms are displaced. Vendura et al. [112] proposed that as with degradation of crystalline silicon solar cells, the degradation of a-Si:H solar cells is governed by displacement damage. In literature electron-beam degradation of crystalline silicon solar cells has been compared to degradation by protons having various kinetic energies, in order to study the degradation mech-

anism further [85]. In this way the ratio between the ionizing and non-ionizing energy deposition is altered between each degradation experiment and the governing defect-creation mechanism could be established. However, for a-Si:H solar cells contradictory findings have been reported. Srour et al. [28] found that the degradation of the short-circuit current density of triple-junction a-Si:H solar cells following high-energy charged-particle irradiation had a strong correlation with the ionizing dose. They assumed that the ionization-induced charge is captured on pre-existing defects in the material leading to distortion of the internal electric field, which in turn reduces the solar-cell performance. Danesh et al. [41, 42] and Yelon et al. [43] suggested that high-energy charged-particle irradiation has the same effect on a-Si:H as light soaking. Important in their conclusion is that defect creation following electron-beam irradiation is initiated by electron-hole pair recombination events, as found for light soaking [60, 89]. Later, Walters et al. [113] did not find a clear correlation of the drop in power output of solar cells with ionizing dose. However, they did not give an alternative explanation. Lord et al. [66] also presented simulations of a-Si:H solar cells irradiated with 40-keV electrons to extract the defect-density changes. He only matched experimental and simulated results of the the dark  $J$ - $V$  curve and only assumed changes in defect density. They found an increase in defect density of a factor 200 following a fluence of  $1 \times 10^{17}$  electrons/cm<sup>2</sup>.

In this chapter we present the results of three different irradiation experiments, which were carried out in order to study the processes that underly the degradation of a-Si:H solar cells. First, we have studied the fluence dependency of the degradation of the solar-cell performance. Secondly, we have investigated the flux dependency on the performance degradation, in order to verify literature reports (e.g., [41, 43]) that defect creation by high-energy charged-particle irradiation is similar to light soaking and linked to recombination events. If this were the case, it is expected that the particle flux has an influence on the degradation, because the particle flux may be considered the equivalent of the light intensity during light soaking. For a similar reason we have studied the solar-cell performance degradation under open- and short-circuit condition. If defect creation is indeed initiated by recombination events following the generation of charge carriers by electron-beam irradiation, then in this way the recombination profile in the cell is altered during irradiation, because under short-circuit condition the internal electric field in the cell is higher.

We have irradiated the solar cells with 1-MeV electrons, which has two main

advantages. Firstly, 1-MeV electron-beam irradiation is generally used to degrade solar cells within the research field concerning the application of photovoltaic devices on spacecraft, because it is readily available and is seen as a benchmark for radiation hardness experiments [85]. Secondly, the energy deposition is uniform over the thickness of solar cells, as indicated by the Constant-Stopping-Derivation-Approach stopping range of  $0.54 \text{ g/cm}^2$  [22]. Using a mass density of  $2.1 \text{ g/cm}^3$  for silicon, a penetration depth of 2.6 mm is obtained, which means that the energy deposition profile may be assumed to be uniform throughout the whole solar cell and therefore will simplify the simulations. The experimental data are matched to computer simulations using our procedure presented in chapter 3 for the description of electron-beam irradiated solar cells. In addition, the fluence dependency of the defect-density increase may be extracted, as well as the defect-creation depth profile (DCDP), i.e., where the defects are created in the cells by the irradiation. This information may give further insights in the degradation mechanism. In order to extract this DCDP we irradiated cells with i-layer thickness varying from 150 nm to 900 nm.

In section 5.3.1 the a-Si:H cells with different intrinsic layer thickness used in the irradiation are presented and the measured cell performances are discussed. As described above, these cells are subjected to three degradation experiments. In section 5.3.2 the dependency of the fluence on the degradation is investigated. The influence of the incident electron flux on the degradation is studied in section 5.3.3. The effects of open- versus short-circuit degradation are presented and discussed in section 5.3.4. The measured results are then matched to computer simulations. Section 5.4.1 gives the simulations of the as-deposited state, which will provide the base parameter set needed to describe the degraded solar cells. Based upon the results of the experiments, our procedure to simulate electron-beam irradiated solar cells is introduced in section 5.4.2. In this section the simulations related to the degraded state of the solar cells are also presented and the match with the experimental results is discussed. On the basis of the simulations, the fluence dependency of changes in the activation energy of the doped layers as well as the increase in defect density are extracted and discussed. Finally, section 5.5 summarizes the most important conclusions of this chapter.

## 5.2 Experimental details

For the degradation experiments described in this chapter we used single-junction a-Si:H solar cells, having the following structure: 0.5-mm thick CMZ glass, 700-nm thick texture-etched ZnO:Al front contact, 5-nm thick p-type  $\mu\text{c-Si:H}$ , 9-nm thick p-type a-SiC:H, 15-nm thick intrinsic a-SiC:H, an intrinsic a-Si:H layer with varying thickness, 15-nm thick n-type a-Si:H, and as back contact 100-nm Ag covered with 200-nm Al. The thickness of the i-layer was varied between 150 and 900 nm. The cells were deposited on radiation-tolerant CMZ glass (see section 2.2.1) to minimize the reduction of transmission following irradiation. The sputtered ZnO:Al layer was texture etched to improve the light-trapping in the cell [114, 115]. In order to reduce the band mismatch between the p-type a-SiC:H and the ZnO:Al, an extra  $\mu\text{c-Si:H}$  p-layer was included in the structure [116, 117]. Finally, an a-SiC:H buffer layer was used between the p-layer and the i-layer to improve the interface quality [118].

The solar cells were characterized before and after irradiation by measuring the external parameters under AM 1.5 illumination [23] and the quantum efficiency (QE). The QE was measured on the most efficient solar cell in all cases. In the section 5.3.1 only the results of solar cells used in section 5.3.2 are presented. The cells used in the other degradation experiments showed similar performance and trends with respect to the intrinsic layer thickness. In order to obtain better statistics, for each solar cell thickness, 60 cells with an area of  $4\text{ mm} \times 4\text{ mm}$  were produced to be irradiated with 6 different fluences.

## 5.3 Experimental results

### 5.3.1 Experimental results for the as-deposited solar cells

The obtained external parameters of the series of the as-deposited cells are given in Table 5.1. Here, the averages of the best 50 of these 60 cells are given together with the corresponding standard deviation. The fill factor,  $FF$ , varies between 0.64 and 0.70. Increasing the i-layer thickness lowers the  $FF$  due to a decrease of the built-in electric field in the cells. Note the high standard deviation in the  $FF$  of the 150-nm cells, which is often observed for thin a-Si:H solar cells and is linked to shunting effects [119]. The short-circuit current density,  $J_{\text{sc}}$ , increases from  $114\text{ A/m}^2$  to  $153\text{ A/m}^2$  with increasing i-layer thickness. This increase results from an enhancement of the optical path length of the light in the solar

**Table 5.1:** Measured and simulated external parameters under AM1.5 for the thickness series of as-deposited solar cells.

thickness (nm)	type	$V_{oc}$ (V)	$J_{sc}$ (A/m <sup>2</sup> )	$FF$	eff. (%)
150	exp	$0.84 \pm 0.01$	$114 \pm 2$	$0.68 \pm 0.05$	$6.5 \pm 0.6$
150	sim	0.847	126.2	0.730	7.80
300	exp	$0.839 \pm 0.004$	$133 \pm 3$	$0.695 \pm 0.005$	$7.8 \pm 0.2$
300	sim	0.849	141.9	0.681	8.20
450	exp	$0.836 \pm 0.006$	$143 \pm 3$	$0.69 \pm 0.01$	$8.3 \pm 0.1$
450	sim	0.849	148.6	0.644	8.14
600	exp	$0.831 \pm 0.006$	$148 \pm 3$	$0.68 \pm 0.01$	$8.4 \pm 0.3$
600	sim	0.850	149.5	0.632	8.03
900	exp	$0.833 \pm 0.004$	$153 \pm 2$	$0.64 \pm 0.01$	$8.2 \pm 0.2$
900	sim	0.850	146.5	0.631	7.86

cell, leading to more light absorption in the intrinsic layer and a higher electron-hole pair generation rate. The open-circuit voltage,  $V_{oc}$ , of approximately 0.84 V is largely unaffected by the thickness of the intrinsic layer. Overall, good single-junction a-Si:H solar cells were produced having an efficiency between 6.5% and 8.4%, depending on the i-layer thickness. The external parameters found here are slightly less favorable compared to the parameters of the solar cells on Asahi U-type substrates used in the light-soaking experiments in chapter 4. The lower  $J_{sc}$  presented here is largely due to the lower transmission of the CMZ glass as compared to the Asahi U-type substrates. The lower  $FF$  could be caused by a hole or electron barrier at the ZnO:Al/p-layer interface, despite the insertion of the  $\mu\text{c-Si:H}$  p-layer.

The results of QE measurements on the as-deposited solar cells are presented in figure 5.1. The QE measurements were carried out at zero voltage and no bias light was used. At 375 nm the QE is in between 0.12 and 0.22, depending on the i-layer thickness, where the thicker cells have a higher QE. We think that this increase in QE as a function of the solar-cell thickness may be due to a higher internal electrical field near the p-i interface in the thicker cells. For longer wavelengths the QE increases and this effect is partly related to the increase of transmission of the CMZ glass substrates and ZnO:Al. Between 500 and 600 nm the QE shows a maximum, and for longer wavelengths the QE is decreased again. This QE decrease is due to a lower light absorption of the a-Si:H at these

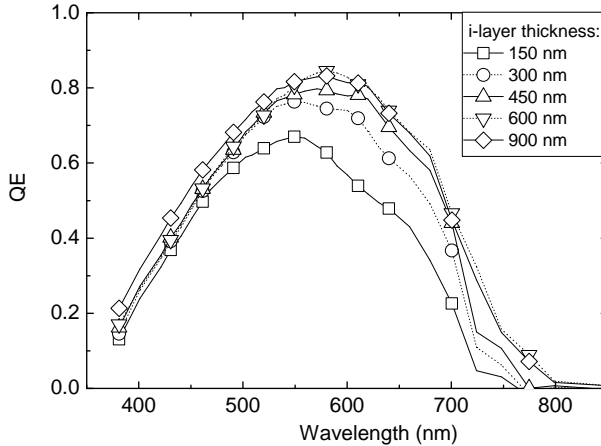


**Figure 5.1:** Quantum efficiency of the as-deposited series of solar cells on CMZ glass with a varying i-layer thickness. The measurements were carried out at a bias of 0 V.

wavelengths leading to a lower electron-hole pair generation rate. The increase in  $J_{sc}$  when increasing the i-layer thickness as presented in previous subsection is illustrated by higher QE of the thicker cells at longer wavelengths, where the optical absorption of the a-Si:H is low.

When the results of the QE measurements on the as-deposited cells presented in this chapter are compared to the results on the cells used for the light-soaking experiments (see figure 4.1), a much lower QE at shorter wavelengths is noted: around 0.2 versus 0.6 at a wavelength of 400 nm. The lower QE at short wavelengths for the solar cells in this chapter is due to more light absorption in the CMZ glass and ZnO:Al layer. In addition, the cells presented in this chapter employ a stack of two p-layers, which is thicker than the p-layer used in the cells for the light-soaking experiments. The thicker p-layers will further decrease the QE at short wavelengths [120].

### 5.3.2 Fluence dependency

The series of solar cells described in section 5.3.1 were irradiated under open-circuit condition using 1-MeV electrons. For the electron irradiation we employed a Van de Graaff accelerator. The cells were irradiated with fluences ranging from  $1 \times 10^{15}$  electrons/cm<sup>2</sup> up to  $1.9 \times 10^{16}$  electrons/cm<sup>2</sup> using a beam current of  $1.5 \times 10^{12}$  electrons/cm<sup>2</sup>s. Due to non-uniformity of the electron beam, there is a

10% uncertainty in the fluence. Irradiation was performed at room temperature ( $< 25^\circ\text{C}$ ) by placing the solar cells on a temperature-controlled table. Further, the samples were put in a nitrogen atmosphere in order to prevent ozone formation. In the remainder of this chapter, the state of the solar cells or material after irradiation using  $1.9 \times 10^{16}$  electrons/cm<sup>2</sup> will be called the degraded state.

The external parameters as a function of the electron-beam-irradiation fluence are shown in figure 5.2. Following high-energy electron-beam irradiation a statistical deviation of up to 20% has been found in the external parameters of solar cells of a particular thickness and irradiated with a particular fluence. This deviation seems to be correlated to the fluence: the higher the fluence, the higher the deviation. Furthermore, approximately 5% of the cells were shunted after irradiation. Shunt repair was not used to reactivate the cells and these cells were not analyzed nor used in the statistics any further. The results for the external parameters given here are averaged over the 6 most efficient out of 10 cells that were irradiated at that particular condition. All cells were characterized within 3 days after irradiation in order to minimize room-temperature annealing effects. After irradiation using the highest fluence the efficiencies of the solar cells dropped to approximately 1.4% to 3.3% and degradation was observed in all external parameters. The results for the external-parameter and QE degradation are discussed in more detail below.

The  $FF$  is often seen as a good indication for the total recombination in the cell, because it is closely related to the defect density of states in the material [48]. It is also the largest contributor to the degradation of the solar cells following electron-beam irradiation, especially for thin solar cells. The experimental results (markers) for the  $FF$  are given in figure 5.2. As-deposited  $FF$ s were in between 0.64 and 0.72, depending on the thickness, where the thinner cells had the highest  $FF$ . After degradation,  $FF$  dropped to values between 0.286 and 0.472. The drop in  $FF$  is larger for cells with a thick i-layer: the 150-nm cell drops 0.25 (35%) in  $FF$ , while the 900-nm cells drops 0.354 (55%). Remarkably, the thin solar cells show some initial stability against the irradiation before  $FF$  degradation is observed.

The  $V_{oc}$  degradation is the smallest contribution to the performance degradation. Figure 5.2 shows the experimental results (markers) for the  $V_{oc}$  as a function of the fluence. As-deposited open-circuit voltages of  $0.835 \pm 0.06$  V were obtained, with thinner cells having the highest  $V_{oc}$ . However, this dependence on the i-layer thickness is small. After irradiation the  $V_{oc}$  shows a decrease between 0.07 V (8%)

## 5. Degradation of solar cells by high-energy electrons

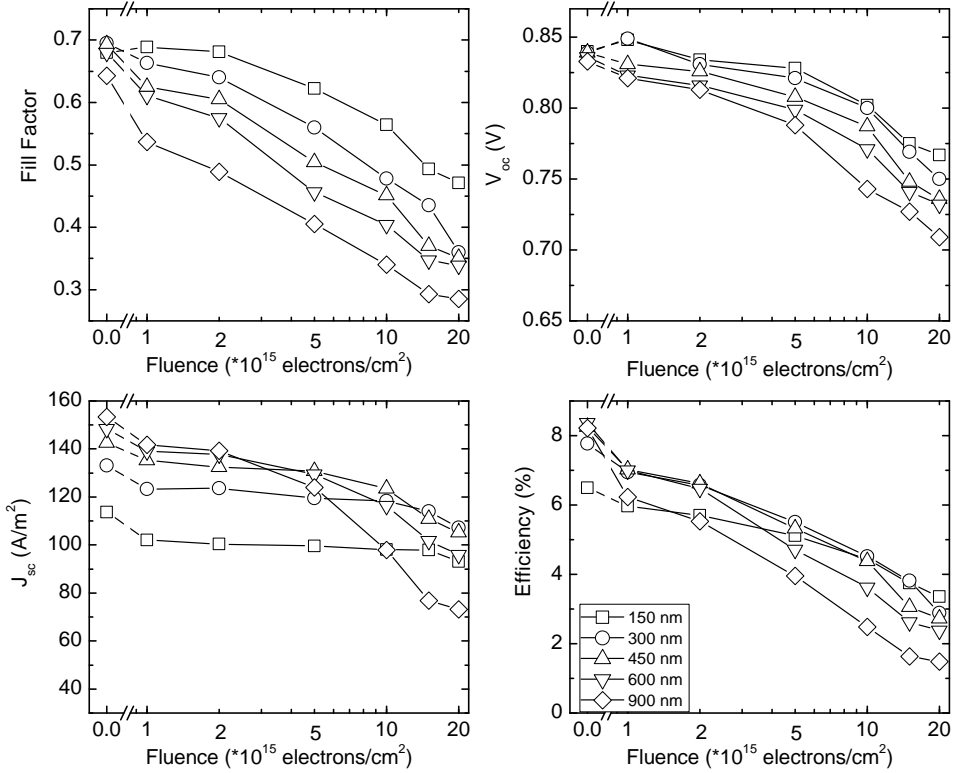


**Figure 5.2:** The external parameters of a-Si:H solar cells with different i-layer thickness as a function of the electron-beam-irradiation fluence.

and 0.12 V (14%) depending on the i-layer thickness, where the thinner cells are more stable, especially at lower fluences.

The influence of the i-layer thickness is most obvious on the degradation of the  $J_{sc}$  as can be seen in figure 5.2. In the as-deposited state the  $J_{sc}$  ranged from 112 to 153 A/m<sup>2</sup>, where thick solar cells have the highest  $J_{sc}$ . In the degraded state this situation is almost reversed. The 150-nm shows almost no degradation, while the 900-nm cell degraded more than 80 A/m<sup>2</sup> to value of 72 A/m<sup>2</sup> (a drop of 52%). The thinner solar cells also show initial stability against the irradiation and only for higher fluences significant degradation is found. The  $J_{sc}$  for each i-layer thickness shows the similar dependency on the fluence as was found by Srour et al. [28] in the degradation of proton- and electron-beam-irradiated tandem solar cells. They used the following equation to describe the  $J_{sc}$  variation:

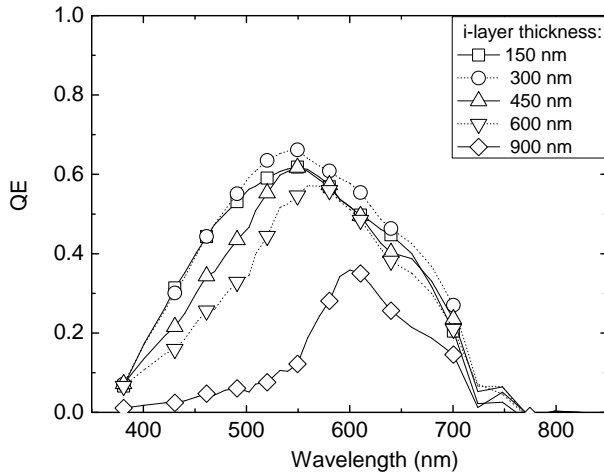


**Figure 5.3:** The quantum efficiency, QE, of cells with different i-layer thickness following electron-beam irradiation at the highest fluence.

$$J_{sc}(D_i) = J_{sc}(0)(1 - k_i D_i), \quad (5.1)$$

where  $D_i$  is the incident ionizing dose, which is directly related to the fluence, and  $k_i$  a constant that was experimentally determined to be  $1.1 \times 10^{-9} \text{ rad(Si)}^{-1}$  (here 1 rad(Si) corresponds to a fluence of  $3.4 \times 10^7 \text{ electrons/cm}^2$ ). Using equation 5.1 in our case we found values for  $k_i$  between  $1.3 \times 10^{-10} \text{ rad(Si)}^{-1}$  for 150-nm thick cell and  $1.0 \times 10^{-9} \text{ rad(Si)}^{-1}$  for the 900-nm cell. These values indicate that the  $J_{sc}$  in our single-junction a-Si:H solar cells is more tolerant to electron-beam irradiation than for the tandem a-Si:H solar cells used by Srour et al. [28]. We note that they did not specify the thickness of the tandem solar cells.

Of course, the most important parameter to determine the usability of these cells for space application is the efficiency. After the highest irradiation fluence the efficiencies of the solar cells dropped to 1.5% and 3.4%, depending on the i-layer thickness (figure 5.2). For each thickness significant degradation is observed, but the thinner cells are more stable against the irradiation at lower fluences. The efficiency of the 150-nm thick solar cells degraded 48%, while that of the 900-nm thick cell degraded more than 82% following the highest irradiation fluence.

Changes in QE at zero bias are closely related to the  $J_{sc}$  degradation. Figure 5.3 shows the QE of the series of solar cells in the degraded state. In agreement with the  $J_{sc}$  data, the QE of thicker cells degrade more. Compared to the as-

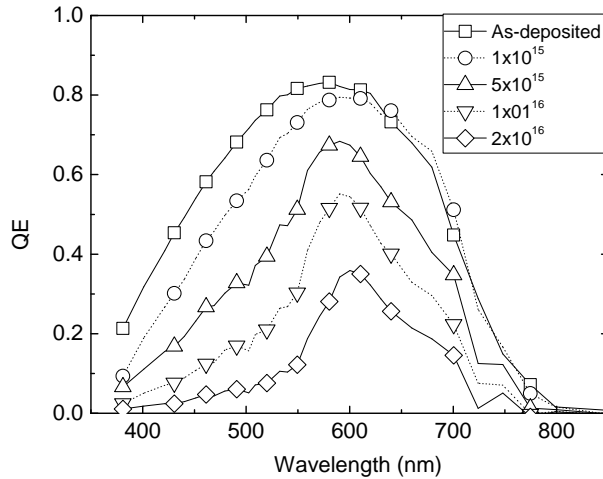


**Figure 5.4:** The quantum efficiency, QE, of 900-nm cells following electron beam irradiation versus the fluence. Note that for each QE curve a different solar cell was used.

deposited state of the solar cells (figure 5.1), the thin solar cells degrade most in the short wavelength range of up to around 550 nm. For thicker solar cells the QE degradation is more pronounced and is observed across the entire wavelength range. After irradiation the 900-nm cells show a distinct peak in QE around 600 nm. For lower fluences the similar trends were observed.

In figure 5.4 the fluence dependency of the QE of the 900-nm cells is shown. For the lowest fluence used, only a drop in the QE is observed for the wavelength range below 600 nm. When increasing the fluence further a decrease in QE across the entire wavelength range is observed, with a peak in QE around 600 nm. In the degraded state the QE is reduced more than 50% over the whole wavelength range and at some wavelengths even more than 90%.

When comparing these results to degradation by light soaking (chapter 4), the  $FF$  degradation shows a similar dependence on the  $i$ -layer thickness: thin solar cells are more stable than thick cells. This  $i$ -layer dependence is also observed in  $J_{sc}$  degradation. Degradation of the  $V_{oc}$  to the extent as observed for electron-beam irradiation was not found in the light-soaked cells. The narrowing of the QE of the 900-nm cell following electron-beam irradiation is also observed for solar cells subjected to light soaking.

### 5.3.3 Flux dependent degradation

It has been noted by Danesh et al. [41] that there are many similarities between electron-beam and light-induced degradation. Therefore it was suggested that the degradation in a-Si:H solar cells due to high-energy-charged-particle irradiation is due to similar or even the same degradation processes as with light soaking. Many groups have studied the Staebler-Wronksi effect and it is generally accepted that electron-hole pair recombination initiates the defect-creation process, see for instance Biswas et al. [89] and Branz et al. [91]. For the case of continuous light-soaking of a-Si:H, the following relation was found [87]:

$$\Delta N_D(t) = a \cdot t^{1/3} \cdot G^{2/3}, \quad (5.2)$$

where  $\Delta N_D(t)$  is the increase in defect density over time,  $t$ ,  $a$  is a rate constant, and  $G$  is the electron-hole-pair generation rate density due to the illumination. A similar dependence has been reported for light soaking of a-Si:H solar cells [121, 122]. If the defect-creation mechanism in electron-beam irradiated a-Si:H is also initiated by electron-hole-pair recombination, it is expected that the degradation would depend on the incident electron flux, because this flux is equivalent to the light intensity during light soaking.

In order to verify if recombination events play a role in the degradation of a-Si:H due to electron-beam irradiation, we have irradiated single-junction solar cells with different i-layer thickness using varying electron fluxes, while keeping the fluence constant. The electron flux was varied from  $5 \times 10^{11}$  to  $1 \times 10^{13}$  electrons/cm<sup>2</sup>s and the fluence was  $5 \times 10^{15}$  electrons/cm<sup>2</sup>. Due to the increased incident energy flux when increasing the electron flux, the temperature of the samples during irradiation increased up to 35°C at the highest flux.

We like to point out that compared to the space environment the electron flux used in this experiment is very high: within 10 minutes of electron-beam irradiation in this experiment an incident fluence is achieved that is similar to the equivalent electron fluence for a one year space mission in a high-radiation orbit [85, 123].

Figure 5.5 shows the external parameters following irradiation as a function of incident electron flux. For low fluxes similar degradation behavior with respect to the i-layer thickness and fluence is observed as found in section 5.3.2: thick solar cells degrade more than thin cells. Also the amount of degradation is comparable. The  $FF$  decreased to 0.4 and 0.6, where the thicker cells had the lowest  $FF$ . The  $V_{oc}$  was between 0.79 V and 0.84 V, with the thicker cells having the lowest  $V_{oc}$ .

## 5. Degradation of solar cells by high-energy electrons

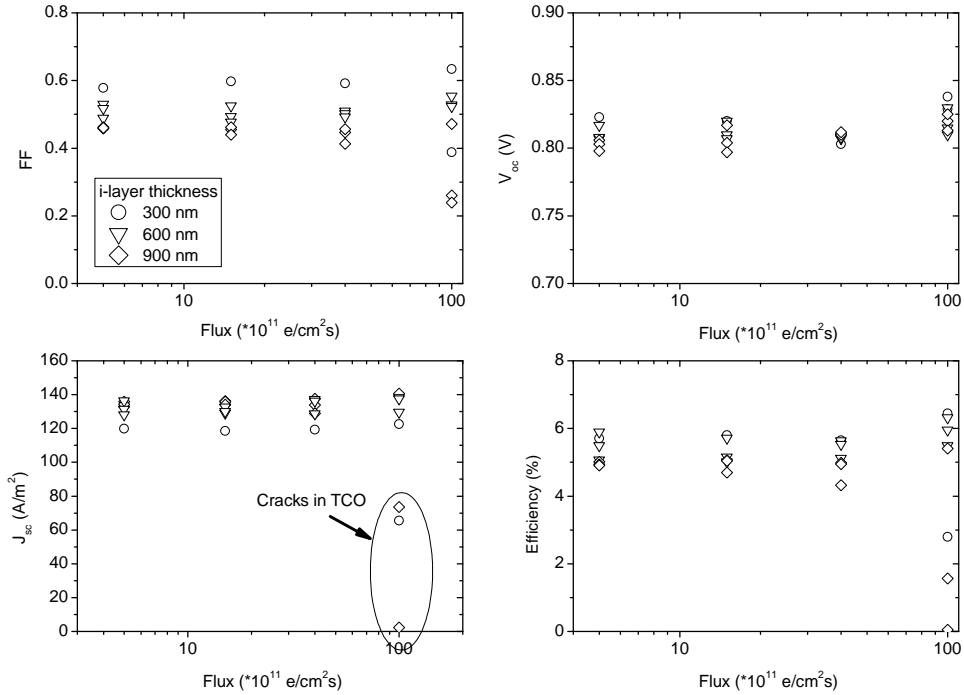


**Figure 5.5:** The variation of the external parameters as a function of the incident electron flux following 1-MeV electron irradiation using a fluence of  $5 \times 10^{15}$  electrons/cm<sup>2</sup>.

The  $J_{sc}$  was lowered to 100 A/m<sup>2</sup> and 120 A/m<sup>2</sup>. In agreement with the results presented in figure 5.2 no significant thickness trend is found for *this* fluence. The cell efficiencies were in between 5% and 6% following irradiation using low fluxes, whereas at higher fluxes some cells showed much more degradation. This larger degradation at high electron fluxes is most notably due to  $J_{sc}$  and  $FF$  degradation.

On the basis of the results shown in figure 5.5 we think that the degradation of the external parameters is unaffected by the flux, except for the highest flux. At this high flux a large increase in degradation is observed for some cells. However, we think that this extra degradation is not due an increase in defect density in the solar cell. In the cells subjected to these high electron fluxes visible cracking of the TCO layer was observed following the irradiation with the highest flux.

Figure 5.6 shows a picture of such a crack in the TCO near an Al bus bar used to collect the current from the TCO. The cracks are visible by a change in color

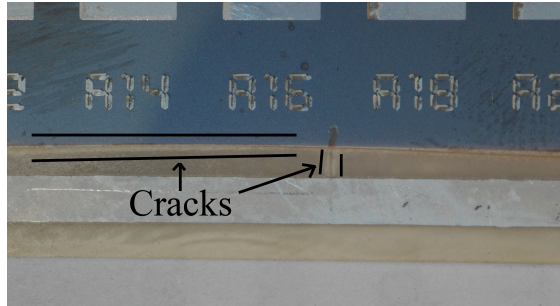


**Figure 5.6:** A crack in the TCO near the Al bus bar due to electron-beam irradiation using a high flux of  $1 \times 10^{13}$  electrons/cm<sup>2</sup>s.

of the substrates, because of ZnO:Al coating appeared to be removed. The cracks were only observed in the uncovered ZnO:Al. No cracking underneath the a-Si:H solar cell was found. The cracks are typically observed parallel along the Al bus bar on the front contact. The cracks are typically less than 0.5 mm wide and may be a few centimeters long. In the picture also a crack perpendicular to the Al bus bar is observed. These cracks lead to a higher series resistance between the actual solar cells and the bus bar, which suppresses the  $FF$  and  $J_{sc}$ . The cells unaffected by the cracks appear to show even a higher radiation tolerance when subjected to the highest flux as compared to the cells irradiated with lower fluxes. This can be explained by a slightly higher substrate temperature during the irradiation because of the higher energy flux. The temperature of the table where the cells during the irradiation was approximately 10°C higher during the irradiation with the highest flux as compared to the lowest flux. This higher temperature could have resulted in in-situ annealing during the irradiation, leading to less degradation. Another explanation could be the larger inaccuracy in determining the total fluence incident the sample when using higher fluxes.

In conclusion, we do not observe differences in the performance degradation of solar cells when increasing the incident electron flux, which might indicate that electron-hole pair recombination does not play a role in the degradation of a-Si:H by electron-beam irradiation. It may be argued, however, that the density of electron-hole recombination events was unaffected by increasing the electron flux, because of the different way the electron-hole pairs are generated in a-Si:H during electron-beam irradiation in comparison to light soaking. With high-energy-charged-particle irradiation the electron-hole pairs are generated al-

most instantly along the traveled path of the incident particle, thus creating a tube of electron-hole pairs in the cell. Only when two of these tubes overlap, an increase in the recombination rate is expected. We have estimated that a tube has a lifetime of approximately 100 ps to 10 ns due to e-h pair recombination within the tube. However, a lifetime for the tubes of at least 56 ns to 0.8  $\mu$ s is needed to have overlap between tubes for the highest fluence used,  $1 \times 10^{13}$  electrons/cm<sup>2</sup>s. For this reason we assume that there is virtually no overlap between the tubes, implying that no increase of electron-hole pair recombination events will occur when increasing the electron-beam flux with more than one order of magnitude. This calculation is discussed in more detail in appendix A. It is therefore difficult to conclude from this experiment if electron-hole pair recombination plays a role in the degradation due to electron-beam degradation.

We like to point out that compared to the space environment the electron flux used in this experiment is very high: within 10 minutes of electron-beam irradiation in this experiment an incident fluence is achieved that is similar to the equivalent electron fluence for a one year space mission in a high-radiation orbit [85, 123].

### 5.3.4 Degradation under open- versus short-circuit condition

We carried out another experiment in order to establish if defect creation in a-Si:H solar cells subjected to electron-beam irradiation is initiated by electron-hole pair recombination. In this experiment the difference in degradation of open- and short-circuited cells is investigated. Short-circuiting the cells leads to a higher internal electric field in the cell and therefore increases the current collection and reduces the recombination rate. If electron-hole pair recombination plays a role in electron-beam degradation, then irradiating the cells under short-circuit condition would lead to less degradation of the performance as compared to irradiating the cell under open-circuit condition, like has been demonstrated for light-induced degradation (chapter 4). If no difference in the performance degradation is observed, it is unlikely that the defect-creation mechanism is indeed initiated by electron-hole pair recombination.

A series of solar cells with different i-layer thickness (from 150 to 900 nm) were irradiated under both open- and short-circuit conditions. The fluence was varied between  $5 \times 10^{15}$  and  $2 \times 10^{16}$  electrons/cm<sup>2</sup> using a beam current of

$1.5 \times 10^{12}$  electrons/cm<sup>2</sup>s. Half of the cells were short-circuited by applying silver paste between the front and back contacts. For each short-circuited cell, the resistance between both contacts was measured to be less than  $5 \Omega$  before and after the irradiation. After irradiation the connections were removed by cleaning with iso-propanol and no extra shunting due to traces of silver paste was found.

The results of the degradation in the external parameters of the solar cells under open and short-circuit conditions are presented in figure 5.7. Similar to the results presented in section 5.3.2 the degradation in  $FF$  is the major contributor to the drop in efficiency. The thickness dependency is most obvious in the degradation of the  $J_{sc}$ , in which we observe again that the thin cells are more tolerant against the irradiation. Finally, the  $V_{oc}$  in this experiment shows a similar decrease as shown in section 5.3.2. The most important conclusion from this experiment is that there does not appear to be a difference in the degradation of the external parameters, irrespective if the solar cells are degraded under open- or short-circuit condition.

Granata et al. [30] suggested that the load conditions may play a role in the degradation by charged particle irradiation. However, we find no difference in degradation rate between open- and short-circuited cells when irradiating the cells with 1-MeV electrons. This observation is quite different when compared to degradation results due to light soaking and therefore suggests that the degradation by electron-beam irradiation is not initiated by electron-hole pair recombination. Therefore, we assume that the degradation mechanism is due to collisions of incident electrons with the a-Si:H lattice. In chapter 6 we will discuss the idea further. We have found similar results as Wagner et al. [124] and Herbst et al. [125], who found that the  $J_{sc}$  degradation using keV electrons was the same for irradiation under open- or short-circuit conditions. However, keV irradiation leads to a non-uniform degradation profile and most damage is induced in the back of the solar cell, where the internal electric field is high both in open- and short-circuit conditions resulting in similar recombination statistics at that location. It could have masked a dependency of the degradation on the electron-hole pair generation rate in their case.

## 5. Degradation of solar cells by high-energy electrons

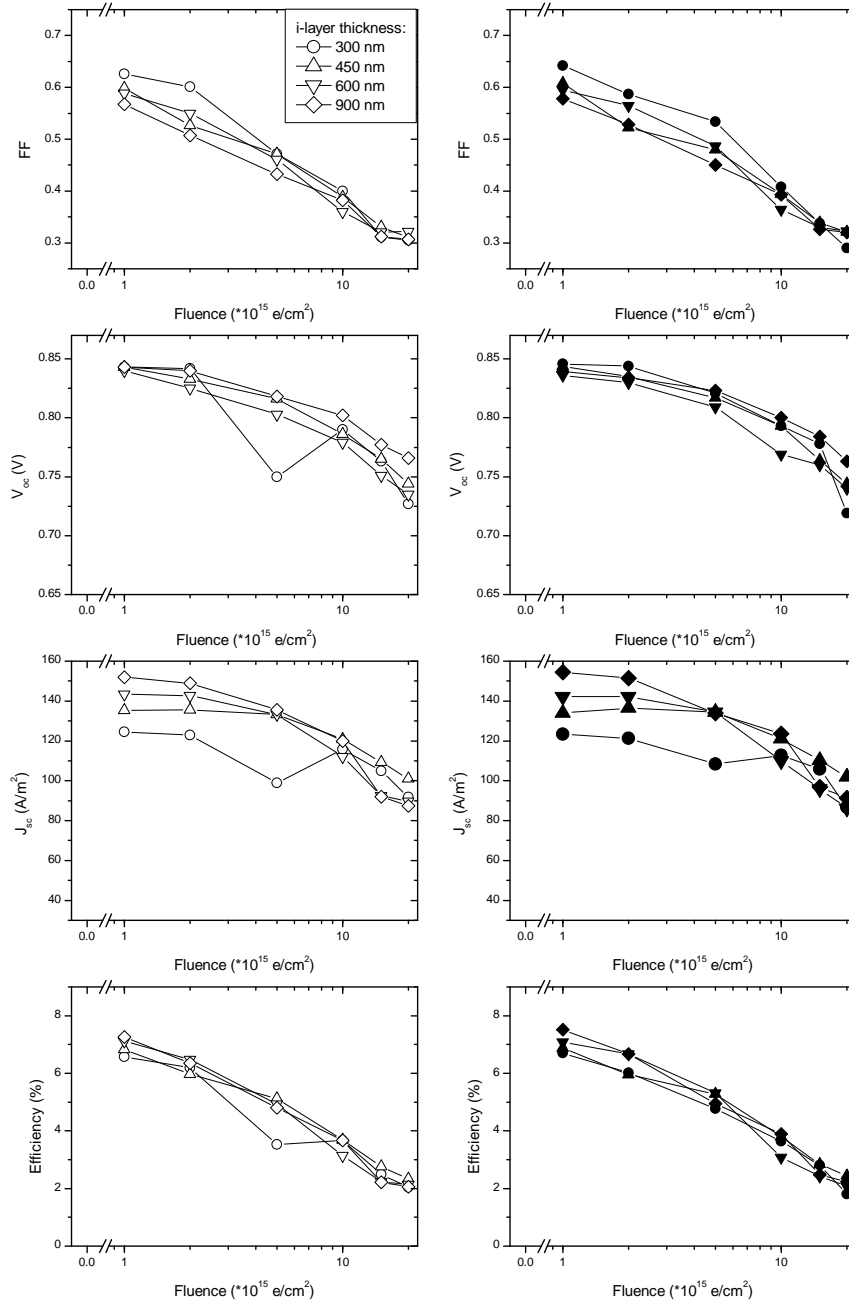


**Figure 5.7:** Variation of the external parameters as a function of the electron-beam fluence following 1-MeV electron-beam irradiation under both open-circuit (left-hand graphs) and short-circuit conditions (right-hand graphs).

**Table 5.2:** Input parameters used for the electrical simulations of a-Si:H solar cells in the as-deposited state.

Doped layers	
Activation energy p-layer	0.55 eV
Activation energy n-layer	0.35 eV
Intrinsic layer	
Mobility gap	1.75 eV
Effective DOS valence band	$4 \times 10^{26} \text{ m}^{-3}$
Effective DOS conduction band	$4 \times 10^{26} \text{ m}^{-3}$
DOS at valence band edge	$2 \times 10^{27} \text{ m}^{-3} \text{ eV}^{-1}$
Characteristic energy valence band tail	0.045 eV
Hydrogen concentration	$5 \times 10^{27} \text{ m}^{-3}$
Si-Si bond concentration	$2 \times 10^{29} \text{ m}^{-3}$
Width of defect pool	0.185 eV
Position of defect pool (relative to valence band)	1.20 eV
Electron mobility	$28 \times 10^{-4} \text{ m}^2 \text{ V}^{-1} \text{ s}^{-1}$
Hole mobility	$8 \times 10^{-4} \text{ m}^2 \text{ V}^{-1} \text{ s}^{-1}$

## 5.4 Simulation results

### 5.4.1 Simulations of the as-deposited cells

The experimental results presented in section 5.3.1 have been matched with simulations using the computer program called ASA to obtain a base parameter set, which is used in our method to simulate the degradation of a-Si:H solar cells by particle irradiation and light soaking. More explanation on the method and the ASA simulation program can be found in chapter 3. In this section we focus on the parameter set, the simulation results, and the match between the simulations and experiments.

The multi-rough-interface optical model GENPRO3 was used to calculate the electron-hole pair generation profile in the solar cell under an AM 1.5 spectrum. In this optical model light-trapping effects are included.

Relevant ASA input parameters corresponding to the as-deposited state are given in table 5.2. In the simulations of each solar cell only the i-layer thickness is varied, while the other parameters are kept constant. Using this parameter set, ASA provides a good match between the experimental and simulated results of

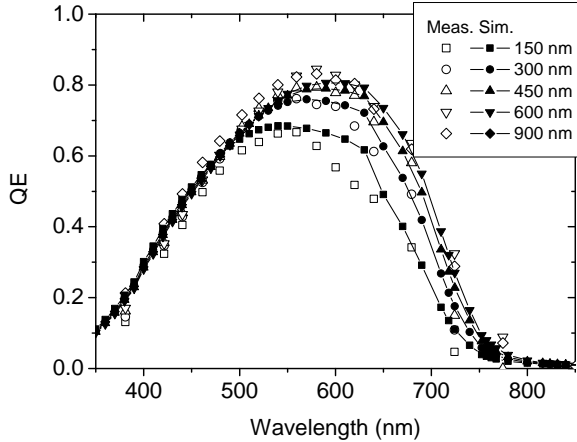


**Figure 5.8:** The experimental (open markers) and simulation results (lines and closed markers) of the QE for cells with different i-layer thickness.

the as-deposited solar cells as well as for the QE for each i-layer thickness.

Table 5.1 compares the simulation results of the external parameters with the measurements of the solar cells for the thickness series in the as-deposited state. Overall, the difference between the measurement and simulation result is within 10% for each external parameter and in the simulations the same trends are found for the external parameters as a function of the i-layer thickness as reported in section 5.3.1. Increasing the i-layer thickness leads to an increase in  $J_{sc}$ , a lowering of the  $FF$  and has little effect on the  $V_{oc}$ . The 900-nm thick solar cell, however, has a slightly lower  $J_{sc}$  than the 600-nm cell, which was not observed in the measurement data. Examining the results in more detail we notice that the simulated  $V_{oc}$  is slightly too high for each solar cell thickness. Furthermore, the difference between the  $FF$  of the thickest and thinnest cell is slightly higher in the simulations. For the thinner cells the  $FF$  is overestimated in the simulations. We note, however, that the spread in the  $FF$  results of the 150-nm thick solar cells is quite large and some cells did have an experimental  $FF$  above 0.72. We ascribe this large spread in results to some shunting effects, which are frequently observed when the i-layer thickness is decreased. In the  $J - V$ -simulations a higher  $J_{sc}$  is found for the thin cells (150 and 300 nm) than in the experimental results.

Figure 5.8 shows the match between the measurements (markers) and the simulations (lines) of the QE. At shorter wavelengths the simulated and measured

QE are almost similar and in this wavelength range the QE is mainly determined by the low transmission of the substrates. At longer wavelengths the thicker solar cells show a higher QE, because of an increase in the electron-hole pair generation rate in the thicker cells in comparison to thin cells. Overall, the simulations follow the measurements within 10%, except in the wavelength range between 550 nm and 600 nm. In this region the QE is overestimated in the simulations, especially for the 150-nm cell.

### 5.4.2 Simulations of electron-beam irradiated cells

In order to improve our understanding of the degradation of electron-beam irradiated solar cells, we matched the experimental results presented in section 5.3.2 to results of computer simulations, using our procedure to describe changes in the defect-density profile in degraded a-Si:H solar cells. If a satisfactory match is obtained, this procedure could be used to predict the EOL-efficiency for a space mission. Our procedure is explained in more detail in chapter 3. The parameter set presented in section 5.4.1 is taken as the baseline set. In chapter 2 three major degradation effects in a-Si:H solar cells irradiated by electrons were identified: reduction of the transmission of the glass, increase in the activation energy of doped a-Si:H, and increases in the defect density in the intrinsic a-Si:H. By matching experimental to simulation results we are able to extract the fluence dependence of the activation energy and the defect density in irradiated a-Si:H solar cells.

Part of the degradation of the solar cells is due to the reduction of the transmission of the glass substrate following electron-beam irradiation and in order to take this effect into account the results obtained from the transmission measurements following irradiation (see section 2.2.1) are used to calculate the absorption spectrum of the glass related to that particular fluence. Therefore in the optical simulations in ASA the absorption of the substrates related to the as-deposited state is exchanged for the absorption spectrum of the irradiated state in order to simulate the transmission reduction of the substrates. The real part of the refractive index is kept constant at 1.5. From simulations in which only the transparency of the CMZ substrates is altered it is concluded that this effect will only result in a drop of the  $J_{sc}$  of 13 to 14 A/m<sup>2</sup> at most, while lowering the QE for wavelengths shorter than 600 nm. The  $V_{oc}$  and  $FF$  change less than 1% due the reduction of the transmission. This effect is not used as a matching parameter.

In section 2.2.4 we showed that activation energy of p- and n-doped layers

increased following irradiation. An increase of up to 0.25 eV was found. However, this result cannot be directly converted to a change in Fermi-level position in the thin doped layers of an a-Si:H solar cell, because in the solar cell the position of Fermi level in the doped layers is also dependent on the properties of the Schottky front and back contacts. In the ASA program the position of the Fermi level is controlled by the activation-energy parameter. In the simulations the activation-energy parameter,  $\Delta E_{act}$ , for the doped layers following irradiation is chosen in such a way that a good match for the  $V_{oc}$  is obtained. We think that this procedure is justified, because we showed in section 3.4.2 that the  $V_{oc}$  is mainly determined by the activation energy of the doped layers and is much less affected by changes in the defect density of states and distribution, or by transmission loss of the glass. More details on the effects of increasing activation energy of the doped layers on the solar-cell performance are presented in section 3.4.2.

In chapter 2 we showed that the defect density in the material increases significantly as a result of electron-beam irradiation[41, 53, 126–128]. The results of section 5.3.3 and 5.3.4 suggest that the degradation following electron-beam irradiation is not linked to electron-hole pair recombination, but is most likely due to damage by direct interaction of the incident electrons with the a-Si:H. Because the energy deposition of the incident electron beam is uniform across the cell, we assume in this chapter that the induced defect-creation-depth profile in each solar cell is also uniform. In addition, we assume the same profile for each solar-cell thickness irradiated with the same fluence. Further, we have found in section 3.4.3 that the distinct QE peak of the degraded 900-nm solar cell (see section 5.3.2) could only be reproduced in the simulations by increasing the mid-gap defect density of states. Therefore, in the simulations presented here only the as-deposited  $D_z$  defect-state distribution is increased, which leads to a higher defect density of states in the middle of the band gap. The  $D_e$  and  $D_h$  densities are not changed. At each fluence this  $D_z$  density is changed by choosing the  $C_z$  parameter in equation 3.5 in such a way that at that particular fluence the best match between the experimental and the simulation results is obtained. Note that the induced defects states do not need to be neutral in the degraded state.

With the two thickness-independent input parameters,  $C_z$  and  $\Delta E_{act}$ , in our method, the experimentally observed degradation of the external parameters and the QE can be matched satisfactory for each solar-cell thickness as will be shown in more detail below.

In figure 5.9 we have plotted the simulation (lines) and experimental (mark-

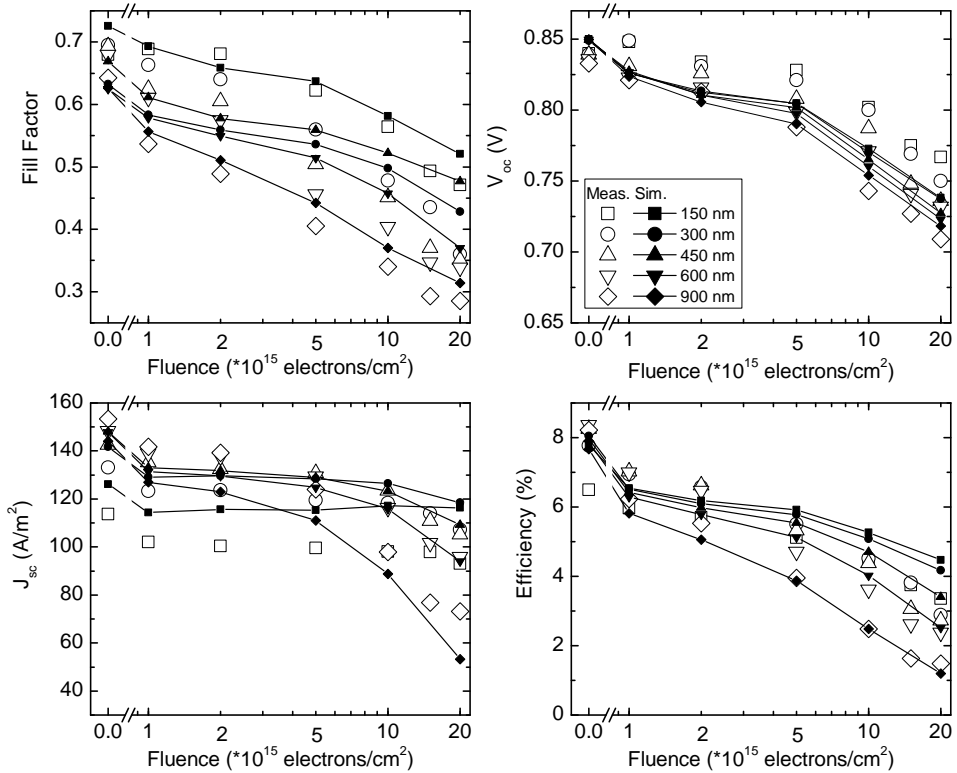


**Figure 5.9:** Measured (open markers) and simulated (lines with closed markers) external parameters for solar cells with different i-layer thickness as a function of the irradiation fluence.

ers) results of the external parameters versus the fluence. Simulated as-deposited  $FF$ s were in between 0.63 and 0.73, with the thinner solar cells having a higher  $FF$ . The as-deposited solar cells had an  $FF$  of 0.64 to 0.70, with the same thickness trend. After degradation the simulated  $FF$ s dropped between 0.20 and 0.32, where the thicker solar cells are less tolerant against irradiation. In the measurements a drop between 0.23 and 0.35 is observed, where the thicker cells showed more degradation. At higher fluence the simulations tend to underestimate the degradation. Further, the simulated  $FF$ s of the 300-nm, 450-nm, and the 600-nm thick cell are smaller at lower fluences and larger at higher fluences when compared to the experimental results.

A reasonable match is found for the  $J_{sc}$  degradation as can be seen in figure

5.9. The simulation as well as the experimental results can be fitted satisfactory using equation 5.1 as suggested by Srour et al. [28]. For the 300-nm, 450-nm and 600-nm solar cells the  $k_i$  value (see equation 5.1) found in the simulations is within 10% from the experimentally obtained values. Compared to the measurements, the simulation of the 150-nm thick solar cell has a lower  $k_i$  value, which implies that the cell degrades less, whereas the 900-nm thick cells show more degradation in the simulations as was found experimentally. We suggest that the mismatch in the  $J_{sc}$  for the thinner solar cells is due to the used optical parameter set for the silver contacts. We think that these properties are not entirely correct, resulting in a reflection at the back contact that is too high and thus an overestimation of the  $J_{sc}$ .

Included in figure 5.9 are the simulations of the  $V_{oc}$  (lines) for each i-layer thickness. For the solar cells in the as-deposited state the  $V_{oc}$  hardly varies with i-layer thickness and values of  $0.835 \pm 0.006$  V are obtained. In the simulations the degradation leads to a decrease between 0.11 V and 0.15 V and also in this case the thin solar cells are more stable against irradiation. A good match between the simulations and the measurements is obtained for the thicker cells, however, for the thin cells the simulations seem to overestimate the degradation of the  $V_{oc}$  slightly, especially at higher fluences.

The match between simulation and measurement results is best for the efficiency of the thicker cells. For the thinner cells at higher fluences, the simulations lead to an overestimation of the efficiency. This overestimation is mainly due to the mismatch between the measured and simulated  $J_{sc}$ , although the simulated  $FF$ s are also higher than the measured results.

In figure 5.10 the simulated (lines and closed markers) and experimentally-obtained (open markers) QE are shown following irradiation using the highest fluence. A reasonable match is obtained over the whole wavelength range and for each solar-cell thickness. The difference between the measured and simulated QE is typically smaller than 0.1, although in some regions this difference is somewhat larger. The simulations of thinner cells overestimate the QE around 500 to 700 nm, which according to us is also an indication that the optical properties of the Ag-Al contacts are not entirely correct. Further, the distinct peak in QE observed for the 900-nm thick solar cell is shifted to higher wavelengths in the simulations and this effect may be related to the chosen ratio between the hole and electron mobilities in the simulations or to a slight mismatch in the energy location of the induced defects in the bandgap.

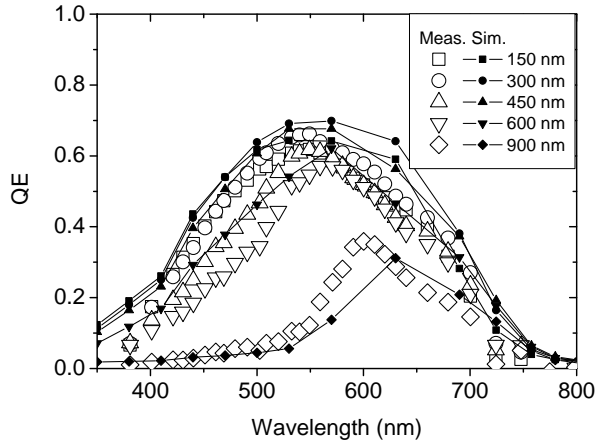


**Figure 5.10:** Measured (markers) and simulated (lines and closed markers) QE for solar cells with a varying i-layer thickness after irradiation using a fluence of  $1.9 \times 10^{16}$  electrons/cm<sup>2</sup>

By matching the experimental to the simulation results the fluence dependency of the change in Fermi-level position in the doped layers,  $\Delta E_{act}$ , and the increase in defect density in a degraded solar cell,  $C_z$ , are extracted. In case the degradation is due to collision events in the material as was assumed by the simulations presented in this chapter, a linear relation of the defect density with the fluence is expected. If a degradation mechanism similar to the Staebler-Wronski effect is expected, the defect density is expected to have a fluence dependency between 0.33 and 0.66, as was found when a-Si:H samples were degraded using high-energy lasers [60].

Figure 5.11 shows  $C_z$  versus the fluence and figure 5.12 shows the change in activation energy of the doped layers. We find that  $C_z$  shows a more or less linear dependence on the fluence, which indicates that the damage induced in the a-Si:H solar cells is directly due to incident electrons and thus is governed by collision events. Using these  $C_z$  values in the simulations the defect density is increased by a factor of 50 at the highest fluence. The experimental results presented in chapter 2 suggest that the defect density increases by one to two order of magnitude following irradiation using the highest fluence. It is expected that  $C_z$  is dependent on the properties of the as-deposited material, but this has not been verified in our investigations.

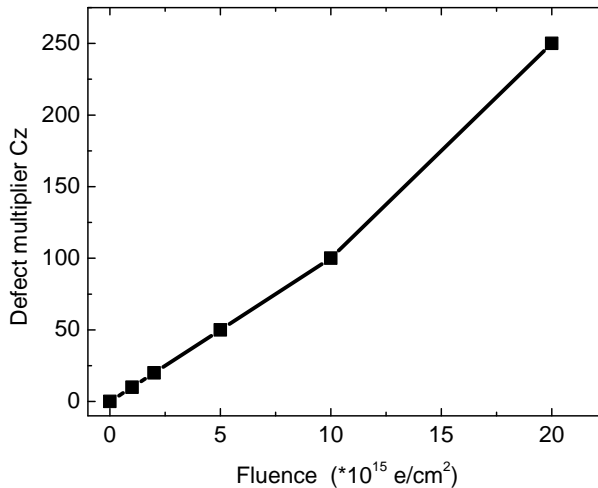


**Figure 5.11:** The  $C_z$  value, found by matching the experimental results with simulations, as a function of the fluence.

The increase in activation energy extracted from the simulations is slightly smaller to the observed changes found in section 2.2.4: experimentally a change of 0.25 eV was found and the simulations suggest only a change of 0.15 eV for the highest fluence. The activation-energy increase in the simulations shows also more or less a linear dependency on the fluence.

## 5.5 Conclusions

In this chapter the degradation of a-Si:H solar cells by electron-beam irradiation has been studied in order to develop a model to predict the EOL performance. Therefore, a series of solar cells with different i-layer thickness was deposited and exposed to 1-MeV electron-beam irradiation. We have varied the fluence, the beam current, and performed irradiation under open- and short-circuit conditions. The cells were characterized by their external parameters and the QE. We found that thinner cells are more stable against the irradiation, similar to light soaking. The drop in  $FF$  is the most important parameter in the degradation of the cell efficiency. The thickness dependence was strongest for the  $J_{sc}$ . In contrast to light soaking, the  $V_{oc}$  degradation played a more substantial role in the degradation.

In literature it was suggested that electron-hole pair recombination events may play a role in the degradation by high-energy electrons. In order to study

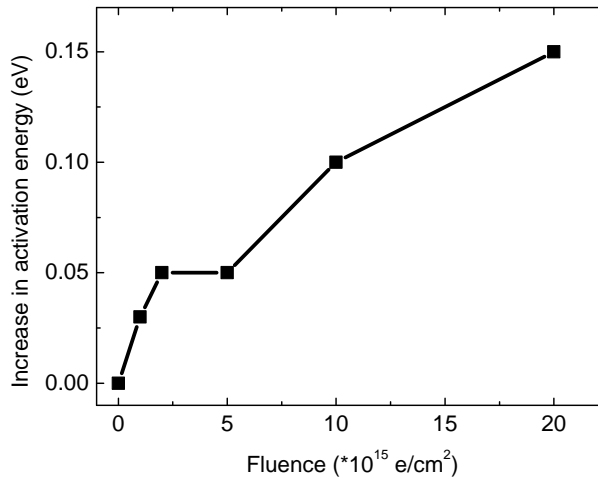


**Figure 5.12:** The activation energy of the doped layers used in the simulations as a function of the fluence.

the degradation mechanism in more detail two dedicated experiments were carried out. In the first experiment the influence of the incident electron flux on the degradation was studied. No dependency of the a-Si:H solar-cell degradation on the flux was found, apart from cracking of the TCO layer. In the second experiment the difference was investigated between electron-beam induced degradation of open- and short-circuited solar cells. However, also in this experiment no difference in degradation rate was observed. Neither experiment provided evidence that electron-hole pair recombination events play a role in the degradation and we suggest that the degradation is governed by collisions of the incident electrons in the a-Si:H.

In chapter 2 three material-property changes were identified that contribute to the a-Si:H solar cell degradation by electron-beam degradation: (i) an increase in the density of defect states, (ii) increases in activation energy of the doped a-Si:H layers, and (iii) reduction of the light transmission of the substrates. Using our procedure as presented in chapter 3 to simulate degraded solar cells, the experimental results of the solar-cell performance following electron-beam irradiation have been matched to computer simulations. Overall, a reasonable match of the external parameters and QE between the experimental and simulation results was obtained. It was found that the  $V_{oc}$  degradation is mainly affected by the change in the activation energy of the doped layers and is hardly influenced by

the other two effects. The transmission loss of the glass mainly reduces the  $J_{sc}$  by approximately  $14 \text{ A/m}^2$ , independent of the solar-cell thickness. The best results to model the  $FF$  and  $J_{sc}$  degradation are obtained by increasing the as-deposited  $D_z$  state density depth profile uniformly for each solar cell. Using computer simulations we found that the defect density and the activation energy of the doped layer increase more or less linear with fluence, which also suggests that electrons induce displacements in the material.

## Chapter 6

# Degradation of solar cells by high-energy protons

### 6.1 Introduction

During a space mission solar cells are not only subjected to irradiation by electrons, but also to a range of other particles, like protons. For certain orbits like the Medium Earth Orbits (MEO), the proton flux is even higher than the electron flux [30]. It has been reported that a-Si:H solar cells are less tolerant to proton irradiation [28]. In principle, no fundamental difference is expected between the degradation mechanism by either proton or electron irradiation. Both particles lose most energy through Coulomb interaction with electrons in the material, leading to ionization events and generation of electron-hole pairs in the material. Both incident electrons and protons may also produce displacements in the material by elastic collisions with the lattice, provided the kinetic energy is sufficient. However, because of the higher rest mass of the protons, the energy deposition into a-Si:H is higher for proton irradiation when the same kinetic energy of the incident particle is assumed, leading to more ionizing and displacement events during irradiation.

Woodyard et al. [40] studied the  $J_{sc}$  degradation of a-Si:H solar cells using various proton and electron energies. They found no clear link between the displacement damage induced in the material by the incident particles and the solar-cell degradation. Similarly, Srour et al. [28] concluded that the  $J_{sc}$  degrada-

tion is not correlated to the so-called Non-Ionizing-Energy-Loss (NIEL) value of the incident particles, but to the Ionizing Energy Loss (IEL), which is in contrast to the  $J_{sc}$  degradation of c-Si solar cells. Here, the NIEL value may be considered as a measure for the amount of energy dissipated into displacement events by the incident particle. Because of the observed correlation between the  $J_{sc}$  degradation and the IEL, they suggested that free charge carriers, generated by the high-energy charged-particle irradiation, become trapped on the pre-existing defects leading to a lowering of the internal electric field over the cell and consequently to  $J_{sc}$  degradation. They claimed that displacement damage is only significant for low-energy proton irradiation. In addition, they found that annealing at temperatures as low as 70°C during the irradiation results in an End-of-Life (EOL) efficiency close to the Beginning-of-Life efficiency.

Lord et al. [129] found similarities in degradation behavior of single and triple junction solar cells due to 1-MeV proton irradiation. They reported no significant difference in degradation between single and triple-junction solar cells, although they found that for triple cells  $FF$  degradation is dominant at low fluences, whereas at higher fluences the  $J_{sc}$  degradation takes over. For single-junction solar cells  $FF$  degradation dominated for all investigated fluences (up to  $2 \times 10^{15}$  protons/cm<sup>2</sup>).

Kishimoto et al. [53] investigated the change in conductivity following 17-MeV proton-beam irradiation. They concluded that dangling bonds are created following irradiation and that the induced dangling-bond density can be reduced by annealing up to 450 K. No change in band gap was observed following irradiation. They also described a model to explain the high radiation tolerance of a-Si:H. In this model relaxation of defect sites in irradiated a-Si:H occurred by a collective rearrangement of the lattice surrounding these sites. In addition, free charge carriers generated near a defect site during proton irradiation may facilitate the restructuring of a-Si:H as well, removing the newly-created dangling bonds.

In order to investigate if our model to calculate the EOL performance of a-Si:H solar cells following electron-beam irradiation can be applied to other particles, we study in this chapter the influence of the kinetic energy and the type of incident particle on the performance degradation of a-Si:H solar cells. Therefore, we have irradiated single junction solar cells with 1-MeV and 65-MeV protons and compare the results to electron-beam irradiation and light soaking. In this way we vary the ratio between the IEL and NIEL values of the incident particles and we can gain further insight in the degradation mechanism following irradiation.

In the next section (6.2) we will first describe some details concerning this experiment. In section 6.3.1 the performance of the as-deposited cells used in the irradiation experiments is shown. The degradation results using 1-MeV and 65-MeV protons are shown and discussed in section 6.3.2. In the following section 6.4 we present and discuss a comparison of proton-beam degradation to electron-beam and light-induced degradation. We will provide evidence suggesting that the NIEL values used by Srour et al. [28] to calculate the amount of induced displacements in a-Si:H are not correct. Finally, in section 6.5 the main conclusions of this chapter are drawn.

## 6.2 Experimental details

In our proton-beam irradiation experiments a series of a-Si:H single-junction solar cells was used of which the thickness of the i-layer was varied between 150 and 900 nm. The solar cells were deposited on radiation-tolerant CMZ glass covered with a ZnO:Al front contact. The following stack of layers was used for the solar cell: a 5-nm thick p-type doped  $\mu$ c-Si:H layer, a 7-nm thick p-type doped a-SiC:H layer, a 10-nm thick intrinsic a-SiC:H buffer layer, an intrinsic a-Si:H layer, a 20-nm thick n-doped a-Si:H, 200-nm Ag, and finally 100-nm Al. The double p-layer structure was used to overcome the band mismatch between the p-type a-SiC:H layer and the ZnO:Al [114]. The a-SiC:H buffer layer in between the p-layer and the i-layer was implemented to improve the interface quality [118]. The cells are characterized by measuring the quantum efficiency (QE) at zero bias and the external parameters under AM 1.5 illumination. For the deposition of the solar cells one substrate of ZnO:Al covered CMZ glass was used on which two rows of fifteen cells were made. The size of each cell was 4 mm  $\times$  4 mm. The deposited solar cell was then cut into three pieces consisting of two rows of five solar cells for the irradiation experiments.

Solar cells were irradiated using a proton-beam energy of 1 MeV and 65 MeV. 1-MeV proton irradiation was performed in the TANDEM accelerator in the Physics Department of Naples University. The 65-MeV irradiation was done in the Hahn-Meitner-Institut. With the 1-MeV beam fluences up to  $1 \times 10^{14}$  protons/cm<sup>2</sup> have been used and with the 65-MeV beam  $5 \times 10^{14}$  protons/cm<sup>2</sup>. The latter is more than one order of magnitude higher as used by Srour et al. [28] or Woodyard et al. [40] in their degradation experiments. Nuclear reactions of the protons with Si atoms, leading to a decay of Si into P, may be neglected

**Table 6.1:** Measured external parameters under AM1.5 illumination for as-deposited solar cells used in the proton-irradiation experiments.

i-layer (nm)	set	$V_{oc}$ (V)	$J_{sc}$ (A/m <sup>2</sup> )	$FF$	efficiency (%)
150	1-MeV	$0.84 \pm 0.01$	$111 \pm 2$	$0.69 \pm 0.01$	$6.5 \pm 0.06$
150	65-MeV	$0.87 \pm 0.01$	$108 \pm 2$	$0.71 \pm 0.01$	$6.7 \pm 0.05$
300	1-MeV	$0.84 \pm 0.01$	$137 \pm 1$	$0.66 \pm 0.01$	$7.5 \pm 0.02$
450	65-MeV	$0.84 \pm 0.01$	$143 \pm 2$	$0.66 \pm 0.02$	$7.8 \pm 0.02$
600	1-MeV	$0.84 \pm 0.01$	$148 \pm 2$	$0.66 \pm 0.01$	$7.9 \pm 0.03$
900	1-MeV	$0.84 \pm 0.01$	$157 \pm 2$	$0.64 \pm 0.01$	$8.4 \pm 0.02$
900	65-MeV	$0.83 \pm 0.01$	$155 \pm 3$	$0.63 \pm 0.02$	$8.1 \pm 0.03$

[130]. Due to the limited area that could be irradiated, only three fluences for each beam energy were used. After irradiation, the data of the 6 best performing solar cells irradiated at a particular condition were included in the statistics.

In addition to the proton-beam degradation of a-Si:H solar cells, CMZ substrates were irradiated separately as well to investigate changes in the transmission of the substrates. Extra light absorption in the substrates will severely lower the absorption in the active layers of the solar cell and could obscure the irradiation-induced degradation of the a-Si:H solar cells. However, no transmission loss of the substrates was observed in the wavelength range of 350 nm to 1000 nm and thus it was concluded that the measured degradation of the cells may be fully attributed to changes in the optical and electrical properties of the solar cell itself.

## 6.3 Experimental results

### 6.3.1 Experimental results for the as-deposited solar cells

The measured external parameters for the as-deposited solar cells used in the 1-MeV and 65-MeV proton irradiation experiment are given in table 6.1. The cells used in each irradiation experiment were fabricated at different dates and a small difference in the as-deposited solar-cell performance is noted. The values presented in table 6.1 were obtained by averaging first the external parameters of the best performing 7 cells of each piece, and subsequently the average of the three pieces.

The external parameters obtained for these solar cells are comparable to the

parameters found for the cells used in the electron-irradiation experiments presented in section 5.3.1. The difference between the as-deposited external parameters of cells used for the 1-MeV and 65-MeV proton irradiation on one hand and of cells used for 1-MeV electron irradiation on the other hand is less than 5%. The  $J_{sc}$  increases with i-layer thickness from 108 to 157 A/m<sup>2</sup>. Increasing the i-layer thickness leads to an increase in  $J_{sc}$  because of the increase in the optical path length. The  $V_{oc}$  is approximately 0.84 V for all cells. The  $FF$  varies from 0.71 to 0.62, where the  $FF$  is highest for the thin cells. Increasing the thickness lowers the  $FF$ , due to decrease of the overall internal electrical field in the cell, which in turn leads to an increased recombination rate. These values for the external parameters lead to efficiencies in between 6.5 and 8.4%.

### 6.3.2 Degradation with 1-MeV and 65-MeV protons

Single-junction a-Si:H solar cells with different thickness were irradiated using 1-MeV and 65-MeV protons. In both cases a uniform energy deposition depth profile for all solar cells is achieved, because the projected range of 1-MeV and 65-MeV protons in Si is estimated to be 20  $\mu$ m and 2.2 cm, respectively [22]. The results for the external parameters versus the fluence are presented in figure 6.1. For the 1-MeV irradiation closed markers are used and for the 65-MeV open markers. Note that there is some scatter in the data, as indicated by the standard deviation for the 150-nm and 900-nm thick solar cell irradiated with  $1 \times 10^{14}$  protons/cm<sup>2</sup>. A possible reason for this scatter in the data is the flux non-uniformity over the irradiated surface where all 10 solar cells were placed. This non-uniformity led to a large deviation in the irradiation fluence and thus in the degradation of the external parameters. The deviation increased for higher fluences and it was found that the  $FF$  had the highest deviation: at the highest fluence a standard deviation of 20% was found.

Similar to what was observed for light-induced (chapter 4) and electron-beam degradation (chapter 5), for both 1-MeV and 65-MeV irradiation the performance of thinner cells is less sensitive to irradiation than of thicker cells, although this thickness dependence is somewhat obscured due to the scatter in the results. The thickness dependence is most noticeable in the  $J_{sc}$  and least in the  $V_{oc}$ .

The  $FF$  of the 150-nm cell dropped from 0.69 to 0.64 after 1-MeV irradiation using the highest fluence of  $1 \times 10^{14}$  protons/cm<sup>2</sup>, a decrease of 7.2%. For this cell the  $V_{oc}$  decreases from 0.84 V to 0.80 V (4.8%), while the  $J_{sc}$  was reduced

## 6. Degradation of solar cells by high-energy protons

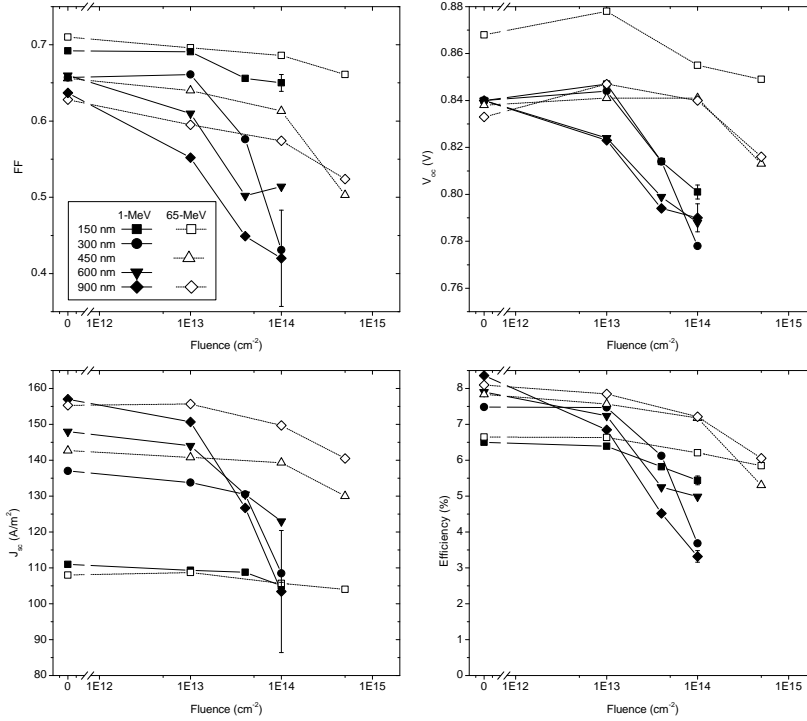


**Figure 6.1:** External parameters as a function of the fluence for solar cells with different *i*-layer thickness following 1-MeV and 65-MeV proton-beam degradation. Closed and open markers represent the solar-cell data following 1-MeV and 65-MeV irradiation, respectively. For the 150-nm and 900-nm thick solar cells irradiated using 1-MeV protons the standard deviation of each external parameter is plotted as well at a fluence of  $1 \times 10^{14}$  protons/cm<sup>2</sup>

from 111 A/m<sup>2</sup> to 105 A/m<sup>2</sup> (5.4%). These changes lead to an efficiency decrease from 6.5% to 5.4% (17%). After 1-MeV proton-beam degradation the 150-nm cell has the highest efficiency when compared to the other cells in the thickness series. The 900-nm cell shows a large decrease in *FF*: from 0.64 to 0.42 (34%). The *V*<sub>oc</sub> degradation of the 900-nm cell is slightly larger than of the 150-nm cell: from 0.84 V to 0.79 V (6.0%). In contrast to the 150-nm cell, the 900-nm cell shows a large *J*<sub>sc</sub> reduction: from 157 A/m<sup>2</sup> to 103.4 A/m<sup>2</sup> (34%). This results in an efficiency following irradiation of only 3.3%, a decrease of more than 60%.

Single-junction a-Si:H solar cells were also irradiated by 65-MeV protons. Fluences up to  $5 \times 10^{14}$  protons/cm<sup>2</sup> were used in this experiment. The performance

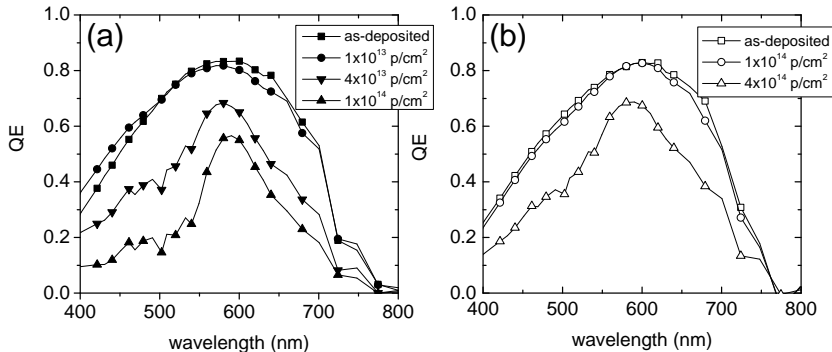


**Figure 6.2:** QE versus the fluence for the 900-nm solar cells following (a) 1-MeV (closed markers) and (b) 65-MeV (open markers) proton-beam irradiation.

degradation in this experiment was much lower. Following the highest fluence of 65-MeV proton irradiation, the  $FF$ ,  $V_{oc}$ ,  $J_{sc}$ , and efficiency of the 150-nm cell dropped to 0.66 (7%), 0.85 V (2.2%), 104 A/m<sup>2</sup> (3.7%), and 5.9% (12%), respectively. For the 900-nm cell more degradation in the external parameters is observed: the  $FF$ ,  $V_{oc}$ , and  $J_{sc}$  decreased to 0.52 (17%), 0.82 V (2.0%), and 141 A/m<sup>2</sup> (9.5%), respectively, reducing the efficiency to 6.1% (25%).

The QEs of the 900-nm cells following 1-MeV and 65-MeV proton irradiation are presented in figure 6.2. For the cells irradiated with 65-MeV protons, only at the highest fluence of  $4 \times 10^{14}$  protons/cm<sup>2</sup> significant degradation of the QE is observed. The QE degradation by 1-MeV protons is found to be faster and already for a fluence of  $4 \times 10^{13}$  protons/cm<sup>2</sup> a significant decrease in QE is observed. Similar to electron-beam irradiation and degradation by light soaking, the QE decreases most for shorter and longer wavelengths and shows a distinct peak around 550 to 600 nm. Not shown here is the thickness dependency of the QE degradation, but similar to the  $J_{sc}$  the thinner cells are more tolerant to the irradiation.

When comparing the solar-cell data of the two proton irradiation experiments we conclude that a-Si:H solar cells are more tolerant to 65-MeV than to 1-MeV irradiation, in agreement with the findings of Srour et al. [28]. They assumed that the degradation is related to ionizing events. However, we will show below in figure 6.3 and in more detail in section 6.4 that this observation can also be explained by the difference in the total deposited displacement energy in the solar cells as a result of the irradiation.

## 6. Degradation of solar cells by high-energy protons

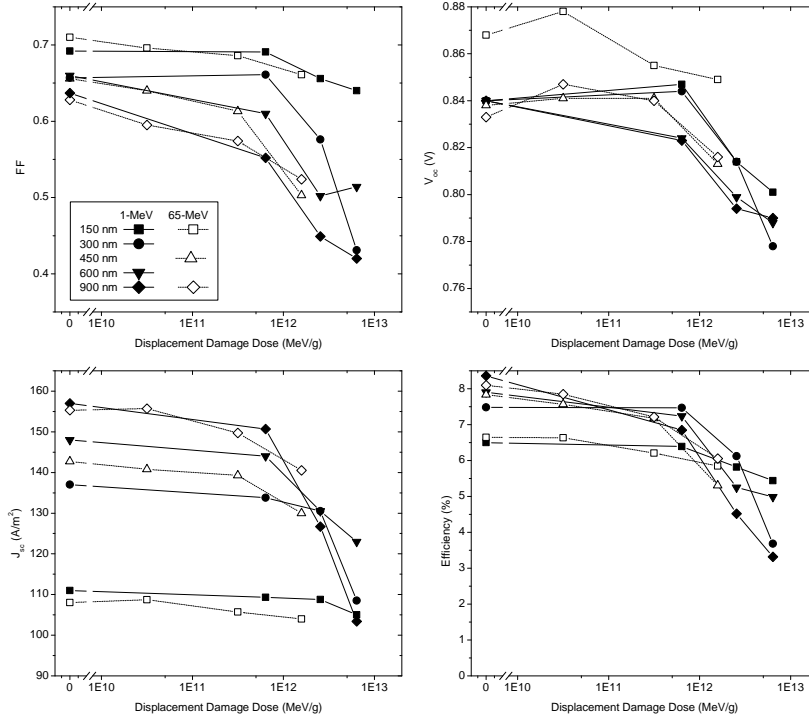


**Figure 6.3:** External parameters as a function of the displacement damage dose for solar cells with different i-layer thickness following 1-MeV and 65-MeV proton-beam degradation. Closed and open markers represent the solar-cell data following 1-MeV and 65-MeV irradiation, respectively.

From the results in chapter 5 we concluded that the solar-cell performance degradation following irradiation is most likely related to non-ionizing collision events of incident protons with the a-Si:H. It has been reported that the NIEL values are a good indication of the amount of displacements induced in c-Si by incident particles [85]. Figure 6.3 shows the same results as presented in figure 6.1, but now the fluence is converted to the so-called displacement damage dose using the NRL method by Messenger et al. [85]. The NIEL values used in the calculations were  $6.38 \times 10^{-2} \text{ MeV cm}^2/\text{g}$  and  $3.16 \times 10^{-3} \text{ MeV cm}^2/\text{g}$  for the 1-MeV and 65-MeV irradiation, respectively. The data of all external parameters of the 150-nm and 900-nm solar cells now show much more overlap for the 1-MeV and 65-MeV irradiation, suggesting that all data fall on the same curve. This figure suggests that the degradation of the external parameters by high energy

## 6.4. Comparison with light soaking and electron-beam irradiation

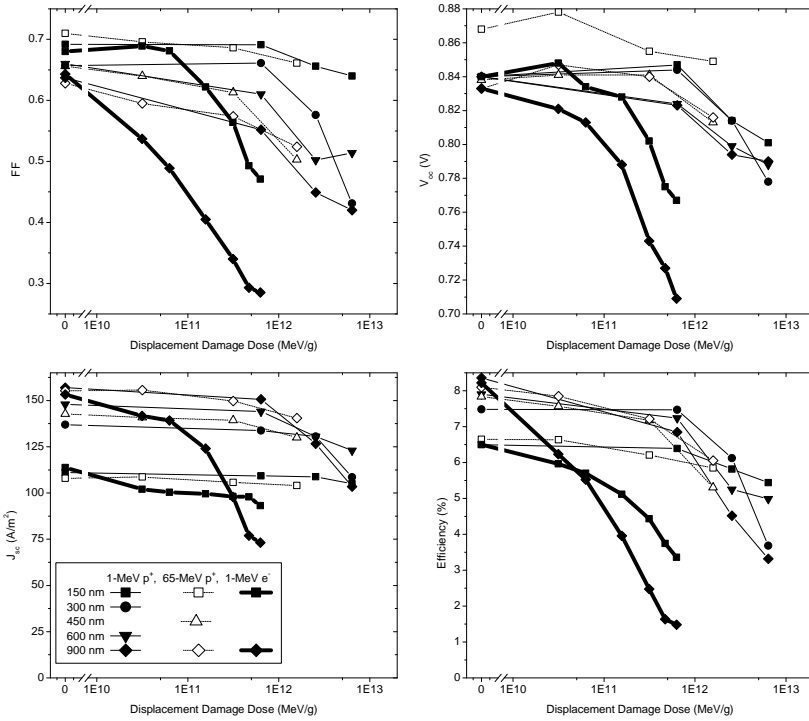


**Figure 6.4:** External parameters of solar cells with different i-layer thickness following 1-MeV and 65-MeV proton-beam degradation and 1-MeV electron irradiation versus the displacement damage dose using the NIEL values as given by Srour et al. [28]. Closed and open markers are for the 1-MeV and 65-MeV irradiation, respectively. The thick lines connect the electron-beam data. For clarity, only the electron-beam data of the 150-nm and 900-nm thick solar cells are plotted.

protons is strongly correlated to the displacement damage dose.

## 6.4 Comparison with light soaking and electron-beam irradiation

For the 1-MeV and 65-MeV proton irradiation experiments the ratios between the NIEL and IEL values as used by Srour et al. [28] are approximately equal for both energies. Therefore, based on the results obtained by the proton irradiation, it is not possible to verify if degradation is governed by ionizing or displacement

events. However, for the electron irradiation the ratio of IEL over NIEL is shifted towards ionizing events. Based on this difference we may be able to learn more about the degradation mechanism by comparing electron-beam to proton-beam degradation.

In a similar way as for the proton-beam irradiation results, the electron-beam fluence can be converted to the displacement damage dose. For 1-MeV electron-beam irradiation of a-Si:H solar cells Srour et al. [28] used a NIEL value of  $3.14 \times 10^{-5}$  MeV cm<sup>2</sup>/g. In figure 6.4 we compare the external parameter degradation by proton- and electron-beam irradiation by converting the fluence to the displacement damage dose. Note that for clarity only the electron-beam data of the 150-nm and 900-nm thick solar cells are plotted in this figure. In agreement with the results of Srour et al. [28], the proton- and electron-beam results do not overlap. The performance of the electron-beam irradiated solar cells degrades faster and more as function of the displacement damage dose when compared to the performance of proton-beam irradiated cells. This difference in degradation rate between proton and electron irradiation would imply that the performance degradation is not related to displacement damage or non-ionizing events induced by charged-particle irradiation, in contradiction to the conclusions presented in chapter 5. In the following we will show that an alternative explanation can clarify this apparent discrepancy and can indeed correlate the degradation to non-ionizing events.

Srour et al. [28] obtained a good correlation between the degradation of proton and electron-beam irradiated samples when the data were plotted as a function of the total ionizing dose induced by the irradiation. The ionizing dose is calculated by multiplying the fluence with the IEL value for the given incident particle. The following IEL values have been used [22]: 1.507, 175.3 and 8.052 MeV cm<sup>2</sup>/g for the 1-MeV electron-beam, 1-MeV proton-beam, and the 65-MeV proton-beam irradiation results, respectively. Figure 6.5 compares the degradation of the external parameters by proton- and electron-beam degradation in case the fluence is converted to the ionizing dose. In agreement with the results of Srour et al. [28] a reasonable overlap is obtained between the results of the proton- and electron-irradiated cells, suggesting a correlation between the performance degradation and the ionizing dose. Some small differences can be observed. At an equal ionizing dose the solar cells are slightly less tolerant to electron-beam irradiation than to proton-beam irradiation, which is particularly visible at higher ionizing doses. If solar-cell degradation by charged-particle irradiation is indeed controlled by the

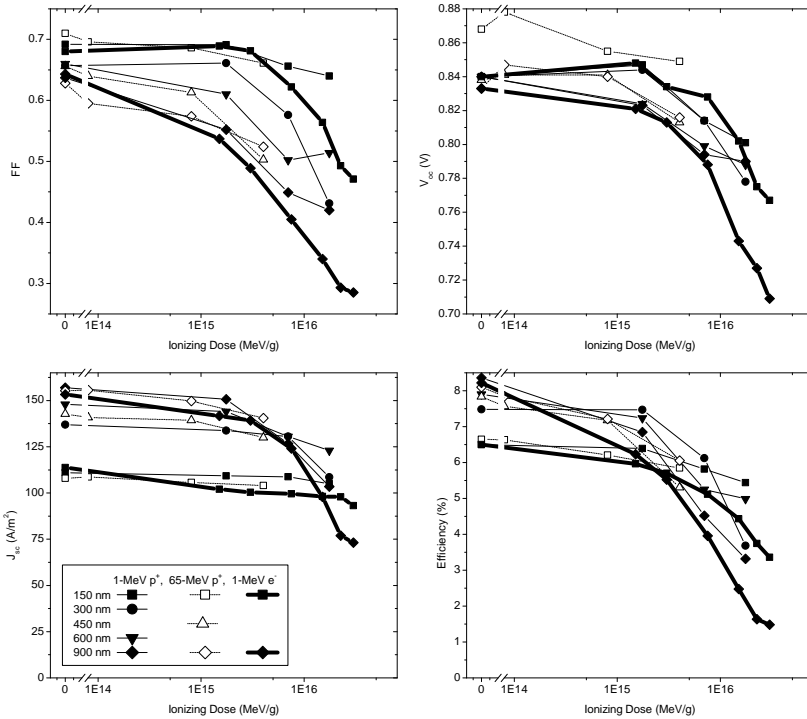


**Figure 6.5:** External parameters of solar cells with different i-layer thickness following 1-MeV and 65-MeV proton-beam degradation and 1-MeV electron irradiation versus the ionizing dose. Closed and open markers are for the 1-MeV and 65-MeV irradiation, respectively. The thick lines connect the electron-beam data. For clarity, only the electron-beam data of the 150-nm and 900-nm thick solar cells are plotted.

ionizing dose, then to our knowledge two degradation mechanisms can explain this observation. We will discuss these degradation mechanisms and explain why we think these mechanisms do not play a role in the degradation of a-Si:H solar cells.

As remarked in the introduction of this chapter, proton-beam irradiation is similar to electron-beam irradiation in many aspects: in both cases the particles lose most energy by Coulomb interaction leading to generation of electron-hole pairs. It has been suggested that the degradation by charged-particle irradiation is related to the Staebler-Wronski effect, i.e., light-induced defect creation in a-Si:H [41, 53]. In that case defect creation is initiated by electron-hole pair recombination [89, 91]. However, in chapter 5 we found no evidence that there

is a link between the electron-hole pair recombination profile and the degradation rate of a-Si:H solar cells following electron-beam irradiation. As the effect of proton-beam and electron-beam irradiation is similar, we therefore conclude that also for proton-beam irradiation of a-Si:H solar cells the degradation is not governed by electron-hole pair recombination.

Srouf et al. [28] suggested another mechanism in which the performance degradation is correlated to the ionizing dose. They proposed that the performance degradation is due to trapping of irradiation-induced charge carriers on pre-existing defect centers. This trapped charge leads to extra space-charge regions in the solar cell, which in turn reduces the magnitude of the internal electric field across the active layer, subsequently reducing the overall performance of the cell. Although not explicitly mentioned by Srouf et al. [28], this mechanism can also explain the drop in  $V_{oc}$  following irradiation. Instead of lowering the activation energy of the doped layers, the trapped charge would reduce the  $V_{oc}$  by a decrease of the internal electric field. However, if the degradation is related to trapping of charge on pre-existing defects as proposed by Srouf et al. [28], the degradation by light-soaking should be huge in our opinion, because the ionizing dose during light soaking is very high as opposed to charged-particle irradiation. The total ionizing dose during our 1-MeV electron-beam irradiation using the highest fluence was  $3 \times 10^{16}$  MeV/g. Using a typical average activation energy of in between 3.4 eV and 6 eV for electron-hole pair generation by charged-particle irradiation [57, 131], we find a total electron-hole pair production of at most  $3 \times 10^{21}$   $\text{cm}^{-3}$  during the electron-beam irradiation experiment. During light-soaking experiments of solar cells using a red laser as described in chapter 4, the incident power density is  $3.4 \text{ kW/m}^2$  and most of this power is absorbed in the material. Using computer simulations the electron-hole pair generation rate in the 150-nm cell is found to be  $2 \times 10^{22} \text{ cm}^{-3}\text{s}^{-1}$ . Thus in one second of light soaking more electron-hole pairs are generated than during the entire electron-beam irradiation experiment, yet the degradation of the solar-cell performance is much higher for the latter experiment. We think that there is also another argument against the explanation of Srouf et al. [28]. If the  $V_{oc}$  degradation is due to trapping of charge carriers on pre-existing defect centers throughout the whole i-layer, a large dependence of the  $V_{oc}$  degradation on the i-layer thickness is expected. However, all results of charged-particle irradiation experiments presented in this thesis show only a small dependence of the  $V_{oc}$  on the i-layer thickness. Therefore, we think that the explanation of Srouf et al. [28] is not correct.

As discussed above, figures 6.4 and 6.5 suggest that the performance degradation of a-Si:H solar cells is not correlated to the displacement damage dose, but to the ionizing dose. However, in the previous paragraph we argued that this observation is not in agreement with other experimental results presented by us. We suggest that the amount of defects induced in a-Si:H is not calculated accurately with the NIEL values used by Srour et al. [28]. Their NIEL values are calculated assuming a displacement energy of 12 eV, similar to values used for c-Si [132]. Here it is assumed that the defects are created by displacing an atom in the a-Si:H lattice leading to vacancies and interstitials. However, the characteristics of defect creation in a-Si:H is somewhat different when compared to c-Si. In a-Si:H, the defect-creation energy is found to be much lower due to inherent disorder of the material and the existence of weak bonds and hydrogen. For instance, from current-injection experiments on thin-film transistors a dangling-bond creation energy of 0.7 to 1.2 eV was found [111]. A defect-creation energy of 1 eV was found in thin-film transistors subjected to gate-voltage stress by Stannowski et al. [133, 134]. Further, Longeaud et al. [107] claimed that an energy of 1.2 eV is needed to initiate the creation of a defect when degrading a-Si:H with light soaking. Finally, Powell et al. [135] found a defect-creation energy of 0.9 to 1.0 eV in the case of light soaking. We think that the increase in defect density following irradiation is underestimated by Srour et al. [28] when assuming that the defects are only created by displacement events with an average activation energy of 12 eV. Instead we think that in order to calculate the increases in defect density in a-Si:H correctly, the displacement energy in the NIEL calculations should be replaced by the defect-creation energy for a-Si:H.

A lower defect-creation energy may also explain the results obtained by Wang et al. [29] and by Lord et al. [66] for 40-keV electron-beam irradiated solar cells. In this case the maximum energy transfer to a Si atom for a knock-on collision is only 3.1 eV. When a displacement energy of 12 eV is used to calculate the NIEL values, like Srour et al. [28], no defect creation would occur at this irradiation energy. The observed degradation following 40-keV electron-beam irradiation then could be explained on the basis of ionization events. However, in that case the increase of the defect density should be faster for 40-keV electron-beam irradiation than for 1-MeV electron-beam irradiation, because the IEL for 40-keV electron-beam irradiation is more than one order of magnitude larger than for 1-MeV electron-beam irradiation. A faster increase in defect density for 40-keV electron-beam irradiation has not been observed. Therefore, we think that the results of Wang

et al. [29] and Lord et al. [66] can be explained on the basis of defect creation following collisions, but that the NIEL values should be calculated using a much lower displacement energy.

Assuming a lower displacement energy leads to higher NIEL values for electron-beam irradiation. If the displacement energy is decreased from 12 to 5 eV, the NIEL value of 1-MeV electrons increases from  $3.14 \times 10^{-5}$  to  $7 \times 10^{-5}$  MeV cm<sup>2</sup>/g [136]. Due to the complex nature of the calculations to determine the NIEL values for electron and proton irradiation, we have not carried out these calculations using lower displacement energies to get a more realistic NIEL value for electron irradiation of a-Si:H. However, we can estimate the NIEL value in order to obtain a similar correlation between proton- and electron-beam irradiation data as presented in figure 6.5. We find that a NIEL value of  $5 \times 10^{-4}$  MeV cm<sup>2</sup>/g must be used for the 1-MeV electron-beam irradiation. The NIEL values for proton irradiation do not need adjustment, because of the higher mass of protons. The energy transfer from the incident proton to a-Si:H is much larger in a collision event. Using classical mechanics we estimate that a 1-MeV proton can transfer up to  $1.3 \times 10^5$  eV to a Si atom, while a 1-MeV electron can only transfer 78 eV for a knock-on collision. The defect-creation energy is therefore much easier to overcome by protons than by electrons and the NIEL values for proton-beam irradiation are expected to be valid for a-Si:H solar cells and material.

In this chapter we have showed that the degradation mechanism by proton-beam irradiation is similar to electron-beam irradiation. Using the method as described by Srour et al. [28] an overlap was obtained in the degradation data by 1-MeV and 65-MeV proton and 1-MeV electron irradiation. Therefore, the simulations of the a-Si:H solar cell degradation as presented in chapter 5 are equally valid to describe the degradation by proton-beam irradiation.

## 6.5 Conclusions

The degradation of a-Si:H single-junction solar cells with different i-layer thickness by 1-MeV and 65-MeV proton irradiation has been studied. It was found that solar cells are more tolerant to 65-MeV proton irradiation and the performance degradation shows a correlation with the displacement damage dose. For thin solar cells the degradation of the  $FF$  is most significant, whereas for thicker cells the  $J_{sc}$  degradation also plays a major role in the overall drop in performance. In contrast to light soaking, and similar to electron-beam irradiation, significant

degradation of the  $V_{oc}$  is found.

In the previous chapter we concluded that the degradation by high-energy electron-beam irradiation is likely due to non-ionizing collision events. However, using the NIEL values as published by Srour et al. [28] to calculate the displacement damage dose in a-Si:H, no correlation between electron-beam and proton-beam irradiation is found. In contrast, it appears that the solar-cell performance degradation is related to the ionizing dose. Two possible degradation mechanisms linked to the ionizing dose are proposed and discussed. The first mechanism is similar to Staebler-Wronski degradation, in which the defect creation is linked to recombination events. As we showed in chapter 4.5, short-circuiting the cells should then lead to a lower degradation rate, which is not observed. The second mechanism was proposed by Srour et al. [28]. They explained the degradation of a-Si:H solar cells by a distortion of the internal electric field due to the build-up of space-charge regions. These space-charge regions were formed as a result of trapping of irradiation-induced charge carriers on pre-existing defects. However, when comparing charged-particle degradation to light soaking, the ionizing dose during light soaking is much higher than for charged-particle irradiation while the performance degradation is much less for light soaking. This observation indicates that the degradation by charged-particle irradiation is not related to the ionizing dose.

We conclude that the degradation of a-Si:H solar cells is indeed determined by non-ionizing collision events, but that the NIEL values presented by Srour et al. [28] do not accurately predict the amount of displacements or defect creation in a-Si:H. This is due to the occurrence of weak bonds in a-Si:H, which will significantly lower the energy needed for the creation of defects. The activation energy for defect creation in a-Si:H by light soaking or current-injection is assumed to be below 1.5 eV, whereas Srour et al. [28] used a value for the displacement energy of 12 eV to calculate the NIEL values. Assuming a lower displacement energy leads to a higher NIEL value for electron irradiation, which will remove the discrepancy between the degradation of a-Si:H solar cells by proton and electron irradiation.

### **Acknowledgments**

We would like to thank L. Gialanella, M. Romano, and B. Limata of the Physics Department at Naples University for the 1-MeV proton irradiation with the TANDEM accelerator. Also, we gratefully acknowledge the 65-MeV proton irradiations

## 6. Degradation of solar cells by high-energy protons

---

carried out by A. Denker of ISL at Hahn-Meitner-Institut (HMI) in Berlin.

## Chapter 7

# Conclusions and discussion

In this work the behavior of hydrogenated amorphous silicon (a-Si:H solar cells under the influence of electron-beam irradiation is investigated with the aim to predict the End-of-Life (EOL) performance of these cells in a space environment. The main conclusions of this work are as follows.

Degradation of a-Si:H solar cells by light soaking may be simulated by assuming only increases in the defect density in the intrinsic layer. By linking this increase in defect density to the recombination-rate density profile, solar-cell degradation under both open- and short-circuit conditions can be simulated using the same parameter set. By matching experimental to simulation results it is concluded from the simulations that the defect density increases up to two orders of magnitude following 80 minutes of light soaking using a high-energy red laser, depending on the intrinsic layer thickness and circuit conditions. In all cases the defect density shows a  $1/3$  power dependence on the illumination time.

The degradation of a-Si:H solar cells by electron-beam irradiation is the result of three effects: a higher light absorption in the glass substrate, increases in the activation energy of the dark conductivity of the doped layers, and increases in the defect density in the intrinsic layer. The light absorption of Corning glass increased dramatically after 1-MeV electron-beam irradiation and it was not practical to use this glass. We therefore used radiation hard CMZ glass; the absorption of this glass also increased after irradiation, but far less. From measurements on individual layers we found that the activation energy of the doped layers increased approximately 0.25 eV, which will mainly affect the open-circuit voltage of the solar cells. The most important effect of irradiation is the increase in defect

density. Based on the decrease in light conductivity of intrinsic a-Si:H following irradiation, an increase in defect density by a factor of 20 was found following the same fluence of  $2 \times 10^{16}$  electrons/cm<sup>2</sup>. We note that it has been reported in literature that the defect-density increase obtained from the photoconductivity decay may be underestimated. The a-Si:H sub-bandgap absorption, also related to the defect density, increased at most only one order of magnitude. From the measurements no indication of a change in mobility or weak-bond concentration was found, suggesting that the electrons only induce additional defects in the intrinsic layer. Using simulations of solar cells we determined that irradiation with a fluence of up to  $2 \times 10^{16}$  electrons/cm<sup>2</sup> increased the defect density in the intrinsic layer by a factor of 40. In this case the defect density showed a *linear* dependence on the fluence. The activation energy of the doped layers was also adjusted in the simulations, but the increase in activation energy of 0.15 eV is lower than the experimentally obtained value.

Defect creation by electron-beam irradiation is not linked to electron-hole pair recombination events in the material as has been previously suggested, but to energy transfer during collisions of electrons with the lattice in a-Si:H. Varying the recombination profile in the cells during the irradiation by varying the circuit conditions had no effect on the degradation rate: short-circuited cells degraded as fast following irradiation as open-circuited cells. Furthermore, the a-Si:H solar cell degradation was found to be independent on the incident electron flux within the range of  $5 \times 10^{11}$  to  $1 \times 10^{13}$  electrons/cm<sup>2</sup>s apart from cracking of the transparent conductive oxide (TCO) layer observed at higher fluxes. This cracking resulted to additional series resistance, leading to a reduced cell performance.

In agreement with reports in literature, we found no correlation between the solar-cell performance degradation and the displacement damage dose when a displacement energy of 12 eV is used in the calculations to determine the values of the non-ionizing energy loss (NIEL) of the incident particles in the material. A good agreement between the performance degradation of electron-beam and proton-beam irradiated solar cells is found when the ionizing energy loss (IEL) is used, implying that the performance degradation is linked to ionizing or subsequent recombination events in the a-Si:H material. However, a good agreement between the degradation of electron-beam irradiated and proton-beam irradiated a-Si:H solar cells can also be obtained if a displacement energy of less than 2 eV is assumed in the calculation of the NIEL values for a-Si:H rather than using value of 21 eV that was determined for crystalline Si. We think that using a

---

lower displacement energy in the NIEL calculation provides a much more plausible explanation for the observed performance degradation following high-energy particle irradiation, as we have ruled out before that this degradation is initiated by recombination events. Although the initiation of defect formation using electron-beam irradiation is different from light soaking, the induced defects might be similar to the defects induced by light soaking.

In contrast to the previous conclusion, time-resolved microwave conductivity (TRMC) experiments on electron-beam irradiated a-Si:H provided some evidence that the degradation is indeed linked to recombination events. This conclusion is based on the fact that the dependence of the increase in defect density on electron-beam fluence or illumination time when using a pulsed laser are the same. However, during the TRMC experiment the incident electron flux was much higher compared to the degradation experiment on a-Si:H solar cells. During the 80-nC, 20-ns degradation pulse, the electron-hole pair generation rate may be up to  $1 \times 10^{31}$  electrons/cm<sup>2</sup>s, orders of magnitude higher than during typical light soaking conditions. With this high generation rate the degradation initiated by electron-hole pair recombination may be higher than the degradation by electron-collisions within the a-Si:H.

In the simulations, we have found that the degradation is mainly dependent on the total amount of defects induced in the intrinsic layer and that the depth profile of the induced defects only plays a minor role in the degradation. The quantum efficiency of the degraded solar cells do not provide direct information on the depth profile of the induced defects: using significantly different defect creation profiles resulted in similar QE curves. The energy-location of the induced defect states, however, does alter the QE of the degraded solar cells. We found on the basis of quantum-efficiency simulations that the defect states are generated around mid gap. In the simulations of the solar-cell performance following high-energy charged-particle irradiation the increases in activation energy and defect density may not be treated as two independent effects, as they may strengthen each other leading to additional degradation.

We conclude that we have developed a model with which the performance and quantum efficiency following light-soaking or high-energy charged-particle irradiation of a thickness series of a-Si:H solar cells can be modeled at once using computer simulations. To our knowledge it is the first time that such a model has been developed. Although this model is capable of predicting the performance degradation, we note that annealing effects have not been included yet. We also

## 7. Conclusions and discussion

---

think that an iterative procedure would improve the model.

## Appendix A

# Generation, drift and recombination along the incident-particle trajectory

When a high-energy charged particle moves through a material it generates almost instantaneously a tube of electron-hole (e-h) pairs along its trajectory. This tube of e-h pairs later degenerates either by diffusion, drift and/or recombination processes. Yelon et al. estimated that for 20-keV electron-beam irradiation the tubes degenerate completely by recombination events [43]. However, in case of 1-MeV electron-beam irradiation the energy deposition of the incident particle into a-Si:H, and thus the e-h pair density along its trajectory, is much lower, which can affect the recombination statistics in the tube.

In this appendix we will calculate the e-h pair density in a tube and show which processes influence the degeneration of the tube. This information is particularly important for the two experiments presented in chapter 5 in which we attempted to alter the recombination rate and the profile in the solar cells. In the first experiment the incident particle flux was varied, while in the second solar cells were irradiated either under open- or short-circuit conditions. In both experiments it is important to know the lifetime of the induced electron-hole pair tubes created by the incident particles, as this lifetime will determine if irradiation-induced e-h pairs will recombine or will be able to drift.

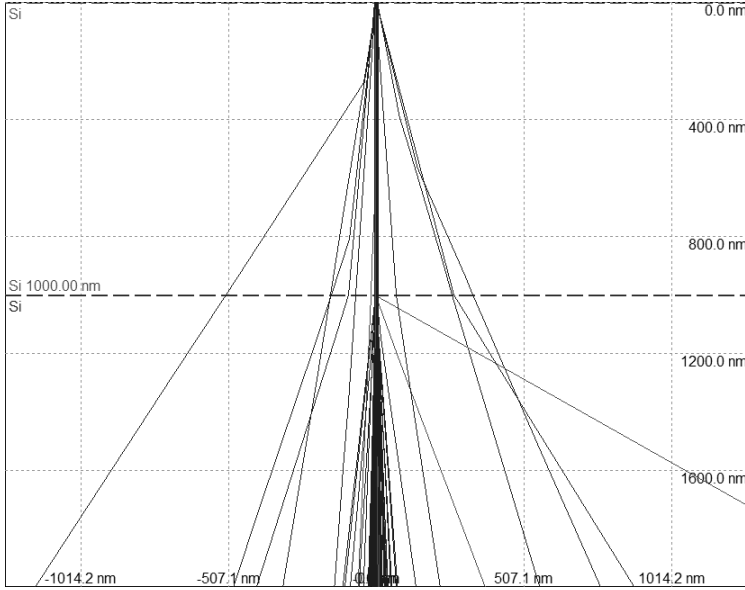


**Figure A.1:** Simulation of scattering of 1-MeV electrons moving through a 2- $\mu\text{m}$  a-Si:H layer.

### Generation

The generation profile of the electron-hole pairs can be estimated from the ionizing energy loss (IEL) of the incident particle. The IEL for a 1-MeV electron is 1.5 MeV  $\text{cm}^2/\text{g}$  [22]. Using a density,  $\rho$ , for a-Si:H of 2.1  $\text{g}/\text{cm}^3$ , it is found that the incident electron dissipates on average 0.3 eV/nm into the material. Given a formation energy of e-h pairs by high-energy electrons,  $E_{e-h\text{ form}}$ , of in between 3.4 and 6 eV [57, 131], it may be estimated by

$$\frac{E_{e-h\text{ form}}}{\text{IEL} \cdot \rho} \quad (\text{A.1})$$

that one e-h pair is generated every 11 to 20 nm. For 20-keV electron-beam irradiation an IEL of 10.2 MeV  $\text{cm}^2/\text{g}$  is found, leading to a much higher e-h pair density along the trajectory of almost 1 e-h pair/nm in agreement with the findings of Yelon et al. [43].

A fraction of the the incident electrons may not move in a straight line through the material but will be scattered because of collisions with the a-Si:H lattice. Using the computer program CASINO (monte CARlo SIMulation of electroNs in sOLids) an estimation of the electron trajectories in the a-Si:H can be made.

---

With this program Monte Carlo simulations of electron trajectories in solids can be carried out and this program is specially designed for low-beam interaction in a bulk and thin foil. Figure A.1 shows the results of a simulation in which 1000 individual electron trajectories through an 2- $\mu\text{m}$  thick a-Si:H film were calculated. At 1  $\mu\text{m}$  an extra interface was defined, which enhances the scattering of electrons. It can be seen that most of the electrons move almost in a straight line through the material and that only a small fraction of the incident electrons is scattered, usually less than 45 degrees.

## Recombination

Information on recombination processes in irradiated a-Si:H can be obtained by comparing the e-h pair density under irradiation to the density following high-intensity laser pulses, under which large e-h pair densities are generated that are comparable to electron-beam irradiation. Schiff [137] reported on the relationship between the e-h pair density,  $N_0$ , and the decay time,  $t_{1/2}$ , required for this density to reduce to half its initial value due to recombination. Several recombination mechanisms contribute to this relationship and it is beyond the scope of this thesis to go into detail on this matter, however, it is clear that much shorter decay times are obtained when increasing the initial e-h pair density. This relationship can be understood intuitively by realizing that at high e-h pair concentration the recombination rate is much larger due to the fact electrons and holes are close enough to annihilate each other. We will now use this relationship to estimate the decay time in an electron-beam induced tube of e-h pairs.

If we take an average distance,  $d$ , of 15 nm in between the e-h pairs in a tube created by a 1-MeV electron, as calculated in the previous section, we find that  $N_0 = d^{-1/3} = 3 \times 10^{17} \text{ cm}^{-3}$ . For this concentration Schiff [137] reported a decay time of at least 100 ps. Note that in his case the generated e-h pairs are located throughout the material, but that following electron-beam irradiation the e-h pairs are only generated along the electron trajectory. Therefore, we believe that the reported decay time of 100 ps only reflects the lower limit for the lifetime of the tube, as some of the charge carriers will diffuse perpendicular to the tube, thereby lowering the e-h pair concentration and as a result increasing the decay time. A decay time substantially longer than the 100 ps reported by Schiff [137] is in agreement with results of our time resolved microwave experiments (see chapter 2); in these experiments we found a decay time of 10 ns following the longest probe pulse [138].

### Drift

In an a-Si:H solar cell generated electrons and holes that do not recombine with each other may drift under the influence of the internal electric field towards the doped layers, depending on the applied bias. The transport time,  $t$ , over a distance,  $x$ , is given by:

$$t = \int \frac{1}{\mu E(x)} dx. \quad (\text{A.2})$$

The drift mobility of electrons is in the range of  $1 \times 10^{-4}$  to  $5 \times 10^{-4}$   $\text{m}^2/\text{Vs}$  [139, 140]. Using the upper value for the mobility it can be estimated that an electron induced near the p-i junction in a short-circuited 300-nm a-Si:H solar cell takes about 500 ps to reach the n-layer where it recombines. For this estimation  $E(x)$  is taken from simulations presented in chapter 3 and is typically above 0.5 MV/m in the intrinsic layer of an as-deposited 300-nm solar cell. Note that carriers are generated uniformly in the intrinsic layer and most electrons need to travel a shorter distance to reach the p-doped layer and therefore require less time than calculated here. For holes a much longer maximum transport time is found due to their lower drift mobility of around  $5 \times 10^{-7}$   $\text{m}^2/\text{Vs}$ .

### Altered recombination statistics?

In the first experiment in chapter 5 in which we attempted to alter the recombination rate in the tube we varied the incident electron flux. If two tubes overlap an increase in recombination rate in the tubes is expected, because this rate scales with the e-h pair density as explained above. In order to establish if we indeed increase the e-h pair density when the incident electron flux is increased, we need to find out if an electron-beam induced tube is struck by another electron before it is degenerated. We will do this by calculating the time difference between tube generation and the arrival of a subsequent electron in the tube region. In the second experiment we tried to change the recombination profile by changing the circuit condition under which the solar cells were degraded. This profile can only be changed if the charge carriers are able to drift some distance before recombination. In order to be sure that the recombination profile is changed, we need to assess how long it takes for electron-beam induced charge carriers to drift through the solar cell before recombination.

First, we will calculate the time difference between tube generation and the arrival of another incident electron in that region. In order to calculate this time difference,  $\tau$ , we need to estimate the tube radius,  $r_{\text{tube}}$ . We assume that

---

this radius is equal to the distance charge carriers can diffuse away from the tube perpendicular to the electron trajectory, which in turn can be estimated when knowing the diffusion constant,  $D$ , and the decay time. We assume for the moment that the generated electrons and holes do not recombine, which in effect implies that the tube radius carries on increasing. The time difference obtained in this way will therefore be a lower limit on the decay time to obtain overlap of the tubes. For the tube radius we find:  $r_{\text{tube}} = \sqrt{D\tau}$ . At a given electron flux,  $\phi_{\text{el}}$ , we then obtain for the time between tube generation and the arrival of a subsequent electron in the tube region:

$$\begin{aligned}\tau &= [\phi_{\text{el}}\pi D\tau]^{-1} \\ \Rightarrow \tau &= \sqrt{\frac{1}{\phi_{\text{el}}\pi D}}.\end{aligned}\tag{A.3}$$

For  $D$  a value of  $0.05 \text{ cm}^2/\text{s}$  was reported by Schiff [137] based on the Einstein relation and assuming an electron mobility of  $2 \text{ cm}^2/\text{Vs}$ , but he also remarked that for large laser intensities very large diffusion constants of  $10 \text{ cm}^2/\text{s}$  have been found. The maximal electron flux in the experiment was  $1 \times 10^{13} \text{ electrons}/\text{cm}^2\text{s}$ . On the basis of the reported diffusion constants, we find that  $\tau$  ranges from  $56 \text{ ns}$  to  $0.8 \mu\text{s}$ . These time differences are much longer than the times reported for the tube to degenerate ( $100 \text{ ps}$  [137] to  $10 \text{ ns}$  [138]). Therefore we can safely assume that the recombination rate in the tube will not increase as a function of the electron flux as the e-h density in the tube is not affected before it degenerates. As the recombination rate is not affected, it is also expected that varying the electron flux will not affect the degradation rate of solar cells.

In the second experiment the solar cells are either degraded under open- or short-circuit condition. Under short-circuit condition we estimated above that the time it takes for an electron to drift towards the n-layer instead of recombining with induced holes in the intrinsic layer is similar to the decay time,  $t_{1/2}$ , of e-h pairs in a tube. The maximum electron-transport time was estimated to be around  $500 \text{ ps}$ , while the decay time of the tube due to recombination events was estimate to be at least  $100 \text{ ps}$ . It is therefore likely that both processes occur simultaneously in the induced tube of e-h pairs. We conclude that under short-circuit degradation a significant fraction of generated electrons in the intrinsic layer drift towards the n-doped layer before recombining with the holes in the tube. Under open-circuit conditions the internal electrical field over the intrinsic layer is much lower and the charge-carrier drift may be ignored. In that case

### A. Generation, drift and recombination along the incident-particle trajectory

---

the tubes mostly degenerate through e-h pair recombination events in the tube. Therefore, we conclude that the recombination profile is significantly different when degrading the solar cells under short-circuit condition than when degrading under open-circuit condition.

---

## Bibliography

- [1] N. S. Fatemi, H. E. Pollack, H. Q. Hou, and P. R. Sharps, “Solar array trades between very high-efficiency multi-junction and Si space solar cells,” in *Conference Record of the Twenty-Eighth IEEE Photovoltaic Specialists Conference*, p. 1083, 2000.
- [2] J. Kuendig, M. Goetz, A. Shah, L. Gerlach, and E. Fernandez, “Thin film silicon solar cells for space applications: Study of proton irradiation and thermal annealing effects on the characteristics of solar cells and individual layers,” *Sol. En. Mater. Sol. Cells*, vol. 79, pp. 425–438, 2003.
- [3] M. A. Green, P. A. Basore, N. Chang, D. Clugston, R. Egan, R. Evans, D. Hogg, S. Jarnason, M. Keevers, P. Lasswell, J. O’Sullivan, U. Schubert, A. Turner, S. R. Wenham, and T. Young, “Crystalline silicon on glass (CSG) thin-film solar cell modules,” *Solar Energy*, vol. 77, p. 857, 2004.
- [4] H. F. Sterling and R. C. G. Swan, “Chemical vapor deposition promoted by r.f. discharge,” *Solid-State electron.*, vol. 653, no. 8, 1965.
- [5] J. Kolodzey, R. Schwarz, S. Aljishi, V. Chu, D. S. Shen, P. M. Fauchet, and S. Wagner, “Optical and electrical properties of an a orphous silicon-germanium alloy with a 1.28 eV optical gap,” *Appl. Phys. Lett.*, vol. 52, p. 477, 1988.
- [6] D. A. Anderson and W. E. Spear, “Electrical and optical properties of amorphous silicon carbide, silicon nitride and germanium carbide by the glow discharge technique,” *Phil. Mag. B*, vol. B35, p. 1, 1977.
- [7] W. E. Spear and P. G. LeComber, “Substitutional doping of amorphous silicon,” *Solid State Commun.*, vol. 17, p. 1193, 1975.
- [8] M. A. Green, K. Emery, D. L. King, Y. Hishikawa, and W. Warta, “Solar cell efficiency tables (version 29),” *Prog. Photovolt: Res. Appl.*, vol. 15, pp. 35–40, 2007.
- [9] J. Meier, J. Sitznagel, U. Kroll, C. Bucher, S. Fay, T. Moriarty, and A. Shah, “Potential of amorphous and microcrystalline silicon solar cells,” *Thin Solid Films*, vol. 451-452, pp. 518–524, 2004.

- 
- [10] M. Yoshimi, T. Sasaki, T. Sawada, T. Suezaki, T. Meguro, T. Matsuda, K. Santo, K. Wadano, M. Ichikawa, A. Nakajima, and K. Yamamoto, "High efficiency thin film silicon hybrid solar cell module on 1m<sup>2</sup>-class large area substrate," in *Conference Record, 3rd World Conference on Photovoltaic Energy Conversion*, pp. 1566–1569, 2003.
- [11] J. Yang, A. Banerjee, T. Glatfelter, K. Hoffman, X. Xu, and S. Guha, "Progress in triple-junction amorphous silicon-based alloy solar cells and modules using hydrogen dilution," in *Conference Record, 1st World Conference on Photovoltaic Energy Conversion*, pp. 380–385, 1994.
- [12] D. L. Staebler and C. R. Wronski, "Reversible conductivity changes in discharge-produced amorphous Si," *Appl. Phys. Lett.*, vol. 31, p. 292, 1977.
- [13] J. Zhao, A. Wang, M. A. Green, and F. Ferrazza, "Novel 19.8% efficient 'honeycomb' textured multicrystalline and 24.4% monocrystalline silicon solar cells," *Appl. Phys. Lett.*, vol. 73, pp. 1991–1993, 1998.
- [14] J. Zhao, A. Wang, F. Yun, G. Zhang, D. M. Roche, S. R. Wenham, and M. A. Green, "20,000 PERL silicon cells for the 1996 world solar challenge" solar car race," *Prog. Photovolt: Res. Appl.*, vol. 5, pp. 269–276, 1997.
- [15] M. D. Andrews, "A search for CMEs associated with big flares," *Solar Physics*, vol. 218, pp. 261–279, 2003.
- [16] L. I. Miroshnichenko, B. Mendoza, and R. P. Enríquez, "Size distributions of the >10 MeV solar proton events," *Solar Physics*, vol. 202, no. 1, pp. 151–171, 2001.
- [17] P. Brekke, "Effects of space weather on technology infrastructure," *NATO Science Series*, vol. 176, p. 116, 2003.
- [18] S. G. Bailey and D. J. Flood, "Space photovoltaics," *Prog. Photovolt: Res. Appl.*, vol. 6, pp. 1–14, 1998.
- [19] H. Y. Tada, J. R. Carter, B. E. Anspaugh, and R. G. Downing, *The solar cell radiation handbook, 3rd edition*. JPL Publications, 1982.
- [20] G. P. Summers, E. A. Burke, P. Shapiro, S. R. Messenger, and R. J. Walters, "Damage correlations in semiconductors exposed to gamma, electron and proton radiation," *IEEE Trans. Nucl. Sci.*, vol. 40, p. 1372, 1993.

- 
- [21] G. P. Summers, E. A. Burke, and M. A. Xapsos, "Displacement damage analogs to ionizing radiation effects," *Radiat. Meas.*, vol. 24, no. 1, pp. 1–8, 1995.
- [22] National Institute of Standards and Technology, "Stopping-power and range tables for electrons, protons, and helium ions."
- [23] R. E. Bird, R. L. Hulstrom, and L. J. Lewis, "Terrestrial solar spectral data sets," *Solar Energy*, vol. 30, p. 563, 1983.
- [24] J. Tauc, *Amorphous and liquid semiconductors*. Plenum press, 1974.
- [25] W. B. Jackson and N. M. Amer, "Direct measurement of gap-state absorption in hydrogenated amorphous silicon by photothermal deflection spectroscopy," *Phys. Rev. B*, vol. 23, no. 8, pp. 5559–5562, 1982.
- [26] B. M. Deblois, R. L. Garwin, R. S. Kamp, and J. C. Marwell, "Star-crossed," *IEEE Spectrum*, 2005.
- [27] A. L. Weigel and D. E. Hastings, "Evaluating the cost and risk impacts of launch choices," *Journal of Spacecraft and Rockets*, vol. 41, no. 1, p. 103, 2004.
- [28] J. R. Srour, G. J. Vendura, D. H. Lo, C. M. C. Toporow, M. Dooley, R. P. Nakano, and E. E. King, "Damage mechanisms in radiation-tolerant amorphous silicon solar cells," *IEEE Trans. Nucl. Sci.*, vol. 45, p. 2624, 1998.
- [29] Q. Wang, K. R. Lord, and J. R. Woodyard, "Effects of 40 keV irradiation," in *Conference Record of the Twenty-Eighth IEEE Photovoltaic Specialists Conference*, p. 1057, 2000.
- [30] J. E. Granata, T. D. Sahlstrom, P. E. Hausgen, S. R. Messenger, R. J. Walters, and J. R. Lorentzen, "Thin-film photovoltaic radiation testing and modeling for a MEO orbit," in *Conference Record of the Thirty First IEEE Photovoltaic Specialists Conference*, p. 607, 2005.
- [31] S. Babras, V. G. Bhide, N. R. Rajopadhye, and S. V. Bhoraskar, "Defect creation by 10-keV electron irradiation in phosphorous-doped a-Si:H" *J. Appl. Phys.*, vol. 67, no. 6, p. 2800, 1990.

- 
- [32] A. Scholz, B. Schehr, and B. Schröder, “Metastability in p- and n-type a-Si:H investigated by keV electron irradiation,” *Solid State Commun.*, vol. 85, no. 9, p. 753, 1993.
- [33] H. C. Neitzert, M. Ferrara, G. D. Licciardo, Y. Ma, W. Fahrner, E. Bobeico, P. D. Veneri, L. V. Mercaldo, L. Gialanella, M. Romano, B. Limata, A. D. Bartolomeo, F. Ravotti, and M. Glaser, “Modification of amorphous and microcrystalline silicon film properties after irradiation with MeV and GeV protons,” in *20th European Photovoltaic Solar Energy Conference*, p. 1627, 2005.
- [34] U. Voget-Grote, W. Kümmerle, R. Fisher, and J. Stuke, “The influence of spin defects on recombination and electronic transport in amorphous silicon,” *Phil. Mag. B*, vol. 41, p. 127, 1979.
- [35] H. Schade and J. Pankove, “Electron-beam induced centers in hydrogenated amorphous silicon,” *Journ. de Physique (Paris)*, vol. 42, p. 327, 1981.
- [36] A. G. Kazanskii, A. S. Korol, E. P. Milichevich, and M. V. Chukichev, “Influence of electron irradiation on the photoconductivity of amorphous hydrogenated silicon,” *Sov. Phys. Semicond.*, vol. 20, p. 1000, 1986.
- [37] S. Gangopadhyay, B. Schröder, and J. Geiger, “Effect of deposition parameters and light and electron irradiation on the density of states of sputtered a-Si:H studied by space-charge-limited current technique,” *Phil. Mag. B*, vol. 56, p. 321, 1987.
- [38] U. Schneider, B. Schröder, and F. Finger, “The creation of metastable defects in a-Si:H films by high dose irradiation with keV-electrons,” *J. Non-Cryst. Solids*, vol. 97-98, p. 795, 1987.
- [39] F. Diehl, W. Herbst, S. Bauer, B. Schröder, and H. Oechsner, “Creation of metastable defects in a-Si:H by keV electron irradiation at different temperatures,” *J. Non-Cryst. Solids*, vol. 198-200, pp. 436–440, 1996.
- [40] J. R. Woodyard and G. A. Landis, “Radiation resistance of thin-film solar cells for space photovoltaic power,” *Solar Cells*, vol. 31, p. 297, 1991.
- [41] P. Danesh, B. Pantchev, I. Savatinova, E. Liarokapis, S. Kaschieva, and A. G. Belov, “Electron irradiation of a-Si:H films prepared from hydrogen-diluted silane,” *Vacuum*, vol. 69, p. 79, 2003.

- 
- [42] P. Danesh, B. Pantchev, and E. Vlaiskova, "18 MeV electron irradiation-induced metastability in hydrogenated amorphous silicon," *Nucl. Instrum. Methods Phys. Res. B*, vol. 239, pp. 370–374, 2005.
- [43] A. Yelon, H. Fritzsche, and H. M. Branz, "Electron beam creation of metastable defects in hydrogenated amorphous silicon: hydrogen collision model," *J. Non-Cryst. Solids*, vol. 266-269, p. 437, 2000.
- [44] J. Russel and G. Jones, "Radiation testing of coverglasses," in *1st International Energy Conversion Engineering Conference*, p. 6036, 2003.
- [45] D. Han and H. Fritzsche, "Study of light-induced creation of defects in a-Si:H by means of single and dual-beam photoconductivity," *J. Non-Cryst. Solids*, vol. 59-60, p. 397, 1983.
- [46] P. Stradins, H. Fritzsche, and M. Q. Tran, "Light induced defects in a-Si:H, temperature dependence of their creation and anneal and their effect on photocarrier lifetime," in *MRS Proc.*, vol. 336, p. 227, 1994.
- [47] B. von Roedern, "Shortfall of defect models for amorphous silicon solar cell performance," *Appl. Phys. Lett.*, vol. 62, no. 12, p. 1368, 1993.
- [48] A. Gordijn, L. Hodakova, J. K. Rath, and R. E. I. Schropp, "Influence on cell performance of bulk defect density in microcrystalline silicon grown by VHF PECVD," *J. Non-Cryst. Solids*, vol. 352, pp. 1868–1871, 2006.
- [49] H. Meiling, *Deposition of amorphous silicon thin films and solar cells*. PhD thesis, Utrecht University, 1991.
- [50] R. E. I. Schropp and M. Zeman, *Amorphous and Microcrystalline Silicon Solar Cells – Modelling, Materials and Device Technology*. Kluwer Academic Publishers, Boston, 1998.
- [51] R. A. Street, *Hydrogenated amorphous silicon*. Cambridge University Press, 1991.
- [52] S. Knief, W. von Niessen, and T. Koslowski, "Defects in a-Si and a-Si:H: A numerical study," *Phys. Rev. B*, vol. 58, no. 8, pp. 4459–4472, 1998.
- [53] N. Kishimoto, H. Amekura, K. Kono, and C. G. Lee, "Stable photoconductivity in metastable a-Si:H under high-energy proton irradiation," *J. Non-Cryst. Solids*, vol. 227-230, pp. 238–242, 1998.

- 
- [54] L. Jiang, J. H. Lyou, S. Rane, E. A. Schiff, Q. Wang, and Q. Yuan, "Open-circuit voltage physics in amorphous silicon solar cells," in *MRS Proc.*, vol. 609, p. A18.3.1, 2000.
- [55] J. M. Warman, M. P. de Haas, and H. M. Wentinck, "The study of radiation induced conductivity changes in microheterogeneous materials using microwaves," *Radiat. Phys. Chem.*, vol. 34, no. 4, pp. 581–586, 1989.
- [56] H. M. Wentinck, *Carrier injection in amorphous silicon devices*. PhD thesis, Delft University of Technology, 1988.
- [57] R. Coelho, *Physics of Dielectrics*. Elsevier, Amsterdam, 1979.
- [58] P. P. Infelta, M. P. de Haas, and J. M. Warman, "The study of transient conductivity of pulse irradiated dielectric liquids on a nanosecond timescale using microwaves," *Radiat. Phys. Chem.*, vol. 10, p. 353, 1977.
- [59] S. M. Sze, *Semiconductor Devices – Physics and Technology, 2nd ed.* John Wiley and Sons, New York, 2002.
- [60] M. Stutzmann, M. C. Rossi, and M. S. Brandt, "Pulsed-light soaking of hydrogenated amorphous silicon," *Phys. Rev. B*, vol. 50, p. 11592, 1994.
- [61] H. Fritzsche, ed., *Amorphous silicon and related materials*. World scientific Publishing company, 1988.
- [62] M. N. Meytin, M. Zeman, B. G. Budaguan, and J. W. Metselaar, "Kinetics of light-induced degradation in a-Si:H films investigated by computer simulations," *Semiconductors*, vol. 34, no. 6, p. 717, 2000.
- [63] D. Caputo, U. Forghieri, and F. Palma, "Low-temperature admittance measurement in thin film amorphous silicon structures," *J. Appl. Phys.*, vol. 82, p. 733, 1997.
- [64] D. Caputo, "Degradation and annealing of amorphous silicon solar cells by current injection experiments and modeling," *Sol. En. Mater. Sol. Cells*, vol. 59, pp. 289–298, 1999.
- [65] U. Dutta, M. Uspolewitz, P. R. i Cabarrocas, and P. Chatterjee, "Evolution of current-induced defects in hydrogenated amorphous silicon P-I-N solar cells : inference from simulations of experimental characteristics," in *20th European Photovoltaic Solar Energy Conference*, pp. 1557–1560, 2005.

- 
- [66] K. R. Lord and J. R. Woodyard, "Measured and simulated dark J-V characteristics of a-Si:H single junction p-i-n solar cells irradiated with 40 keV electrons," in *Conference Record of the Twenty-Ninth IEEE Photovoltaic Specialists Conference 2002.*, pp. 986–989, 2002.
- [67] M. Zeman, J. A. Willemen, L. L. A. Vosteen, G. Tao, and J. W. Metselaar, "Computer modelling of current matching in a-Si:H/a-Si:H tandem solar cells on textured TCO substrates," *Sol. En. Mater. Sol. Cells*, vol. 46, pp. 81–99, 1997.
- [68] J. A. Willemen, *Modelling of amorphous silicon single- and multi-junction solar cells*. PhD thesis, Delft University of Technology, 1998.
- [69] M. Zeman, R. A. C. M. M. van Swaaij, E. Schrotten, L. L. A. Vosteen, and J. W. Metselaar, "Device modelling of a-Si:H alloy solar cells: Calibration procedure for determination of model input parameters," in *MRS Proc.*, vol. 507, pp. 409–414, 1998.
- [70] R. A. C. M. M. van Swaaij, M. Zeman, S. Arnoult, and J. W. Metselaar, "Performance dependence on grading width of a-SiGe:H component solar cells," in *Twenty Eighth IEEE Photovoltaic Specialist Conference*, pp. 869–872, 2000.
- [71] B. E. Pieters, M. Zeman, R. A. C. M. M. van Swaaij, and W. J. Metselaar, "Optimization of a-SiGe:H solar cells with graded intrinsic layers using integrated optical and electrical modeling," *Thin Solid Films*, 2004.
- [72] M. A. Kroon, R. A. C. M. M. van Swaaij, M. Zeman, V. I. Kuznetsov, and J. W. Metselaar, "Hydrogenated amorphous silicon transverse junction solar cell," *Appl. Phys. Lett.*, vol. 72, no. 2, pp. 209–210, 1998.
- [73] M. Kroon, *The transverse junction solar cell*. PhD thesis, Delft University of Technology, 2001.
- [74] B. E. Pieters, J. W. Metselaar, and M. Zeman, "Modelling of  $\mu$  c-Si:H solar cells," in *Conference Record of the 20th European Photovoltaic Solar Energy Conference and Exhibition*, 2005.
- [75] M. Zeman, V. Nádaždy, and J. W. Metselaar, "The role of charged states in light-induced degradation of single junction a-Si:H solar cells," in *MRS Proc.*, vol. 808, p. 189, 2004.

- 
- [76] M. J. Powell and S. C. Deane, “Improved defect-pool model for charged in amorphous silicon,” *Phys. Rev. B*, vol. 48, no. 15, p. 10815, 1993.
- [77] C. T. Sah and W. Shockley, “Electron-hole recombination statistics in semiconductors through flaws with many charge conditions,” *Phys. Rev.*, vol. 109, pp. 1103–1115, 1958.
- [78] J. van den Heuvel, *Optical properties and transport properties of hydrogenated amorphous silicon*. PhD thesis, Delft University of Technology, 1989.
- [79] G. Tao, *Optical modeling and characterization of hydrogenated amorphous silicon solar cells*. PhD thesis, Delft University of Technology, 1994.
- [80] G. Tao, M. Zeman, and J. W. Metselaar, “Accurate light absorption profile in tandem a-Si:H solar cells on textured TCO substrates,” in *MRS Proc.*, vol. 336, pp. 705–710, 1994.
- [81] M. Zeman, R. A. C. M. M. van Swaaij, M. Zuiddam, J. W. Metselaar, and R. E. I. Schropp, “Effect of front and back contact roughness on optical properties of single junction a-Si:H solar cells,” *Sol. En. Mater. Sol. Cells*, vol. 66, pp. 353–359, 2001.
- [82] M. Isomura, T. Takahama, S. Tsuda, and S. Nakano, “Dependence of open circuit voltage of amorphous silicon solar cells on thickness and doping level of the p-layer,” *Jpn. J. Appl. Phys.*, vol. 32, p. 1902, 1993.
- [83] D. M. Sawyer and J. I. Vette, “AP8 trapped proton environment for solar maximum and solar minimum,” *NASA Publication NSSCE*, vol. 76-06, 1976.
- [84] J. I. Vette, “The AE8 trapped electron model environment,” *NASA Publication NSSDC*, vol. 91-42, 1991.
- [85] S. R. Messenger, G. P. Summers, E. A. Burke, R. J. Walters, and M. A. Xap-sos, “Modeling solar cell degradation in space: a comparison of the NRL displacement damage dose and the JPL equivalent fluence approaches,” *Prog. Photovolt: Res. Appl.*, vol. 9, p. 103, 2001.
- [86] H. Dersch, J. Stuke, and J. Beichler, “Light induced dangling bonds in hydrogenated amorphous silicon,” *Appl. Phys. Lett.*, vol. 38, p. 456, 1980.

- 
- [87] M. Stutzmann, W. B. Jackson, and C. C. Tsai, "Light-induced metastable defects in hydrogenated amorphous silicon: A systematic study," *Phys. Rev. B*, vol. 32, no. 23, 1985.
- [88] S. T. Pantelides, "Defects in amorphous silicon: A new perspective," *Phys. Rev. Lett.*, vol. 57, p. 2979, 1986.
- [89] R. Biswas and B. C. Pan, "Mechanisms of metastability in hydrogenated amorphous silicon," *Sol. En. Mater. Sol. Cells*, vol. 78, p. 447, 2003.
- [90] V. Nádaždy and M. Zeman, "Origin of charged gap states in a-Si:H and their evolution during light soaking," *Phys. Rev. B*, vol. 69, no. 16, p. 165213, 2004.
- [91] H. M. Branz, "The hydrogen collision model of metastability after 5 years: experimental tests and theoretical extentions," *Sol. En. Mater. Sol. Cells*, vol. 78, p. 425, 2003.
- [92] P. Chaudhuri, S. Ray, A. K. Batabyal, and A. K. Barua, "Thickness dependence of light-induced effects in a-Si:H solar cells," *Solar Cells*, vol. 31, p. 13, 1991.
- [93] L. Yang and L. Chen, "Thickness dependence of light-induced degradation in a-Si:H solar cells," *J. Non-Cryst. Solids*, vol. 137-138, p. 1189, 1991.
- [94] B. Rech and H. Wagner, "Potential of amorphous silicon solar cells," *Appl. Phys. A.*, p. 155, 1999.
- [95] M. Block, "Defect distribution in a-Si:H-pin solar cells before and after degradation," *J. Non-Cryst. Solids*, vol. 164-166, p. 701, 1993.
- [96] D. L. Staebler, R. S. Crandall, and R. Williams *Appl. Phys. Lett.*, vol. 39, p. 733, 1981.
- [97] L. Yang, L. Chen, J. Y. Hou, and Y. M. Li, "The mechanism for defect generation studied by photodegradation of a-Si:H solar cells under electrical bias," in *MRS Proc.*, vol. 258, p. 365, 1992.
- [98] N. Wyrsh and A. Shah, "Degradation of a-Si:H solar cells: new evidence for a bulk effect," in *Proceedings of the First World Conference on Photovoltaic Energy Conversion*, p. 583, 1994.

- 
- [99] M. S. Haque, H. A. Naseem, and W. D. Brown, "Degradation and failure mechanisms of a-Si:H solar cells with aluminum contact," in *Proceedings of the First World Conference on Photovoltaic Energy Conversion*, pp. 642–645, 1994.
- [100] N. Wyrsh and A. Shah, "Depth profiles of mobility lifetime products and capture cross-sections in a-Si:H," *Solid State Commun.*, vol. 80, p. 807, 1991.
- [101] P. Hotaling, H. Antoniadis, and E. A. Schiff, "Electron mobility-lifetime product and D0 defect density in hydrogenated amorphous silicon," *J. Non-Cryst. Solids*, vol. 114, p. 420, 1989.
- [102] J. A. Schmidt, R. D. Arce, R. R. Koropecski, and R. H. Buitrago, "Light-induced creation of metastable defects in hydrogenated amorphous silicon studied by computer simulations of constant photocurrent measurements," *Phys. Rev. B*, vol. 59, no. 7, p. 4568, 1999.
- [103] I. Sakata, M. Yamanaka, S. Numase, and Y. Hayashi, "Deep defect states in hydrogenated amorphous silicon studied by a constant photocurrent method," *J. Appl. Phys.*, vol. 71, p. 4344, 1992.
- [104] S. Wagner, X. Xu, X. R. Li, D. S. Shen, M. Isomura, M. Bennett, A. E. Delahoy, X. Li, and J. K. Arch, "Performance and modeling of amorphous silicon solar cells soaked at high light intensity," in *Conference Record of the Twenty Second IEEE Photovoltaic Specialists Conference*, p. 1307, 1991.
- [105] M. Stutzmann, "Weak bond-dangling bond conversion in amorphous silicon," *Phil. Mag. B*, vol. 56, p. 63, 1987.
- [106] G. Schumm, "Chemical equilibrium description of stable and metastable defect structures in a-Si:H," *Phys. Rev. B*, vol. 49, p. 2427, 1994.
- [107] C. Longeaud, "Mediation of light-induced metastable defect formation in hydrogenated amorphous silicon by interstitial hydrogen and voids," *J. Optoelectr. and Adv. Mater.*, vol. 4, no. 3, pp. 461–479, 2002.
- [108] H. C. Kang, "Correlation between bond distortion and the band-tail electronic density of states in amorphous silicon: a tight-binding recursion study," *J. Non-Cryst. Solids*, vol. 261, pp. 169–180, 2000.

- 
- [109] B. R. Djordjevic, M. F. Thorpe, and F. Wooten, "Computer model of tetrahedral amorphous diamond," *Phys. Rev. B*, vol. 52, p. 5685, 1995.
- [110] B. Stannowski, *Silicon-based thin-film transistors with a high stability*. PhD thesis, Utrecht University, 2002.
- [111] S. C. Deane, R. B. Wehrspohn, and M. J. Powell, "Unification of the time and temperature dependence of dangling-bond-defect creation and removal in amorphous-silicon thin-film transistors," *Phys. Rev. B*, vol. 58, no. 19, p. 12625, 1998.
- [112] G. J. Vendura, M. A. Kruer, R. M. Kurland, and J. Newton, "The effects of radiation and annealing on amorphous silicon solar cell space arrays," in *Conference Record of the Twenty Fourth IEEE Photovoltaic Specialists Conference 1994*, vol. 2, p. 2049, 1994.
- [113] R. J. Walters, J. H. Warner, G. P. Summers, S. R. Messenger, J. R. Lorentzen, P. Tlomak, J. E. Granata, and P. E. Hausgen, "Radiation response and annealing characteristics of thin film photovoltaics," in *19th European Photovoltaics Solar Energy Conference*, p. 3606, 2004.
- [114] B. Rech, S. Wieder, C. Beneking, A. Loffi, O. Kluth, W. Reetz, and H. Wagner, "Texture etched ZnO:Al films as front contact and back reflector in amorphous silicon p-i-n and n-i-p solar cells," in *Conference Record of the Twenty Sixth IEEE Photovoltaic Specialists Conference*, p. 619, 1997.
- [115] O. Kluth, A. Loffi, S. Wieder, C. Beneking, W. Appenzeller, L. Houben, B. Rech, H. Wagner, S. Hoffmann, R. Waser, J. A. A. Selvan, and H. Keppner, "Texture etched Al-doped ZnO: a new material for enhanced light trapping in thin film solar cells," in *Conference Record of the Twenty Sixth IEEE Photovoltaic Specialists Conference 2002*, pp. 715–718, 1997.
- [116] M. Kubon, E. Boehmer, F. Siebke, B. Rech, C. Beneking, and H. Wagner, "Solution of the ZnO/p contact problem in a-Si:H solar cells," *Sol. En. Mater. Sol. Cells*, vol. 41-42, pp. 485–492, 1996.
- [117] S. Y. Myong and K. S. Lim, "Natural hydrogen treatment effect during formation of double amorphous silicon-carbide p layer structures producing high-efficiency pin-type amorphous silicon solar cells," *Appl. Phys. Lett.*, vol. 86, p. 33506, 2005.

- 
- [118] G. Munyeme, M. Zeman, R. E. I. Schropp, and W. F. van der Weg, "Performance analysis of a-Si:H p-i-n solar cells with and without a buffer layer at the p/i interface," *Physica Status Solidi C*, vol. 1, no. 9, p. 2298, 2004.
- [119] M. K. van Veen and R. E. I. Schropp, "Amorphous silicon deposited by hot-wire CVD for application in dual junction solar cells," *Thin Solid Films*, vol. 403, p. 135, 2002.
- [120] M. Zeman, R. A. C. M. M. van Swaaij, J. W. Metselaar, and R. E. I. Schropp, "Optical modeling of a-Si:H solar cells with rough interfaces: Effects of back contact and interface roughness," *J. Appl. Phys.*, vol. 88, no. 11, pp. 6436–6443, 2000.
- [121] L. Yang, L. Chen, and A. Catalano, "Intensity and temperature dependence of photodegradation of amorphous silicon solar cells under intense illumination," *Appl. Phys. Lett.*, vol. 59, p. 840, 1991.
- [122] M. C. Rossi, M. S. Brandt, and M. Stutzmann, "Accelerated stability test for amorphous silicon solar cells," *Appl. Phys. Lett.*, vol. 60, p. 1709, 1992.
- [123] G. P. Summers, S. R. Messenger, E. A. Burke, M. A. Xapsos, and R. J. Walters, "Low energy proton-induced displacement damage in shielded GaAs solar cells in space," *Appl. Phys. Lett.*, vol. 71, no. 6, p. 832, 1997.
- [124] C. Wagner, S. Gangopadhyay, B. Schröder, and J. Geiger, "Different generation processes of metastable defects in sp-a-Si:H material by light soaking and keV-electron irradiation," in *AIP Conf. Prof.*, vol. 157, p. 48, 1987.
- [125] W. Herbst, J. Dudel, A. Scholz, B. Schröder, and H. Oechsner *Sol. En. Mater. Sol. Cells*, vol. 37, p. 55, 1995.
- [126] U. Schneider, A. Scholz, B. Schröder, F. Karg, and H. Kausche, "A comparative study of the electronic stability of hydrogenated amorphous silicon and silicon-germanium alloy material," *Jpn. J. Appl. Phys.*, vol. 30, no. 2, pp. 228–232, 1991.
- [127] A. Scholz and B. Schröder, "Interpretation of the saturation behavior of the metastable defect density created in intrinsic a-Si:H by keV-electron irradiation," *J. Non-Cryst. Solids*, vol. 137-138, pp. 259–262, 1991.

- 
- [128] H. Stitzl, G. Krötz, and G. Müller, “Accumulation and annealing of implantation damage in a-Si:H,” *Appl. Phys. A.*, vol. 53, pp. 235–240, 1991.
- [129] K. R. Lord, M. R. Walters, and J. R. Woodyard, “Investigation of light and dark I-V characteristics of a-Si:H alloy solar cells, irradiated with 1.0 MeV protons,” in *Proceedings of the 23rd Photovoltaic Specialists Conference*, p. 1448, 1993.
- [130] I. Abril, R. Garcia-Molina, K. M. Erokhin, and N. P. Kalashnikov, “Phosphorus doping of silicon by proton induced nuclear reactions,” *Appl. Phys. Lett.*, vol. 66, no. 22, p. 3036, 1995.
- [131] J. Dubeau, L. A. Hamel, and T. Pochet, “Radiation ionization energy in a-Si:H,” *Phys. Rev. B*, vol. 53, no. 26, p. 10740, 1996.
- [132] G. P. Summers, R. J. Walters, M. A. Xapsos, E. A. Burke, S. R. Messenger, P. Shapiro, and R. L. Statler, “A new approach to damage prediction for solar cells exposed to different radiations,” in *Proceedings of the First World Conference on Photovoltaic Energy Conversion*, p. 2068, 1994.
- [133] B. Stannowski, R. E. I. Schropp, and A. Nascetti, “High energy-barrier for defect creation in thin-film transistors based on hot-wire amorphous silicon,” *Appl. Phys. Lett.*, vol. 75, p. 3674, 1999.
- [134] B. Stannowski, A. M. Brockhoff, A. Nascetti, and R. E. I. Schropp, “Metastability of hot-wire amorphous-silicon thin-film transistors,” *J. Non-Cryst. Solids*, vol. 266-269, p. 464, 2000.
- [135] M. J. Powell, S. C. Deane, and R. B. Wehrspohn, “Microscopic mechanisms for creation and removal of metastable dangling bonds in hydrogenated amorphous silicon,” *Phys. Rev. B*, vol. 66, p. 155212, 2002.
- [136] S. R. Messenger, E. A. Burke, G. P. Summers, R. J. Walters, E. M. Jackson, and B. D. Weaver, “Nonionizing energy loss (NIEL) for heavy ions,” *IEEE Trans. Nucl. Sci.*, vol. 46, no. 6, p. 1595, 1999.
- [137] E. A. Schiff, “Diffusion-controlled bimolecular recombination of electrons and holes in a-Si:H” *J. Non-Cryst. Solids*, vol. 190, pp. 1–8, 1995.
- [138] A. Klaver, J. M. Warman, M. P. de Haas, J. W. Metselaar, and R. A. C. M. M. van Swaaij, “Study of 3-MeV electron radiation damage in amorphous silicon with TRMC,” in *MRS Proc. 808*, p. 165, 2004.

- [139] Q. Wang, H. Antoniadis, and E. A. Schiff, “Electron drift mobility measurements on annealed and light-soaked hydrogenated amorphous silicon,” *Appl. Phys. Lett.*, vol. 60, p. 2791, 1992.
- [140] M. Despeisse, D. Moraes, G. Anelli, P. Jarron, J. Kaplon, R. Rusack, S. Saramad, and N. Wyrsh, “Hydrogenated amorphous silicon sensors based on thin film on asic technology,” in *Proceedings of the Nuclear Science Symposium and Medical Imaging Conference 2005*, 2005.

# List of abbreviations and symbols

---

$a$	rate constant in eq. 5.2
a-Si:H	hydrogenated amorphous silicon
C	constant used in eq. 1.5
$C_e$	multiplication factor for the as-deposited, negatively charged defect states distribution
$C_h$	multiplication factor for the as-deposited, positively charged defect states distribution
$C_z$	multiplication factor for the as-deposited, uncharged defect states distribution
c-Si	crystalline silicon
CSDA	Constant Stopping Derivation Approach
$D_d$	displacement damage dose
$D_i$	ionizing dose
DBP	Dual-Beam Photoconductivity
$E$	energy position in band diagram
$E_u$	Urbach energy
$E_{cc}$	characteristic energy of the conduction band tail
$E_c$	energy position of the bottom of the conduction band
$E_v$	energy position of the top of the valence band
$G$	electron-hole pair generation rate density
IEL	Ionizing Energy-Loss function
$J_{sc}$	short-circuit current density
$k_i$	experimental-determined rate constant in eq. 5.1

$k$	Boltzmann constant
$K$	kinetic energy
LEO	Low Earth Orbit
MEO	Medium Earth Orbit
$n$	free electron concentration
$n_i$	complex part of the refractive index
$N$	density of states
$N_D$	defect density
$N_c$	effective density of states of the conduction band
$N_v$	effective density of states of the valence band
NIEL	Non-Ionizing Energy-Loss function
$p$	free hole concentration
RT	Reflection-Transmission
$t$	time
TRMC	Time-Resolved Microwave Conductivity
$T$	temperature
$\alpha$	absorption
$\Delta E_{act}$	change in activation energy of both doped layers
$\Delta N_D$	increase in defect density
$h\nu$	photon energy
$\Phi_n$	incident electron flux
$\Phi_p$	incident proton flux
$\sigma$	capture cross-section
$\sigma_{pv}$	hole-capture-cross section of valence band tail states
$\sigma_{ev}$	electron-capture-cross section of valence band tail states
$\sigma_{pc}$	hole-capture-cross section of conduction band tail states
$\sigma_{ec}$	electron-capture-cross section of conduction band tail states
$\sigma_{pc}$	hole-capture-cross section of defect states
$\sigma_{ec}$	electron-capture-cross section of defect states

---

# Summary

Solar cells are the prime power supply for satellites in space. Space is, however, a hostile environment for electronic devices, such as solar cells: in space the devices are subjected to large temperature cycles, atomic oxygen, space dust, meteorites, and high-energy charged-particle irradiation. For medium earth orbit and geostationary orbits the lifetime of solar cells is mainly limited by this charged-particle irradiation. Hydrogenated amorphous silicon (a-Si:H) solar cells show favorable properties, which may enable the application of these solar cells in space missions, especially in high-radiation environments. It has been established that thin-film silicon solar cells have greater radiation tolerance compared to conventional solar cells based on crystalline Si or GaAs. Furthermore, a-Si:H cells exhibit low-temperature annealing behavior, meaning damage induced by irradiation is reversed, when subjecting the cells to temperature in the range of 100°C. In addition, thin-film silicon solar cells can be produced on flexible substrates, inexpensively and lightweight, because no cover-glasses is needed to protect the cells from irradiation.

In order to investigate if a-Si:H are cost competitive with c-Si and GaAs solar cells for particular missions, several factors need to be taken into account. The most important cost factors are the production of the solar-cell panels, the (un)folding mechanism of the panels, and the launch costs. The launch costs are directly related to the mass of the solar cells and the required folding mechanism. The costs for the entire system are related to the area of the solar cells needed to provide enough power to the satellite at the end of the mission, the so-called End-of-Life (EOL) performance. Therefore, if a-Si:H solar cells are to be used for space applications it is essential that the EOL-performance for a particular mission is predictable and understood.

In this thesis we present the development of a model with which the EOL-

performance of a-Si:H solar cells can be predicted for a high-radiation space mission. For this development we have performed light-soaking, electron-beam, and proton-beam irradiation experiments on a-Si:H layers and solar cells in order to study the degradation cell performance under these conditions. Furthermore, we present a procedure for the simulation of solar-cell performance degradation and this method has been applied to our measurement results to study some aspects of the degradation in more detail.

In chapter 2 we show results of electron-beam irradiation experiments on a-Si:H and a-Si:H-related materials to investigate which and how material properties change when subjected to radiation. Intrinsic a-Si:H has been characterized by measuring the absorption spectrum, and dark and photo-conductivity. Furthermore, a-Si:H degradation has been studied using time-resolved microwave-conductivity measurements. For doped layers the activation energy of the dark conductivity is determined following irradiation. For the glass only optical parameters are investigated. From the results three main contributions to the degradation of a-Si:H solar cells by high-energy charged-particle irradiation have been identified: an increase of the defect density in the intrinsic layer, an increase of the activation energy of the doped layers, and additional absorption in the glass substrates. No change in the charge-carrier mobility or the weak-bond concentration was observed.

In chapter 3 we present our procedure to simulate the degradation of a-Si:H solar cells. In this procedure the electrical and optical device simulator, Advanced Semiconductor Analysis (ASA), is used to calculate the performance characteristics of the solar cells based on an input parameter set. In our procedure the as-deposited parameters set is correlated to the degraded set by changing the input parameters related to the material properties that vary upon radiation as described in chapter 2. Changes in other material properties, for instance a change in the valence-band tail width, are not taken into account as a degradation effect, but can be easily included in this procedure if required. In this chapter we also present a sensitivity study of this procedure. Using our procedure we found that the increase of the glass absorption leads mainly to a decrease in short-circuit current,  $J_{sc}$ . Changes in the activation energy of the doped layers will mainly lead to a lowering of the open-circuit voltage,  $V_{oc}$ , and the fill factor,  $FF$ , while the  $J_{sc}$  is hardly affected or may even increase. Increasing the defect density of states will result in  $FF$  and  $J_{sc}$  degradation, while the  $V_{oc}$  remains unaffected. When combining the increase in activation energy of the doped layers with the increase

---

in defect density, an enhancement in  $FF$  degradation is observed. Finally, it was found that the quantum efficiency degradation, which is highly dependent on the defect density, is only slightly dependent on the depth location of the induced defects. Therefore during light soaking, the total recombination in the solar cell, and thus the total induced defect density, explains mainly the differences in performance degradation between the solar cells with different thickness and not the depth differences in recombination profiles.

The procedure to simulate the degradation of a-Si:H solar cells was verified by applying it to light soaking of these cells. In chapter 4 we present the results of light-soaking experiments on a-Si:H solar cells under both open- and short-circuit conditions. These conditions were chosen in order to alter the recombination profile in the solar cells. The degradation of the solar-cell performance is mostly due to lowering of the  $FF$  and the  $J_{sc}$ . It was found that solar cells with a thicker i-layer degrade faster. Further, we observe that short-circuited solar cells are more stable than the solar cells light-soaked under open-circuit condition. The experimental results of the degradation by light soaking have been matched to simulations obtained using our procedure. In the simulations only changes in the defect density of states were included. When the defect-creation profile is related to the electron-hole pair recombination rate profile during the light soaking, a reasonable good match between the simulations and the experiments is obtained for all the external parameters and the quantum efficiency under both open- and short-circuit conditions for each i-layer thickness. We stress that this match is obtained by adjusting only one parameter, namely the parameter controlling the increase of the density of neutral defect states. From the simulations it was concluded that the increase in defect density in the intrinsic layer as a result of light soaking follows a  $t^{1/3}$  dependence, in agreement with literature reports on light soaking of a-Si:H.

The degradation of a-Si:H solar cells by electron-beam irradiation is studied in chapter 5. A series of solar cells with different i-layer thickness was deposited and exposed to 1-MeV electron-beam irradiation. In the experiments we have varied the fluence, the beam current, and performed the irradiation under open- and short-circuit condition. Similar to light soaking, the thinner cells are more stable against the irradiation. The drop in the  $FF$  is the most important parameter in the degradation of the cell efficiency. The thickness dependence was strongest for the  $J_{sc}$ . In contrast to light soaking, lowering of the  $V_{oc}$  played a major role in the degradation. In literature it was suggested that electron-hole

pair recombination events also play a role in the degradation by high-energy electrons. In order to study the degradation mechanism in more detail two dedicated experiments were carried out. In the first experiment the influence of the incident electron flux on the degradation was studied. No dependency of the a-Si:H solar-cell degradation on the flux was found, apart from cracking of the TCO layer. Further, we found no difference between open- and short-circuit degradation when subjected to electron-beam irradiation. Neither experiment could provide indications that electron-hole pair recombination events play a role in the degradation and we therefore suggest that the degradation is initiated by collisions of incident electrons with the a-Si:H lattice. The experimental results of the solar-cell performance following electron-beam irradiation have also been matched to computer simulations using our procedure. This time a uniform increase of defect density over the entire solar cell was assumed in the simulation. Furthermore, in the simulations the activation energy of the doped layers was increased, in agreement with experimental observations presented in chapter 2. Overall, for the external parameters and QE a reasonable good match between the experimental and simulation results was obtained. We found that the defect density and the activation energy of the doped layer increase more or less linearly with the fluence following irradiation, which also indicates that defect formation in a-Si:H following electron-beam irradiation is not initiated by electron-hole pair recombination events.

The degradation of a-Si:H single-junction solar cells with different i-layer thickness by 1-MeV and 65-MeV proton irradiation has been studied in chapter 6. It was found that proton-beam irradiation induces more damage in the solar cells as compared to electron-irradiation. Furthermore, the cells are more tolerant to 65-MeV proton irradiation than to 1-MeV proton irradiation. In the previous chapter we concluded that the degradation by high-energy electron-beam irradiation is likely due to non-ionizing collision events of incident electrons with a-Si:H. However, when using the non-ionizing energy loss (NIEL) values published by Srour et al. [28] to calculate the displacement damage dose in a-Si:H, no correlation between electron-beam and proton-beam irradiation is found. In contrast, it appears that the solar-cell performance degradation is related to the ionizing dose, because a correlation between electron- and proton-beam irradiation can be found when using the ionizing energy loss (IEL) values. However, when comparing charged-particle degradation to light soaking, the ionizing dose during light soaking is much higher than for charged-particle irradiation, while the perfor-

---

mance degradation is much less for light soaking. We think that this observation indicates that the degradation by charged-particle irradiation is not linked to the ionizing dose. Therefore, we conclude that the degradation of a-Si:H solar cells is indeed related to non-ionizing collision events, but that the NIEL values presented by Srour et al. [28] to predict the amount of defect creation in a-Si:H are not correct. We think that the NIEL values for electron irradiation of a-Si:H should be higher in order to reflect the occurrence of weak bonds in a-Si:H, which will significantly lower the energy needed for the creation of defects. Assuming a higher NIEL values for electron irradiation will remove the discrepancy between the degradation of a-Si:H solar cells by proton and electron irradiation.



# Samenvating

Zonnecellen worden veelal gebruikt als energiebron voor satellieten. De ruimte is echter een vijandige omgeving voor elektronische componenten, zoals zonnecellen. Ze worden blootgesteld aan grote temperatuurverschillen, atomair zuurstof, ruimtestof, meteorieten en bestraling door geladen deeltjes met hoge energie. Voor zogenaamde *medium-earth* en geostationaire satellietbanen wordt de levensduur van zonnecellen op satellieten voor een groot deel bepaald door deze straling. Zonnecellen van gehydrogeneerd amorf silicium (a-Si:H) hebben gunstige eigenschappen welke toepassing in de ruimtevaart mogelijk maken, vooral voor missies waarbij veel deeltjesstraling te verwachten valt. Het is aangetoond dat zonnecellen van dunne lagen van silicium (Si) beter bestand zijn tegen deze straling in vergelijking met conventionele zonnecellen van kristallijn Si (c-Si) of galliumarsenide (GaAs). Tevens kan de schade die door de deeltjesstraling in de cellen wordt geïnduceerd, voor een groot deel worden teruggedraaid door de cellen bloot te stellen aan een temperatuur van ongeveer 100°C. Verder zijn deze zonnecellen goedkoper en lichter, en kunnen ze geproduceerd worden op flexibele substraten. Dit komt mede doordat deze zonnecellen zonder beschermglas kunnen worden gebruikt.

Om te bestuderen of zonnecellen van a-Si:H kostenbesparend zijn ten opzichte van conventionele zonnecellen van c-Si en GaAs voor bepaalde ruimtemissies, moeten verschillende kostenfactoren worden overwogen. De meest belangrijke factoren zijn de productie van de zonnepanelen, het uitklapmechanisme, en de lanceerkosten. De lanceerkosten zijn vooral afhankelijk van de totale massa van de panelen en het bijbehorende uitvouwmechanisme. Deze kosten zijn op hun beurt weer afhankelijk van de grootte en het rendement van de zonnepanelen die nodig zijn om de satelliet van voldoende energie te voorzien aan het einde van de missie. Daarom is het belangrijk om het rendement aan het einde van de missie van de zonnecellen van a-Si:H goed te kunnen voorspellen.

In dit proefschrift presenteren we een model waarmee het rendement van een zonnecel aan het einde van zijn levensduur kan worden voorspeld voor een ruimtevaartmissie met veel straling. Om dit model te kunnen ontwikkelen, hebben we dunne lagen en zonnecellen van a-Si:H blootgesteld aan langdurige belichting en bestraald met elektronen en protonen met hoge energie om zodoende het degradatiegedrag onder deze omstandigheden te bestuderen. Ook presenteren we een procedure voor het simuleren van gedegradeerde zonnellen van a-Si:H en vergelijken we de resultaten van deze methode met meetdata om enkele aspecten van de degradatie in meer detail te onderzoeken.

In hoofdstuk 2 onderzoeken we welke materiaaleigenschappen van a-Si:H veranderen tengevolge van de bestraling en op welke wijze dit gebeurt. Voor dit doel zijn het absorptiespectrum en de donker- en lichtgeleiding van intrinsiek a-Si:H gemeten. Daarnaast zijn lagen van intrinsiek a-Si:H bestudeerd door middel van *time-resolved microwave conductivity* spectroscopie. Het effect van bestraling op gedoteerd a-Si:H is bepaald door de activeringsenergie van de donkergeleiding te meten. De glazen substraten zijn gekarakteriseerd door de lichtabsorptie in deze substraten te meten. Uit de resultaten zijn drie belangrijke effecten naar voren gekomen die de degradatie van zonnecellen van a-Si:H tengevolge van bestraling bepalen: een verhoging van de defectdichtheid in intrinsiek a-Si:H, een verhoging van de activeringsenergie van gedoteerd a-Si:H en een toegenomen absorptie van het inkomende licht in het glas. Er zijn geen veranderingen gevonden in de mobiliteiten van ladingsdragers en in de concentratie van zwakke bindingen in het a-Si:H.

In hoofdstuk 3 tonen we onze procedure voor het simuleren van de prestatie van gedegradeerde zonnecellen van a-Si:H. Hiervoor maken we gebruik van de devicesimulator, *Advanced Semiconductor Analysis* (ASA). Met ASA zijn we in staat de karakteristieken van zonnecellen te berekenen op basis van sets van parameters die eigenschappen van de individuele lagen van de cel beschrijven. Onze procedure correleert parameter sets van individuele lagen voor onbestraalde zonnecellen met die van bestraalde door deze aan te passen op de wijze zoals gevonden in het vorige hoofdstuk. Veranderingen in andere materiaaleigenschappen, zoals de breedte van de valentiebandstaart, zijn niet meegenomen in de procedure, maar kunnen, indien nodig, gemakkelijk worden geïntroduceerd. In dit hoofdstuk worden ook de resultaten van een gevoeligheidsstudie van de procedure gepresenteerd. In deze studie vonden we dat de toename in de absorptie in het glas voornamelijk leidt tot een verlaging van de kortsluitstroomdichtheid

---

( $J_{sc}$ ). Veranderingen in de activeringsenergie van de gedoteerd a-Si:H leidt tot een verlaging van de openklemspanning ( $V_{oc}$ ) en de vulfactor ( $FF$ ), terwijl de  $J_{sc}$  nauwelijks verandert of zelfs licht toeneemt. Verhoging van de toestandsdichtheid voor defecten leidt tot een verlaging van de  $FF$  en de  $J_{sc}$ , terwijl in dit geval de  $V_{oc}$  onveranderd blijft. Wanneer de verhoging van de defectdichtheid in intrinsiek a-Si:H en de activeringsenergie van gedoteerd a-Si:H samengevoegd worden, wordt een sterkere degradatie van de  $FF$  gevonden. Tenslotte wordt opgemerkt dat de zogenaamde *quantum efficiency*, hoewel zeer gevoelig voor de totale hoeveelheid defecten in de zonnecellen, redelijk ongevoelig lijkt voor de positie in de cel waar deze defecten geïnduceerd worden. Om deze reden is dan ook de totale recombinatiesnelheid meer van belang voor de degradatie van de prestatie van de zonnecel dan het diepteprofiel van de recombinatiesnelheid tijdens degradatie tengevolge van langdurige belichting.

De procedure voor het simuleren van gedegradeerde zonnecellen van a-Si:H is geverifieerd door deze toe te passen op zonnecellen gedegrademd door langdurige belichting. In hoofdstuk 4 worden resultaten van experimenten gepresenteerd waarin zonnecellen zijn gedegrademd in zowel openklem als kortgesloten toestand. Het profiel van de recombinatiesnelheid is onder belichting in openklem toestand beduidend anders dan onder kortgesloten toestand. Na langdurige belichting van de zonnecellen wordt voornamelijk een vermindering van de  $FF$  en de  $J_{sc}$  waargenomen. Zonnecellen met een dikkere intrinsieke laag degraderen sneller. Ook zijn de kortgesloten zonnecellen stabielier dan de cellen die langdurig belicht zijn onder openklem toestand. Deze experimentele resultaten worden vergeleken met degene die verkregen zijn uit de simulatieprocedure. In deze simulaties is alleen een verhoging van de defectdichtheid in de intrinsieke laag van a-Si:H in de zonnecel meegenomen. Wanneer het diepteprofiel van de geïnduceerde defecten wordt gerelateerd aan het recombinatieprofiel van elektronen met gaten, dan komen de meet- en simulatieresultaten van de externe parameters van de zonnecellen en de *quantum efficiency* goed overeen voor zonnecellen met verschillende dikte, zowel in kortgesloten als in openklem toestand. We benadrukken dat deze overeenkomst is verkregen door slechts één parameter te variëren, namelijk de vergroting van de defectdichtheid in het midden van de bandkloof. We hebben gevonden dat deze defectdichtheid een  $t^{1/3}$  afhankelijkheid heeft (met  $t$  de belichtingstijd), hetgeen overeenkomt met wat gerapporteerd wordt in de literatuur.

In hoofdstuk 5 wordt degradatie van een aantal series zonnecellen (met verschillende diktes) bestudeerd die door elektronen met een energie van 1 MeV

bestraald zijn. Ten eerste zijn experimenten uitgevoerd waarin de hoeveelheid elektronen wordt gevarieerd waarmee de cellen bestraald worden. Vergelijkbaar met zonnecellen die blootgesteld zijn aan langdurige belichting, hebben we gevonden dat dikke cellen sneller degraderen dan dunne. De vermindering van de  $FF$  heeft de meeste invloed op de totale vermogensreductie na bestraling. De dikteafhankelijkheid komt het sterkst naar voren in de resultaten van de  $J_{sc}$ . In tegenstelling tot zonnecellen blootgesteld aan langdurige belichting, hebben we in dit geval ook een daling van de  $V_{oc}$  gevonden. In de literatuur is geopperd dat recombinatie van door elektronenbestraling geïnduceerde elektronen en gaten een invloed heeft op de degradatie van zonnecellen van a-Si:H, vergelijkbaar met de degradatie gedurende langdurige belichting. Om dit te toetsen zijn twee experimenten uitgevoerd. In het eerste experiment werd het effect van de elektronenflux bestudeerd. Er werd geen afhankelijkheid gevonden tussen de mate van degradatie van de zonnecelprestatie en de elektronenflux, behalve dat breuken in de laag van transparant oxide worden waargenomen wanneer een hoge elektronenflux wordt gebruikt. Als gevolg van deze breuken functioneren deze zonnecellen niet meer. In het tweede experiment is het effect van het al dan niet kortsluiten van de cellen tijdens de bestraling bestudeerd. In dit experiment hebben we geen verschil gevonden tussen cellen bestraald onder kortgesloten en onder openklem toestand. Geen van beide experimenten hebben een indicatie opgeleverd dat recombinatie van elektronen met gaten van invloed is op de degradatie van de zonnecellen gedurende elektronenbestraling. Daarom concluderen we dat de degradatie geïnitieerd wordt door botsingen van de inkomende elektronen met het a-Si:H rooster waarbij bindingen worden verbroken. Dit betekent dat de schade in a-Si:H gecorreleerd kan worden aan het aantal atoomverplaatsingen tengevolge van botsingen van elektronen met het rooster en deze hoeveelheid verplaatsingen kan, in principe, berekend worden met waarden voor de zogenaamde *non-ionizing energy loss* (NIEL). De meetresultaten zijn ook dit keer vergeleken met simulatieresultaten die verkregen zijn met behulp van onze procedure. In dit geval is echter een uniform profiel voor de vergroting van de defectdichtheid in de intrinsieke laag gebruikt. Verder is de activeringsenergie van de gedoteerd a-Si:H aangepast in overeenstemming met de meetresultaten gevonden in hoofdstuk 2. In het algemeen tonen de simulatieresultaten een goede overeenkomst met de meetresultaten. Met behulp van de simulaties hebben we gevonden dat de defectdichtheid en de activeringsenergie min of meer lineair afhankelijk zijn van de stralingsdosis. Dit resultaat is ook een indicatie dat de degradatie tengevolge

---

van elektronenbestraling niet geïnitieerd wordt door recombinatie van elektronen en gaten.

In hoofdstuk 6 is de degradatie van zonnecellen van a-Si:H met verschillende intrinsieke laagdiktes beschreven tengevolge van bestraling met protonen met energieën van 1-MeV en 65-MeV. Vanwege de grotere massa induceren protonen meer schade in het materiaal dan elektronen. Uit de experimenten bleek dat zonnecellen minder gevoelig zijn voor bestraling met protonen met een energie van 65-MeV dan met een energie van 1-MeV. In het vorige hoofdstuk hebben we geconcludeerd dat de schade na bestraling gerelateerd is aan het aantal niet-ioniserende botsingen van de elektronen met het a-Si:H. Echter, als we de waarden voor de NIEL gebruiken om de hoeveelheid atoomverplaatsingen in a-Si:H te berekenen zoals dat door Srour et al. [28] is gedaan, dan vinden we geen goede correlatie tussen zonnecellen bestraald met elektronen en cellen bestraald met protonen. Daarentegen vinden we wel een goede overeenkomst tussen de schade na bestraling en de hoeveelheid ioniserende interacties van geladen deeltjes met het rooster, wat berekend kan worden met waarden voor de *ionizing energy loss* (IEL). Omdat door deze interacties paren van elektronen en gaten worden gecreëerd, zou dit kunnen betekenen dat recombinatie van elektronen en gaten toch aan de basis ligt van de creatie van defecten. Bekijken we echter de resultaten van zonnecellen na langdurige belichting, waarvan we zo goed als zeker weten dat defecten gecreëerd worden door recombinatie van elektronen met gaten, dan zien we dat de hoeveelheid paren van elektronen en gaten die gecreëerd worden veel groter is dan tengevolge van bestraling met deeltjes. Echter, uit de metingen blijkt dat na bestraling met deeltjes veel meer schade wordt toegebracht. Wij denken daarom dat de degradatie van de prestatie van zonnecellen niet gerelateerd is aan de hoeveelheid ionisaties in a-Si:H. Volgens ons zijn de NIEL waarden zoals die door Srour et al. [28] en in eerste instantie ook door ons gebruikt zijn, niet correct om het aantal atoomverplaatsingen in zonnecellen van a-Si:H te voorspellen. De NIEL waarden die gebruikt zijn, zijn bepaald voor c-Si. Wij denken dat de NIEL waarden voor elektronbestraling hoger moeten zijn, omdat er in a-Si:H veel zwakke Si-Si bindingen bestaan die gemakkelijk kunnen breken door interactie met elektronen. Dit betekent dat de energie die nodig is om een defect te maken in a-Si:H lager is dan voorspeld met behulp van NIEL waarden voor c-Si. Als we een hogere NIEL waarde aannemen voor elektronenbestraling kan dit de discrepantie tussen elektronen- en protonenbestraling verklaren.



# Curriculum Vitae

Arjen Klaver was born in Helmond, the Netherlands on 11<sup>th</sup> of June 1977. He obtained his VWO diploma in 1995 from the Bisschoppelijk College in Sittard. Subsequently studied Applied physics at the Eindhoven University of Technology. During his degree work he investigated copper deposition using chemical vapor deposition (CVD), plasma treatment of silicon oxide layers and assisted in the design of a fast-grating infrared spectroscope. In December 2001 he obtained his master degree. From March to May 2002 he worked for Eindhoven University of Technology on the deposition of microcrystalline silicon using Expanding Thermal Plasma CVD. In June 2002, Arjen started his research towards his Ph.D. degree at DIMES, Delft University of Technology. The aim of the project was to develop a model to predict the end-of-life performance of amorphous silicon solar cells for space missions. This project focused on the development of a procedure with which the performance of amorphous silicon solar cells following light soaking or charged-particle irradiation could be simulated using a computer program. This work was carried out in co-operation with Dutch Space b.v. and was supported financially by Technology Foundation STW and SenterNovem. Currently, Arjen is doing research on the use of magnetic tweezers in biophysical applications at MESA<sup>+</sup>, Twente University.



# List of publications

## Publications related to this thesis

A. Klaver and R. A. C. M. M. van Swaaij, "Modeling of light-induced degradation of amorphous silicon solar cells," to be published in *Sol. En. Mater. Sol. Cells*, vol. 92, no. 1, p. 50, 2008.

R. A. C. M. M. van Swaaij and A. Klaver, "Comparison of amorphous silicon solar cell performance following light and high-energy electron-beam induced degradation," accepted for publication in *J. Non-Cryst. Solids*, 2007.

A. Klaver, V. Nádaždy, M. Zeman, and R. A. C. M. M. van Swaaij, "Charge deep-level transient spectroscopy study of high-energy electron-beam irradiated hydrogenated amorphous silicon," *Appl. Phys. Lett.*, vol. 89, p. 22119, 2006.

A. Klaver, J. W. Metselaar, M. Zeman, and R. A. C. M. M. van Swaaij, "Development of a model to predict EOL efficiency of amorphous silicon solar cells for space applications," in *Conference Record of the 20th European Photovoltaic Solar Energy Conference and Exhibition*, 2005.

A. Klaver, J. W. Metselaar, M. Zeman, and R. A. C. M. M. van Swaaij, "Simulation on 1-MeV electron-beam irradiated amorphous silicon solar cells with varying thickness," in *Conference Record of the Thirty First IEEE Photovoltaic Specialist Conference*, p. 1440, 2005.

A. Klaver, J. W. Metselaar, M. Zeman, and R. A. C. M. M. van Swaaij, "Defect-creation mechanisms in high-energy electron irradiated a-Si:H solar cells," in *Proceedings of the 8th Annual Workshop on Semiconductor Advances for Future Electronics and SENSORS (SAFE)*, 2005.

A. Klaver, J. M. Warman, M. P. de Haas, J. W. Metselaar, and R. A. C. M. M. van Swaaij, "Study of 3-MeV electron radiation damage in amorphous silicon with TRMC," in *Mat. Res. Soc. Symp. Proc. 808*, p. 165, 2004.

## Other publications

C. Smit, A. Klaver, B. A. Korevaar, A. M. H. N. Petit, D. L. Williamson, R. A. C. M. M. van Swaaij, and M. C. M. van de Sanden, "High-rate deposition of microcrystalline silicon with an expanding thermal plasma," *Thin Solid Films*, vol. 22, 491(1-2), p. 280, 2005.

M. F. A. M. van Hest, A. Klaver, D. C. Schram, and M. C. M. van de Sanden, "Argon-oxygen plasma treatment of deposited organosilicon thin films," *Thin Solid Films*, vol. 449 (1-2), p. 40, 2004.

M. F. A. M. van Hest, A. Klaver, D. C. Schram, and M. C. M. van de Sanden, "Design of a fast in-situ infrared diagnostic tool," *Review of Scientific Instruments*, vol. 74 (5), p. 2675, 2003.

M. F. A. M. van Hest, A. Klaver, D. C. Schram, and M. C. M. van de Sanden, "A new and fast in-situ spectroscopic infrared absorption measurement technique," in *Proceedings of Frontiers in Low Temperature Plasma Diagnostics IV*, p. 139, 2001.

E. Eisenbraun, A. Klaver, Z. Patel, G. Nuesca, and A. E. Kaloyeros, "Low temperature metalorganic chemical vapor deposition of conformal silver coatings for applications in high aspect ratio structures," *Journal of Vacuum Science & Technology B*, vol. 19, no. 2, p. 585, 2001.

# Dankwoord

Door bemiddeling van Richard van de Sanden kon ik na het behalen van de ingenieurstitel in Eindhoven in Delft starten in een research assistant functie. Dit ter ondersteuning van Chiel Smit bij zijn promotieonderzoek naar de depositie van microkristallijn silicium. Al spoedig kreeg ik de mogelijkheid om zelf een promotieonderzoek te doen. Nu, vijf jaar later, ben ik veel personen dank verschuldigd voor hun bijdrage aan de totstandkoming van dit proefschrift. Zonder hen was het niet mogelijk geweest of was het eindresultaat beduidend minder goed geworden.

Ten eerste wil ik mijn co-promotor en begeleider René van Swaaij bedanken voor al het werk dat hij heeft verricht. Beste René, dank je voor de vele revisies van mijn manuscripten en het structureren van mijn gedachten. Jij hebt mij door een leerzame en waardevolle periode geloodst. Door jouw hulp, adviezen en je enorme kennis van vakliteratuur sta ik nu hier en kunnen wij dit feestje vieren.

Ik bedank Kees Beenakker voor zijn optreden als promotor; de goede werksfeer plus faciliteiten binnen DIMES maakten het plezierig om aan mijn onderzoek te werken.

Geachte leden van de promotiecommissie, hartelijk dank voor uw bereidheid om dit manuscript te beoordelen. Uw aanvullingen en opmerkingen heb ik zeer op prijs gesteld.

Bart, vriend, paranimf en lotgenoot: aan de vooravond van jouw en mijn promotie wil ik je bedanken voor de discussies die wij hebben gevoerd. Tijdens het werk waren ze wetenschappelijk en verantwoord, maar in onze vrije tijd gezellig en ontspannend. Het is fijn om onder het genot van een hartversterkertje te reflecteren op ons werk. Het leven van een promovendus behoeft veel beschouwing.

I would like to thank professor Neitzert for the facilitation of the proton-beam irradiation experiments and the workshop in Salerno.

Marinus Hom ben ik dank verschuldigd voor de elektronen bestralingen. Het

was altijd goed vertoeven in de betonnen bunker van IRI. Nu ik in Enschede woon moet je toch een andere maat zoeken voor het oplossen van je computer problemen. Verder wil ik John Warman en Thijs de Haas van IRI bedanken voor het werk en interpretatie met de time-resolved microwave conductivity setup. Gijs Oomen en Martin Kroon, dank jullie wel voor de begeleiding van mijn project vanuit Dutch Space b.v.

Ik wil de zonnecellen groep hartelijk danken voor de geweldige tijd in Delft. De goede samenwerking en prettige sfeer op onze afdeling werd door jullie gecreëerd: Miro Zeman, Wim Metselaar, Agnès Petit, Bart Pieters, Arjan Driessen, Martijn Tijssen, Kasper Zwetsloot, Chiel Smit, Bas Vet, Gijs van Elzakker, Stefan Luxembourg, Michael Wank, Raúl Jiménez Zambrano, en Vojto Nádaždy. Verder wil ik alle ‘cleanroom’ medewerkers bedanken voor jullie vakkennis, behulpzaamheid en interesse in mijn werk.

De dames van het secretariaat, Marian Roozenburg en Marysia Lagendijk, hartelijk bedankt voor het smeren van de administratieve radertjes. Tom Scholtes, bedankt voor het gebruik van jouw kamer voor onze koffie pauzes.

Mijn burens uit de Ecodusflat in Delft, Carlo, Amber, Noel en Nemo, hartelijk dank voor jullie gastvrijheid en belangstelling in mijn persoon. Het was zo fijn om na een vermoeiende werkdag bij jullie te mogen eten. Deze maaltijden waren heerlijk en gezellig, bij jullie viel de spanning van mij af. Dank voor alles!

Lieve familie en vrienden, daar is het dan, mijn proefschrift! Met veel belangstelling hebben jullie mijn promotietraject gevolgd. Voor jullie was het niet altijd duidelijk waar ik mee bezig was. Ik hoop dat het jullie, na het lezen van dit proefschrift en het lekenpraatje dat ik voorafgaande aan de promotiezitting zal houden, iets duidelijker wordt. Ik ben jullie dankbaar voor het geduld met mij in de weekenden als ik doodmoe en hongerig in het zuiden arriveerde en het tekort aan slaap aanvulde. De rust en gezelligheid gaven mij de energie om er weer tegenaan te gaan. Zie hier, de thesis is klaar. Hoera, er valt een last van mijn schouders!